Recent innovations in analytical methods for the qualitative and quantitative assessment of lignin

Jason S. Lupoi [a,b,*], Seema Singh [b,c], Ramakrishnan Parthasarathi [b,c], Blake A. Simmons [a,b,c], Robert J. Henry [a]

[a] Queensland Alliance for Agriculture and Food Innovation, University of Queensland, St. Lucia, Queensland 4072, Australia
[b] Joint BioEnergy Institute, Lawrence Berkeley National Laboratory, 5885 Hollis Street, Emeryville, CA 94608, USA
[c] Biological and Materials Science Center, Sandia National Laboratories, 7011 East Avenue, Livermore, CA 94551, USA

ARTICLE INFO

ABSTRACT

As the attraction of creating biofuels and bio-based chemicals from lignocellulosic biomass has increased, researchers have been challenged with developing a better understanding of lignin structure, quantity and potential uses. Lignin has frequently been considered a waste-product from the deconstruction of plant cell walls, in attempts to isolate polysaccharides that can be hydrolyzed and fermented into fuel or other valuable commodities. In order to develop useful applications for lignin, accurate analytical instrumentation and methodologies are required to qualitatively and quantitatively assess, for example, what the structure of lignin looks like or how much lignin comprises a specific feedstock's cellular composition. During the past decade, various diverse strategies have been employed to elucidate the structure and composition of lignin. These techniques include using two-dimensional nuclear magnetic resonance to resolve overlapping spectral data, measuring biomass with vibrational spectroscopy to enable modeling of lignin content or monomeric ratios, methods to probe and quantify the linkages between lignin and polysaccharides, or refinements of established methods to provide higher throughput analyses, less use of consumables, etc. This review seeks to provide a comprehensive overview of many of the advancements achieved in evaluating key lignin attributes. Emphasis is placed on research endeavored in the last decade.

© 2015 The Authors. Published by Elsevier Ltd. This is an open access article under the CC BY-NC-ND license (http://creativecommons.org/licenses/by-nc-nd/4.0/).

Contents

* Corresponding author at: Sage Analytics, 1650 38th Street, Boulder, CO 80229, USA. Tel.: +61 510 486 7315.
E-mail addresses: slupoi0213@gmail.com (J.S. Lupoi), seesing@sandia.gov (S. Singh), parthas@lbl.gov (R. Parthasarathi), basimmons@lbl.gov (B.A. Simmons), robert.henry@uq.edu.au (R.J. Henry).

1. Background

Lignin, a major component of land plants, has been routinely analyzed due to its importance in the structural properties of wood and in determining the digestibility of plant material by animals. As the global effort to identify ideal lignocellulosic feedstocks for biofuel production has evolved, the importance of understanding lignin structure, composition, and quantity within plant cell walls has proven to be paramount. Lignin is a three-dimensional, complex biopolymer comprised of phenylpropanoid, units, specifically syringyl (S), guaiacyl (G), and p-hydroxyphenol (H) monomers (Fig. 1), linked via dehydrogenation reactions [1]. These phenylpropanoid moieties originate from hydroxycinnamyl alcohols, and to a lesser degree, cinnamaldehydes. Fig. 2 illustrates a schematic representation of lignin including phenylpropanoid units and lignin–lignin linkages.

The functions of lignin encompass the strengthening of plant cell walls, providing resistance against microbial attack, and playing a crucial part in water transport by reducing cell wall permeability [1]. The ratio of S/G functionalities in the cell wall can help define the degradability of lignin, as some studies have reported that higher S-lignin led to increased removal of lignin with concomitant increases in sugar yields [2–4]. The importance of S/G ratios on lignin deconstruction, and subsequent sugar release appears to be feedstock dependent, however, as decreases in the metric have also been measured to result in higher sugar production [5]. Plants with low lignin content can facilitate enzymatic degradation by allowing the enzymes greater accessibility to cellulose [6]. Lignin also can irreversibly bind cellulase enzymes, thereby diminishing the catalytic potential sugar release, making its reduction highly desirable [4,7–9].

A variety of biomass pretreatment strategies can be employed to deconstruct or delignify plant cell walls. These techniques include treatment with ionic liquids (ILs), bases, such as ammonia, sodium chlorite or sodium hydroxide, organic solvents, and ozone [10–14]. The delignification of plant cell walls generates substantial waste streams that can be utilized in the formation of bio-based chemicals and products. For instance, lignin's diverse marketability includes automotive brakes and tires, wood panel products and preservation, polyurethane foams, a coal substitute, a binder in animal feed, an ingredient in pesticide formulation, industrial cleaners, and concrete, to name a few [15–18]. Zakzeski et al. have provided an elegant, comprehensive review examining the development of catalytic pathways and techniques for the valorization of lignin into useful products [19].

In 2005, Hatfield and Fukushima presented a survey of analytical techniques entitled "Can lignin be accurately measured?" [20]. The authors evaluated a variety of wet chemical techniques such as acetyl bromide, acid detergent, Klason, and permanganate oxidation, as well as instrumental methods like near-infrared (NIR) spectroscopy, nuclear magnetic resonance (NMR) spectroscopy, and ultraviolet (UV) spectrophotometry. Other notable reviews have provided a framework of how specific analytical tools, such as wet chemical techniques [21,22], mass spectrometry (MS) [23], thermochemical conversion [24,25], NMR [21,26–31], and electronic and vibrational spectroscopy [26,29,32–38], have aided in lignin analysis. Additionally, Brunow and Lundqvist recently reviewed functional groups present in lignin and linkages between lignin and carbohydrates [39]. This review seeks to provide an assessment of the progress made in studying lignin qualitatively and quantitatively over the last decade, encompassing wet chemical, chromatographic, microscopic, thermochemical, and spectroscopic advancements (Table 1). A summary of dominant advantages and disadvantages of each technique for lignin assessment is provided in Table 2. Emphasis will be on evaluation of

lignin's structure, lignin–lignin and lignin–carbohydrate linkages, molecular weight, total content, and monomer composition.

2. Lignin structure

2.1. Wet chemistry

As the quest for rigorous analytical tools capable of probing the enigmatic structure of lignin has ensued, a variety of progressive
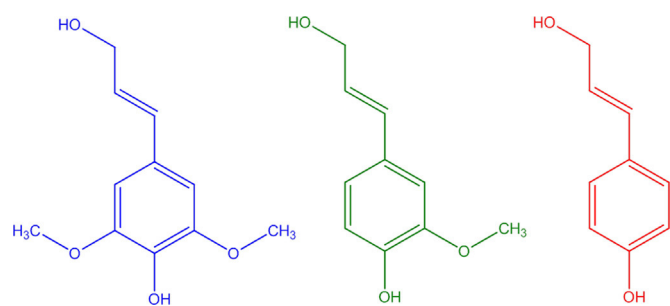

Fig. 1. Three fundamental lignin monomers (and their respective phenylpropanoids): sinapyl alcohol (syringyl (S)), coniferyl alcohol (guaiacyl (G)), and *p*-coumaryl alcohol (*p*-hydroxyphenol (H)).

techniques have emerged. Wet chemical methods for the measurement of specific lignin functional groups have previously been described and reviewed [40–51]. The techniques include detection of carbonyl [40,46,51], carboxyl [43], aliphatic and phenolic hydroxyl [42,48,51], methoxy [41,51], condensed units [49], and free phenolic groups [45,51]. Although these methods have been utilized for decades, the structural complexity of lignin has made the reproducible assessment of specific functionalities challenging. The method used to isolate lignin can change the original structure leading to erroneous measurements of functionalities. Although there have been relatively few advancements in wet chemical techniques for lignin structural analysis, a few recent studies are worth noting. Eshkiki et al. developed a novel method for the titration of free phenolic hydroxyl groups [45]. The analysis of these moieties can aid in developing delignifying strategies. Lignin was reacted with chlorine dioxide (ClO_2) at 0 °C for 30 min. The rate of ClO_2 consumption was monitored using iodometry. The authors found that this protocol could be directly applied to pulps, eliminating the need for extracting the lignin. An inter-laboratory study of analytical methods employed for sulfur-free lignin characterization revealed erroneous results obtained from acetylation of phenolic hydroxyl groups, whereas the use of tetra-n-butylammonium hydroxide in the potentiometric titration of phenolic and carboxyl groups was found to provide correlative results between labs [47]. Ultimately, reproducible, *in situ* measurements of lignin structure have been coveted for decades.
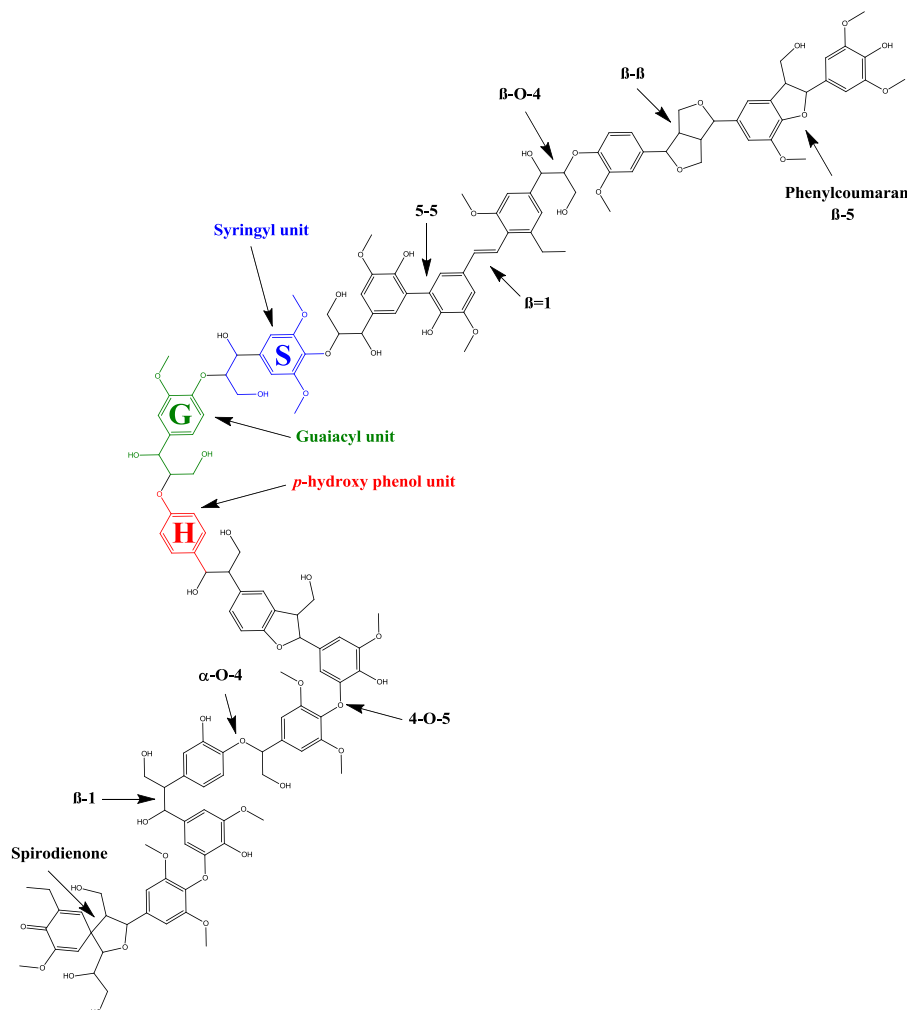

Fig. 2. Schematic representation of lignin including syringyl (S, blue), guaiacyl (G, green), and *p*-hydroxyphenol (H, red) phenylpropanoid moieties, and lignin–lignin linkages. (For interpretation of the references to color in this figure legend, the reader is referred to the web version of this article.)

Table 1
Methods for lignin analysis.

	Wet chemistry	Chromatography	Thermo-chemical	Spectroscopy	Other
Lignin structure	Functionality specific reactions [40–44,47–50]	CZE [52]	APPI-MS [67]	CRS Microscopy [116,117]	AFM [178]
		GC [44] GCMS [171]	DE-MS [62]	Dispersive Raman [92–96]	DFT [88,180]
	ClO$_2$ [45]	GLC-FID [54]	ESI/MS [77]		DSC [60] Potentiometry [44]
	Modified oximation [46]	GLC-MS [54] Headspace GC [55]	MALDI-MSI [68]	Ellipsometry [179]	
		RP-HPLC [53]	MALDI/TOF [73]	Fluorescence [102,103,120,131,176,177]	SEM [71,75] TEM [103]
			MBMS [75]	FTIR [13,44,61,65,75,78,79,81,92,93,109,110,118–139,196]	
			pyGC/FID [66] pyGCMS [60–64]		
			pyTMAH [59,65]	FT-Raman [33,84–91]	
				NMR [13,44,54,59–61,64,67,78–81,91,110,119,121,123,127,128,132–135,137,141–171,196]	
			QqTOF-MS [67] TGA [78–83] TOF-SIMS [69–72,74,76]		
				Optical absorption [75] NIR [181] Raman imaging [97–104] Resonance Raman [105,106,108,112,113] UV-Raman [107–111,114] UV [44,115,128,129,133,174] UVMSP [173,175]	
Lignin–carbohydrate, lignin–lignin linkages	Periodate oxidation/GC [185]	GC [189]	MALDI/TOF [73]	NMR [54,59,61,132,135,137,157–161,165–167,172,182–184,186,190,192–195,319]	
	Permanganate oxidation [60]	GCMS [65,191] GLC-FID [54]	pyGCMS [182,183,190]		
	Ozonation [161] Thioacidolysis [182–185]	GLC-MS [54] LC [187,188] SEC [182,184–186]	pyTMAH [59,65]		
Lignin molecular weight	Acetobromination [221]	GPC [61,134,150,163,167,169–171]	FT-ICR-MS [223]		Light scattering (MALLS)
			MALDI/TOF [73,78]		[178,224]
		SEC [64,77,81,128,129,135,147,183,184,196,222,224]			
Total lignin content	Acetyl bromide [225–227]		pyGC/FID [66,238–240]	Fluorescence [277,278]	Color image analysis [289]
	Acid-insoluble lignin [229,233,234]		pyMBMS [241–243]	FTIR [92–94,252–255,320–323]	
			TGA [244–247]	FT-Raman [248–251]	

Klason [227,228,230,231]

NIR [93,178,241,256–279]

Permanganate oxidation [237]

NMR [80,140,146,152,169,287,288]

TAPPI standard method [230]

Photoacoustic [286]

Van Soest [227,235,236]

UV-Raman [107]
UV–vis [108,125,132,142,232,280–285]

Lignin monomer composition   Acidolysis [297,302]   CZE [52]   DE-MS [62]   Dispersive Raman [95,96]

DFRC/GC [57–59,159]   MALDI-MSI [68]

Cupric oxide [291,292,294,324]

FTIR [65,124,130,134,252,314,317]

GC-FID [135]   pyGC/FID [66,126,240,305]
HS-SPME/GCMS [56]

Permanganate oxidation [291]

FT-Raman [315–317]

pyGCMS [13,59,61–65,156,157,159,183,293,295,298–301,303,308,324]

UPLC-MS/MS [311]   NIR [163,268,304,312,313,317]

Nitrobenzene Oxidation [291,292]

NMR [61,64,78,81,128,134,137,141–143,146,154,156,158,161,166,167,318,325]

Thioacidolysis [196,296,304,307,324]

pyMBMS [4,5,242,243]
SVUV PIMS [306]

UV-Raman [111,112]

TOF-SIMS [70]

Table 2
Advantages and disadvantages of analytical methods used for assessing lignin.

Method	Advantages	Disadvantages
Fluorescence spectroscopy	• 2-3 orders of magnitude more sensitive than UV/vis [37] • Can probe relative lignin content based on brightness in imaging techniques [103] • Capable of localization of lignin in plant cell wall [103,131,176] • Lignin reveals strong fluorescence [96] • Cheap instrumentation [277] • More selective than absorbance [37] • Non-destructive [277]	• Requires fluorophore (intrinsic or through labeling) [277] • Has not led to robust predictive modeling [277]
GC	• Better spectral resolution than HPLC [326] • Selectively analyze only volatile species [326] • Headspace sampling limits clean-up requirements [56,327]	• Destructive [326] • Requires volatile molecules, or must derivatize to promote into gas phase [328]
HPLC	• Diverse separation configurations and molecular polarities [329] • Non-destructive; can collect fractions [330] • Separation of non-volatile or thermally unstable molecules [330]	• Long analysis times [328,331] • May require sample clean-up [327]
MS	• Can be used for MW determination [23] • Rapid analysis [23] • Selectivity [23] • Sensitivity [23] • Variety of different ionization strategies [23]	• Destructive [23]
MIR spectroscopy	• Use of attenuated total reflectance can remove water contribution to spectra [332] • More intense spectra than NIR or Raman [333–335] • Non-destructive [36,332] • Little-to-no sample preparation [332] • High-throughput [332]	• May require specific sample preparation (*i.e.*, KBr pellet) [33] • Spectral sensitivity to water; may require extensive sample drying [332,334]
NIR spectroscopy	• Cheaper instrumentation [336,337] • Field-portable [331,338] • High-throughput [35,331,332] • Non-destructive [35,332] • Little-to-no sample preparation [332] • Water-tolerant [335]	• Requires multivariate analysis [332,338] • Measures predominantly C-H, N-H, O-H, and S-H bonds [332,335] • Physical differences in samples detrimental to spectra [335]
NMR	• Un-paralleled structural information available [27] • Multi-dimensional NMR provides enhanced spectral resolution [26,27] • Non-destructive [27] • Non-invasive [27] • Recent advances probing higher-throughput capabilities [339]	• Lignin quantitation is difficult due to spectral overlap [26] • Most techniques considered low-throughput [95] • Lack of spectral resolution, especially in lignin region [27,162] • Lack of sensitivity [27] • Costly instrumentation [340]
Pyrolysis	• Eliminates need for lignin isolation [23] • High-throughput (MBMS) [242] • Facile sample preparation [239] • Enables detailed structural characterization of pyrolysis products [23,239] • Small sample amounts [23]	• Destructive [23,300] • Potentially complex data analysis (*i.e.*, which fragments should be included in monomer quantitation [59,300]
Raman spectroscopy	• Complimentary to mid-IR [334] • Field-portable [341,342] • High-throughput [95,315] • Multiple excitation sources available [333,343] • Non-destructive [95] • Little-to-no sample preparation [95] • Strong signal from lignin [95] • Surface enhancement capabilities [344] • Water-tolerant [95]	• Self-absorption from colored analytes such as lignin [345] • Relatively weak phenomenon, compared to IR [334] • Cell-wall phenolics can interfere with lignin measurement; need to extract biomass containing high-extractables [95] • Fluorescence can mask signal [96]
SEC	• Conventional instrument [222] • Expansive array of detectable masses in single step [222]	• Association of lignin molecules complicates measurement [23,221] • Complicated by polydispersity [23]

Table 2 (continued)

Method	Advantages	Disadvantages
	• Fast analysis [222] • Coupling w/MALLS enabled higher MW aggregates to be detected (UV and RI detection does not measure these species) [178,224]	• Condensation effects [23]
TGA	• High-throughput [245,246] • Ideal for polymers like lignin [245]	• Destructive [245,246] • Temperature ramping must cause mass changes in analyte [245]
UV/vis spectrophotometry	• Cheap & simple instruments [340] • Convenient [340] • Selective and sensitive [340] • Lignin has UV electronic transition [226]	• Difficulty in determining extinction coefficient for lignin quantitation [37,281] • Ubiquitous absorbance in UV for extraneous molecules requires removal prior to acid-soluble lignin measurement [37]
Wet chemistry	• Well established techniques [22,228] • Selective for specific moieties [22,40–43,48,346]	• Tedious, costly sample preparation and analysis [331] • May alter/destroy the sample [23] • May only detect specific bonds in lignin [21–23] • Toxicity [22,232]

2.2. Chromatography

While chromatographic methods are often employed in conjunction with wet chemical methodology, a few instrumental developments probing lignin structure are worth discussing [44,52–56]. Aromatic lignin compounds, derived from naturally and artificially aged paper were identified using capillary zone electrophoresis (CZE) [52]. Quantitation of acetosyringone, 4-hydroxyacetophenone, 4-hydroxybenzaldehyde, vanillin, vanillic acid, furoic acid, and 4-hydroxybenzoic acid in the aged paper was enabled following the production of respective calibration curves using model lignin derivatives. The authors note that although studies employing CZE detection for lignin derived molecules are relatively scarce, this method has advantages over gas chromatography (GC) since no derivitization is required, and the separation times are shorter. A novel headspace GC technique was developed to quantify the methoxyl content of isolated lignin [55]. Hydroiodic acid effectively cleaves methoxyl functionalities, forming methyl iodide. This method improves upon iodometry, which involves complex and laborious preparatory steps, and the standard GC analysis, as large sampling variance has been measured due to the highly volatile nature of methyl iodide. Sampling the headspace ensures a more accurate quantitation. Grass acylation was evaluated using gas-liquid chromatography (GLC) with flame ionization detection (FID) and MS [54]. Conjugates comprised of coniferyl or sinapyl alcohols (SA) and p-coumarates (p-CA) were found to result from the enzymatic reaction with p-coumaroyl transferase (pCAT). An assay to assess the activity of this enzyme was developed using GLC-FID. This assay was used to probe C3 and C4 grasses such as wheat, tall fescue, and oat (C3) and corn and switchgrass biomass (C4). Despite the preferential reaction of p-CAT with SA, higher S lignin content was not detected in plants with elevated p-CA content. Isolated lignins from various hard- and softwood feedstocks were partitioned and characterized using a reverse phase-HPLC instrument equipped with a wide-pore octadecylsilica column [53]. The authors determined that a 10-step gradient using N,N-dimethylformamide and fluorimetric detection enabled well-defined lignin peaks. Analysis of Klason lignins isolated from aspen, beech, eucalypt, and spruce revealed that each type of biomass produced a unique chromatogram regardless of whether UV or fluorimetric detection was employed.

Derivitization followed by reductive cleavage (DFRC), a technique developed by Lu and Ralph to break α and β-ether linkages, leaving intact the γ-esters [57], was used with GC-FID and GCMS, to study alder, birch, cherry, maple, and oak leaves [58]. Similar to thioacidolysis, DFRC involves the extraction of products representative of the original lignin, followed by the acetylation of the products, and subsequent GC analysis. This technique has been reported to be more advantageous to thioacidolysis due to the less stringent reaction conditions and reagents, and better molecular ion peak resolution in MS. The leaves studied had lower S/G ratios than the xylem. DFRC analysis of wheat straw lignin indicated that limited p-coumaryl functionalities were connected to γ-OH moieties in β-ethers [59].

2.3. Thermochemical methods

2.3.1. Pyrolysis gas chromatography

Although typically employed for the quantitation of lignin monomers (see Section 6.2), pyrolysis gas chromatography/mass spectrometry (pyGCMS) has occasionally been applied to lignin structural analysis [59–65]. Analysis of the pyrograms of Eucalyptus hybrids revealed 37 distinct components stemming from H (3), G (17), and S (17) lignin functionalities [63]. Identical side-chain components were measured for both G and S moieties. No discrete classifications between the samples were illuminated using principal component analysis (PCA); however, PCA did expose differences in the hybrids' lignin content. Evaluation of the scores plot uncovered which lignin structures were significant in building the PCA model.

Herbaceous and softwood industrial lignin samples were characterized using pyGCMS before and after esterification to gauge their potential usefulness for bio-plastic fabrication [60]. While pyGCMS of pine and corn stover revealed G and S/G/H lignin monomeric content respectively, rice straw was measured to lack H lignin. The ratio of monobasic to dibasic monomers was quantified in order to evaluate different lignins based on their degree of condensation. Higher condensation factors indicate the lignin closely resembles a more natural, unaltered lignin. Hu et al. used pyGCMS to characterize S, G, and H lignin compounds generated from the fast pyrolysis of lignin, isolated from industrial black liquor [61]. The analysis of degradation products generated using pyrolysis temperatures of 500, 700, and

900 °C, indicated that below 500 °C, the molecules created predominantly stemmed from inter-unit linkage cleavages and slight side-chain cracking, while phenolic hydroxyl and methoxyl functionalities remained intact. Increasing the temperature from 500 to 900 °C revealed that demethoxylation began to occur, aromatic ring methyl groups were augmented, and side chains exhibited dealkylation. Using this data, a two-step reaction mechanism was proposed for the fast pyrolysis of lignin: inter-unit linkage cleavage followed by free radical reactions that resulted in phenolic species. Lastly, pyGC coupled with FID and PCA allowed the distinction of species and tissue-specific differences in pine, spruce, and larch softwoods [66].

2.3.2. Mass spectrometry

Mass spectrometry, in its numerous configurations, has been employed to characterize the structure of lignin [62,67–77]. Time-of-flight (ToF) secondary ion mass spectrometry (SIMS) is one such MS design that provides enhanced sensitivity to surface measurements of solid analytes with high mass spectral and spatial resolution, requires limited sample preparation, and yields rapid analyses over wide mass ranges [69–72,74,76]. Goacher et al. developed an improved library of secondary ions for the differentiation between lignin and polysaccharide mass fragments [69]. PCA allowed the segregation of mass spectral data as either lignin or polysaccharide peaks from pine. The authors identified 64 new spectral peaks for polysaccharide and lignin characterization beyond the standard fragments reported in the literature. The ions that segregated pure cellulose from the pine sample were likely to stem from lignin. High-resolution images of lodgepole pine were acquired using ToF-SIMS imaging. By localizing specific mass spectral peaks to plant cell wall regions, the classification of a lignin or polysaccharide peak could be facilitated. The images revealed the expected categorization of lignin in the compound middle lamella (CML) and cell corners (CCs), and polysaccharides concentrated in higher proportion inside the cell walls. The novel mass spectral fragments identified using PCA have not been routinely employed in the literature for spectral characterization, despite their high intensity. This library of secondary ion assignments should significantly facilitate both a more accurate characterization and quantitation of lignin and polysaccharides in plant cell walls.

A novel instrument for the analysis of lignin volatilization products from raw biomass was constructed by conjoining pyrolysis or laser ablation with resonance-enhanced multiphoton ionization (REMPI) reflectron ToF-SIMS [72]. A comparison of this instrument with pyrolysis electron impact molecular beam mass spectrometry (pyEI-MBMS) using poplar wood displayed the validity of the REMPI ToF-SIMS to selectively measure lignin, as no peaks from polysaccharides were measured. The mass spectrum resultant from the pyEI-MBMS contained various low molecular weight fragments derived from carbohydrates. The REMPI method also diminishes the splintering of molecular ion peaks into smaller fragments since it is considered a "soft" ionization technique. The energy, for example, of the EI process is ~2.5-fold higher than REMPI, and this excess energy, in turn, cleaves the molecular ion into smaller fragments. Laser ablation was used to preferentially sequester and volatize localized tissues, such as wood growth rings, followed by the subsequent vapor detection using REMPI ToF-SIMS. Using this method, the authors concluded that lignin thermally degrades to a variety of monomeric molecules, with some dimer formation. Overall, this instrument enables the selective measurement of regions of interest with high selectivity and sensitivity, and with fewer spectral peaks compared to more vigorous ionization techniques.

Tokareva and co-authors evaluated a variety of ToF-SIMS sample preparation methods for imaging [76]. The authors concluded that reliable ToF-SIMS imaging required a strict protocol for developing reproducible samples. Another study utilizing ToF-SIMS probed

synthesized lignin polymers and MWL from beech to characterize the depolymerized fragments [74]. A previous study employed gallium primary ions as the bombardment source. Guaiacyl lignin peaks at *m/z* 137 and 151 were easily identifiable, but it remained uncertain whether the 151 peak actually corresponded to two unique fragments. In this study, the use of Au$^+$ ions as the bombardment source led to higher mass resolution, and to the finding that the *m/z* 151 peak is due to only one species, the C_6–C_1 benzoyl ion. Lastly, the surface lignin from the outermost region of rapid displacement heating (RDH) kraft pulp was evaluated using ToF-SIMS equipped with an indium ion source to achieve high mass resolution [70]. The lignin on the surface following the RDH pulping remained a vestige from native lignin, albeit structurally altered during the kraft process. Although the spectral data from birch kraft lignin and MWL show strong similarities, S lignin was more reactive in the kraft process as less S lignin content was measured relative to G lignin. More than half of the surface lignin measured remained on the surface following totally chlorine-free bleaching.

Matrix-assisted laser desorption/ionization (MALDI) ToF mass spectrometry has provided another useful tool for herbaceous lignin analysis [73]. Aromatic acids α-cyano-4-hydroxycinnamic acid (CHCA) or 2,5-dihydroxybenzoic acid (2,5-DHB) were found to provide the best MALDI matrices. Cyclodextrin was added to CHCA to promote the ionization of relatively insoluble lignin samples, and suppress the background noise from matrix-related ions. When used in positive ion mode, this method was found competent for surveying lignins according to "fingerprint" regions (100–800 Da), and discriminating between lignins extracted with ammonia or formic/acetic acid. MALDI mass spectral imaging (MSI) has recently enabled the *in situ* analysis of *Eucalyptus globulus* and *E. grandis* lignin [68]. The authors chose thin-layer chromatography grade silica as a MALDI matrix, since the standard matrices are not suitable for plant materials. Not only were 22 of 24 reported lignin derivative compounds identifiable, but their relative locations inside the plant cell walls were elucidated, providing a tandem approach to characterizing lignin spatial distribution and structure.

In an elegant showcasing of MS techniques, quadrupole (Qq) ToF-MS and atmospheric pressure photoionization (APPI) MS were used to evaluate wheat straw lignin [67]. A novel extraction strategy that selectively partitions biomass into cellulose, hemicellulose, and lignin enabled the isolation of the lignin fractions for MS analysis. APPI-MS was employed to evaluate lignin oligomers incapable of efficient ionization with atmospheric pressure chemical or electrospray ionization (ESI) methods. At least 57 distinguished spectral fragments were identified through the utilization of both positive and negative ion modes. Qq ToF-MS analysis permitted the exact molar mass to be calculated for each ion fragment. Tandem Qq ToF-MS/MS further resolved mass spectral data from a complex series of lignin oligomers, thereby enabling the construction of precise structures. This extensive study of wheat straw lignin unveiled a linear polymeric structure of various poly-condensed coniferyl groups, with a phenylcoumaran repeating unit. The authors contend that lignin is quite reactive under harsh conditions, and can readily be decomposed to new molecules not measured in native lignin, leading to discordance in decades of lignin structural analysis. The authors also express cautionary advice to researchers using ^{13}C cross polarization/magic angle spinning (CP/MAS) nuclear magnetic resonance (NMR) spectroscopy as a singular analytical tool for lignin analysis, explaining that the ratio of 153.1 and 147.5 ppm peaks can be confused, resulting in the misidentification of carboxylic functionalities. Using NMR, these carboxylic functionalities were classified as deriving from proteins or extractives, when, in fact, they stem from the lignin backbone. Other MS techniques employed for lignin analysis include direct exposure MS of waterlogged archaeological wood [62], ESI-MS analysis of the depolymerization of lignin following treatment with

Table 3
Raman spectroscopy vibrational modes characteristic of lignin and model lignin compounds.

Vibrational mode	Assignment
337	Ring deformation, OH torsion [88]
357	Aromatic ring substituents torsion [88]
369	Skeletal deformation [33]; COC symmetric, in-plane bend [88]
468	Ring deformation [88]
531	Skeletal deformation [33]
559	CCO and CCC in-plane bend [88]
582	Ring deformation [88]
597	Skeletal deformation [33]
637–644	Ring and skeletal deformation [32,88]
712	Ring deformation; CC stretch [88]
780	CO stretch [88]; lignin aromatic skeletal vibrations [32,88]
793	Out-of-plane CH bend; ring deformation; CO stretch [88]
799	Ring deformation; CO stretch [88]
805	CO stretch; aryl symmetric CH bend; CH out-of-plane bend [88]
829	CH out-of-plane bend [88]
843	Breathing mode [88]
920–932	CCH wag [32]
921	Ring deformation; in-plane CC stretch; COC stretch [88]
942	lignin CCH wag; aromatic skeletal vibrations [85,88]
977	lignin CCH and −HC=CH deformation; methyl wagging [85,88]
1033	lignin CH_3 wagging; CH_3 out-of-plane rock; aromatic skeletal vibrations, methoxy vibrations [85,88]
1043	OC stretch; ring deformation; CH_3 wagging [88]
1117	lignin methoxy vibrations; aryl CH bend [88]
1130–1136	Coniferaldehyde/sinapaldehyde mode [33]
1147	lignin methoxy vibrations; aromatic CCH bend [88]
1169	lignin hydroxyl COH bend; aromatic skeletal vibrations [88]
1185	lignin methoxy vibrations; COH in plane bend [88]
1199	In-plane CH stretch [88]
1202	lignin methoxy vibrations [88]
1214–1217	Aryl-O of aryl OH and aryl-OCH_3; ring deformation [32,88]
1256	CO stretch [88]
1268	lignin aromatic skeletal vibrations; methoxy vibrations [32,85]
1272	Ring deformation; CO stretch [88]
1288	Ring deformation and in-plane CH and COH bend [88]
1298	CH, CC stretch; ring deformation [88]
1331	Aliphatic OH stretch [33]
1363	Ring Deformation; in-plane COH bend [88]
1372–1383	Phenolic OH stretch
1378–1390	Phenolic OH [32]
1380	Umbrella CH bend [88]
1427	lignin methoxy deformation, methyl bending, aromatic skeletal vibrations [32,85]
1455	CH_3 scissoring; CH_3 out-of-plane bend; umbrella bend [88]
1460	lignin methoxy deformation, CH_2 scissoring [33]
1465	CH_3 scissoring; CH_3 out-of-phase bend [88]
1506–1514	Aryl ring stretch, asymmetric [32]
1517–1521	Asymmetric aryl ring stretch [32]
1605	lignin aromatic skeletal vibrations [32,88]
1632	lignin C~C stretch of coniferaldehyde, sinapaldehyde, phenolic esters [32,85]
1656	lignin C~C stretch of coniferyl alcohol and sinapyl alcohol [32,85]
1704	carbonyl stretch
2842	Out-of-plane CH symmetric stretch [88]
2845	CH stretch in OCH_3, symmetric [33]
2859	Out-of-plane symmetric CH stretch [88]
2867	Out-of-plane symmetric CH stretch [88]
2922	Out-of-plane asymmetric CH stretch [88]
2939	CH stretch in OCH_3, asymmetric [33,88]
3005	In-plane CH stretch [88]
3014	In-plane CH stretch [88]
3039	In-plane CH stretch [88]
3062	In-plane CH stretch [88]
3071	aromatic CH [33]

various organic bases such as sodium phenoxide or guanidine carbonate [77], and the evaluation of ozonation to delignify sugarcane bagasse using molecular beam MS (MBMS) [75].

2.3.3. Thermogravimetric analysis

Thermogravimetric analysis (TGA) has been previously employed in the quest for the structural characterization of lignin [78–83]. Following the pretreatment of Avicel, beechwood, alkaline lignin, switchgrass, and corn stover with the IL 1-butyl-3-methylimidazolium acetate ([C_4mim][OAc]), the thermal decomposition was evaluated using TGA [83]. A wide temperature range was measured for lignin degradation (300–500 °C) resultant from the intrinsic heterogeneity. Following the IL treatment, the DTG curves show two narrow peaks compared to untreated lignin, which the authors infer could stem from a more homogeneous structure. Increases of 50 °C increments did not change

the lignin degradation data, signifying that the structure remained unaltered. The effects of steam pretreatment and incubation with laccase on *E. globulus* chips were evaluated using TGA curves [80]. Lignin in the control sample degraded at approximately 470 °C, while the lignin from steam pretreated *E. globulus* degraded at 490 °C, which the authors conclude could result from condensation reactions during the steam explosion. This trend amplified as the harshness of the steam explosion treatment increased. A 19 °C reduction in lignin degradation temperature was measured following incubation with laccase. This decrease was attributed to changes in the molecular structure or bonding between lignin and carbohydrates due to the experimental conditions employed for the laccase incubation, but not to the laccase itself, as no differences were measured when the laccase-treated biomass was compared to the untreated sample. A recent study explored using TGA to evaluate different preparations of isolated lignin from *Miscanthus* and giant reed [81]. Extraction protocols employing sulfuric acid (H_2SO_4) or hydrogen peroxide (H_2O_2) at an alkaline pH, and a microbial treatment were used to produce the lignins. Following the acid treatment, the giant reed and enzyme-treated sample showed similar degradative patterns, while the *Miscanthus* had a faster rate of degradation up to 673 K, and then conformed to a similarly shaped TGA-curve. Following the alkaline H_2O_2 treatment, all curves expressed similar degradation up to 623 K, where the *Miscanthus* sample began to breakdown more slowly. Differential TGA elucidated which specific chemical moieties in lignin were degrading at explicit temperatures. For example, signals near 593 K were ascribed to the breakage of C–C between lignin monomers and the evaporation of phenolic species. The measured peaks between 673–773 K stemmed from the degradation of aromatic rings.

2.4. Vibrational spectroscopy

2.4.1. Raman spectroscopy

At the United States Department of Agriculture Forest Products Laboratory, Umesh Agarwal and co-authors have been a leading team in developing Fourier-transform (FT) Raman spectroscopy for lignin analysis [32,33,84–86]. The assignment of the characteristic vibrational modes of hard- and softwood lignins have been extensively reported, and are tabulated in Table 3. These assignments have enabled the qualitative assessment of structural differences and similarities between milled-wood, chemically modified, and enzymatically isolated aspen, pine, spruce, and sweetgum lignins [85,87]. Significant spectral differences were measured between hard- and softwoods lignins. Acetylation and methylation produced significant changes in the aliphatic C–H region of the Raman spectra, and gave rise to new vibrational modes not present in unmodified lignin, while measured spectra following alkaline peroxide and hydrogenation reactions were not significantly altered compared to untreated samples. Ethylenic residues in spruce and thermomechanical pulp were measured using the band intensities at 1133 and 1654 cm^{-1}, representative of coniferaldehyde and coniferyl alcohol, respectively [86]. Quantitation based on these vibrational modes provided good correlation with NMR.

FT-Raman spectroscopy and density functional theory (DFT) were used to develop an extensive vibrational mode library for S, G, and H lignin monomers using lignin model monomers [88]. Experimental Raman spectra were compared to the theoretical, calculated spectra, and specific characteristic marker bands for each moiety were identified. In a follow-up study, the authors evaluated how select solvents used for vanillyl alcohol dissolution affected Raman band shape and position [89]. The 1600 cm^{-1} phenolic mode position was strongly correlated with the degree of methoxy substitution on the phenyl ring, whereas the intensity of this mode was not only dependent on the type of lignin monomer (S, G, or H), but also on the solvent or environment. The authors suggest that the shape of the 1600 cm^{-1} vibrational mode could be used to

assess lignin environment. Kihara and co-authors evaluated carbonyl groups in cedar and pine milled wood lignin using FT-Raman spectroscopy [90]. Vibrational modes at 1620 and 1660 cm^{-1} were monitored as chemical modifications were carried out to reduce or enhance C–O groups. The band at 1620 cm^{-1} was identified as a clear marker for carbonyl content. The 1660 cm^{-1} peak was identified as an α,β-unsaturated bond marker. Lastly, FT-Raman spectroscopy was used to gauge the efficiency of lignin removal following an ammonia fiber expansion (AFEX) pretreatment of corn stover [91]. Vibrational modes at 1600 and 1635 cm^{-1} were approximately three times higher in the control relative to the pretreated sample. Additionally, evaluation of the cinnamoyl ester 1170 cm^{-1} peak revealed that the residual lignin had less ferulate and *p*-coumarate functionalities.

Advances in NIR, dispersive Raman spectroscopy instrumentation have enabled applications of this analytical tool to lignin structural research [92–96]. A home-built NIR Raman instrument enabled the analysis of a commercial isolated lignin [96]. The instrument was equipped with a 1064 nm Nd:YVO$_4$ laser and a 1024 element InGaAs multichannel detector. This configuration provided greater sensitivity when compared to a home-built instrument that employed 785 nm excitation, due to the latter instrument's inability to overcome intrinsic lignin fluorescence. The instrument also provided greater signal-to-noise when juxtaposed to a FT-Raman spectrometer when acquisitions longer than 15 s were required. Lignin was dissolved in ethanol, methanol, isopropanol, dioxane, or acetone. The location of the 1600 cm^{-1} phenyl ring breathing mode did not shift in position upon dissolution with any of these solvents; however, when the lignin was dissolved in sodium hydroxide, a pronounced shift was measured. In a follow-up study, applications of the 1064 nm Raman spectrometer were extended to the analysis of raw and ethanol extracted biomass [95]. The intensities of lignin aromatic skeletal vibrational modes near 1600 cm^{-1} were significantly decreased in herbaceous feedstocks, such as orchard grass and red clover, following the extraction, indicative of non-lignin phenolic molecules, such as flavonoids, contributing to this signal. This study showed the necessity of analyzing extractive-free, herbaceous biomass to probe explicit lignin structure with Raman spectroscopy.

At the Joint BioEnergy Institute (JBEI), NIR Raman spectroscopy has been utilized to gauge the delignification efficiency of different pretreatment strategies [92–94]. The removal of lignin from extracted switchgrass was evaluated following dilute acid or IL treatments [93]. A clear reduction in the lignin vibrational modes at 1600 and 1620 cm^{-1} was measured following the IL pretreatment. A follow-up study probed the efficiency of the same pretreatment strategies on eucalypts and pine, with an identical conclusion [94]. A comparison of the AFEX and IL treatment of extracted corn stover also established that the IL treatment more efficiently removed lignin [92]. Researchers at JBEI have also explored Raman imaging to visualize plant compositional distribution inside plant cell walls and to observe the changes in biomass during IL pretreatment [97,98]. Raman hyperspectral imaging was used to map corn stover and *E. globulus* compositional distribution [98]. Lignin was found to be predominantly localized in sclerenchyma cells and tracheids, epidermal cells, and bundle sheath cells using a 2D Raman mapping method. This technique also identified the CCs, followed by the CML and the secondary wall, as containing the highest lignin content. Corn stover lignin dissolution, following an IL treatment with 1-ethyl-3-methylimidazolium acetate ([Emim]OAc), was found to occur most rapidly from the secondary cell walls [97]. Tracheids, despite a thicker wall, showed a faster rate of wall swelling and lignin degradation, compared to sclerenchyma cells. Following just three hours of pretreatment, delignification was 50.7%, 24.2% and 17.9% from tracheids, sclerenchyma cells, and parenchyma cells, respectively.

Uses of Raman imaging to evaluate lignin distribution and delignification extend to a variety of other feedstocks [99–104]. 3D confocal Raman imaging was used to study the delignification of

Miscanthus x giganteus [100]. Following a 20-hour sodium hydroxide (NaOH) pretreatment, complete delignification was observed, while cellulose remained predominantly unscathed. Depth profiling revealed that lignin is initially removed from the interior of the cell wall. The authors also studied the photodegradation of lignin with increasing acquisition time. After about 10 s of exposure to 38 mW of a 532 nm Nd:YAG laser, the Raman scatter measured by integrating the 1550–1650 cm^{-1} spectral region significantly decreased. Confocal Raman microscopy of hybrid poplar normal and tension wood revealed the spatial variation of lignin without requiring staining or chemical pretreatment of the biomass [101]. By integrating the Raman spectra between 1550–1640 cm^{-1}, the lignin distribution of normal poplar wood was determined to be highest in CCs and the CML. Averaged spectra from different cell structures were calculated. As expected, Raman spectra of solely the CCs or CML showed a strong fluorescence background. Analysis of poplar tension wood revealed a relatively lignin-free gelatinous layer, with lignin concentration increasing towards the lumen.

Lastly, stimulated Raman scattering (SRS) microscopy was employed to study maize delignification [104]. In SRS microscopy, two laser beams probe the sample. When the frequency difference between the beams resonates with the sample, vibrational excitation is increased, resultant from this stimulation. A 256 × 256 pixel image could be collected in three seconds compared to two hours using spontaneous Raman scattering. Parenchyma and phloem cells were found to contain relatively little lignin, while vessel, tracheid, and fiber cells contained more lignin. During an acid chlorite delignification treatment, the dominant lignin vibrational mode decreased in intensity by eight-fold, relative to the cellulose signal. Despite containing relative little lignin, the phloem revealed the fastest delignification rate, while the fiber and vessel cells delignified much slower. This study demonstrates the power of real-time, *in situ* analysis of biomass using SRS imaging.

Ultraviolet (UV) and resonance Raman (RR) spectroscopy have routinely been used for lignin analysis since lignin exhibits an UV absorption peak [105–115]. Beech and pine lignin radicals, key intermediate species in lignin biosynthesis, were measured using Kerr-gated RR spectroscopy [105,106]. Kerr-gating is used to reject intrinsic lignin fluorescence. Analysis of lignin radicals using UV-visible spectrophotometry revealed an absorption band at 520 nm. Using an excitation wavelength of 500 nm, Raman bands due to lignin radicals were selectively, resonantly, enhanced. In the initial study, lignin radicals produced from a laccase-mediator treatment were explored [105]. A band was measured at 1610 cm^{-1} following treatment with 2,2′-azino-bis(3-ethylbenzthiazoline-6-sulfonic acid) (ABTS)$^{+\bullet}$, and 400 nm excitation. The authors determined that the lignin spectral intensities were dependent on intermolecular charge-transfer interactions with adjacent groups. In a follow-up study, a lignin radical vibrational mode was measured at 1570 cm^{-1} regardless of the feedstock. For wet beech samples, a peak at 1606 cm^{-1} was detected. DFT calculations revealed that these radicals stemmed from S moieties in beech and G groups in spruce.

The photodegradation of hard- and softwoods was explored using an UV laser to irradiate the samples, and UVRR spectroscopy to evaluate the delignification [115]. The degradation of aromatic moieties, with a concurrent increase of *ortho*- and *para*-quinones, was observed using the Raman spectra. All lignin-derived peaks decreased in intensity, while band-broadening, from the creation of unsaturated molecules, was measured at 1602 cm^{-1}, and in the 1000–1500 cm^{-1} region. The 1602 cm^{-1} vibrational mode was monitored to determine the rate at which hard- and softwoods degrade. The rubber-wood and silver birch hardwood samples were found to degrade more rapidly than pine or spruce. UVRR spectroscopy was also used to study how increases in temperature affected Scots pine samples [109]. As the temperature was ramped from 100–240 °C in 20 °C increments, lignin became more soluble in acetone at

Table 4
Mid-infrared spectroscopy vibrational modes characteristic of lignin and lignin model compounds.

Vibrational mode	Assignment
827	S-mode [347]
1035	aromatic CH in-plane deformation [348,349]
1050	aromatic CH in-plane deformation [348,349]
1116	CH stretch in S-ring [139]
1127	aromatic CH in-plane deformation [348,349]
1142	aromatic CH in-plane deformation [348,349]
1151	CH stretch in G-ring [139]
1215	CC, CO stretch [139]
1226	CC, CO, C″O stretches [348,349]
1252	aryl ring breathing mode; CO stretch [348,349]
1270	aryl ring breathing mode; CO stretch; G-mode [348–350]
1330	aryl ring breathing mode; CO stretch; S-mode [139,348,349]
1379	aromatic skeletal vibration; CH in-plane deformation [348,349]
1425	OCH$_3$ CH deformation, asymmetric; S-mode [347–349]
1428	aromatic skeletal vibration; CH in-plane deformation [348,349]
1440	OH in-plane bending [350]
1465	CH deformation, asymmetric [348,349]
1500	S-mode [347]
1506–1513	aryl ring stretch, asymmetric [348,349]
1589	S-mode [347]
1596–1600	aryl ring stretch, symmetric [348,349]
1682	C″O stretch [139]
1704	C″O stretch [139]
1737	C″O stretch [348,349]
2840	CH stretch [139]
2938	CH stretch [348,349]
3430–3440	OH stretch [348,349]

or greater than 180 °C. Un-extractable lignin did not change in structure even when heated to 200 °C. Lastly, the effects of pH on lignin analysis were explored using UVRR spectroscopy [114]. Changes in pH were found to shift Raman bands by 25–35 cm^{-1} in model compounds lacking *para*-substitution, 8–12 cm^{-1} with *para*-substitution, and 2–7 cm^{-1} in pine/spruce mixed pulps. When the phenolic hydroxyl functionalities were increased, the shift was more pronounced. More alkaline pH levels resulted in more intense aromatic vibrational modes. Therefore, the authors suggest appropriate pH adjustments be made prior to Raman analysis.

Coherent anti-Stokes Raman (CARS) microscopy has been used to measure biomass, in part because it does not suffer from fluorescence interference, while still providing strong lignin signal [116,117]. Wild-type and transgenic alfalfa and corn stover were studied using CARS imaging [117]. There was no indication of sample degradation after ten minutes of acquisition time. CARS images were acquired from different sections of the plant cell wall, with the more heavily lignified regions, such as the fiber and xylem cells, revealing the strongest spectral signals. Down-regulated hydroxycinnamoyl CoA: shikimate hydroxycinnamoyl transferase (HCT) or coumaroyl shikimate 3-hydroxylase (C3H) alfalfa lines revealed decreased lignin intensities in CCs compared to the secondary walls. Recently, CARS was employed to gauge the chemical and structural composition of birch, oak, and spruce samples [116]. A strong absorption of excitation light and photodegradation of lignin necessitated the measurement of lignin in an aqueous matrix. CARS spectra of spruce revealed stronger lignin bands, which the authors attribute to the higher lignin content of softwoods.

2.4.2. Mid-infrared spectroscopy

FT-infrared (IR) spectroscopy has been extensively utilized for determining lignin structure [13,44,61,65,75,78,79,81,92,93,109,

110,118–139]. Characteristic IR vibrational modes are listed in Table 4. Nuopponen and co-authors used FTIR coupled with PCA to characterize 25 tropical hardwoods [110]. Analysis of PCA loadings plots revealed key vibrational modes integral to classifying the various feedstocks according to acetyl groups from hardwood xylans, S and G lignin content, tannins or tannin-like structures, and conjugated carbonyl groups. A similar technique was applied to the study of thermal modifications in Scots pine [109]. Analysis of these PCA loadings plots unveiled characteristic vibrational modes of wood resin including methylene, carbonyl, and carboxylic acid functionalities. The spectra could be partitioned according to whether they had been thermally treated at low or high temperatures. FTIR spectra also showed increases in aromatic skeletal vibrations, which the authors attribute to increases in Klason lignin content due to the degradation of hemicellulose into pseudo-lignin. A variety of herbaceous, and hard- and softwood Organosolv lignin preparations were classified using FTIR spectral data and PCA [130]. The three classifications of biomass were lucidly fractionated along PC1 and PC2. Subsequent analysis of the loadings plot identified which vibrational modes distinctly segregated the three types of feedstocks. The predominant variations included G (829, 1140, 1221, 1266, 1270, 1505 cm^{-1}) and S (1325 cm^{-1}) lignin differences, and the presence of secondary alcohols and aliphatic ethers (1086 cm^{-1}) and ester functionalities (1166 cm^{-1}). Thus, it was determined that G lignin concentration is one of the main structural differences between softwood and grass lignin.

The thermal degradation of lignins extracted from wheat straw, oak, birch, and pine was also studied using an FTIR instrument conjoined with a thermogravimetric analyzer and a mass spectrometer [118].This instrumentation enabled the discrimination of the release and formation of acetic acid and furfural from Organosolv birch lignin. Carbon monoxide and dioxide formation were also monitored using FTIR spectra. The decomposition of sugarcane bagasse lignin, following ozonation, revealed significant structural variation in the spectral data when probed with FTIR [75]. The predominant changes were in the 830, 1030, 1240, 1510, 1596, and 1732 cm^{-1} vibrational modes. The band at 1510 cm^{-1}, due to phenyl ring skeletal vibrations, is a known marker for the presence of lignin in pulp. The peak at 1240 cm^{-1} was assigned to the asymmetric stretching vibrations of C–O–C bonds in G lignin. The absence of the two aforementioned vibrational modes, as well as the carbonyl mode at 1732 cm^{-1} following a four hour ozonation period were indicative of delignification. Xu et al. monitored the degradation of bamboo lignin following a treatment with brown- and white-rot enzymes [136]. The calculated ratio of the peak heights resultant from the lignin phenyl ring skeletal vibration at 1511 cm^{-1} or the phenyl ether mode at 1248 cm^{-1} and the carbohydrate peak at 1739 cm^{-1} unveiled the extent of lignin degradation. The white-rot fungi were measured to cause significant decay of lignin, while the calculated ratio of lignin-to-carbohydrate peaks increased following incubation with brown-rot fungi.

Attenuated total reflectance (ATR)–FTIR enabled the analysis of regenerated switchgrass biomass following an IL pretreatment using [Emim]OAc [131]. After the addition of water as an anti-solvent to precipitate out the cellulose, leaving all other biomass components solubilized, the ATR-FTIR spectra exhibited characteristics parallel to Avicel cellulose. Thus, this methodology was able to easily identify the power of the IL treatment to efficiently delignify switchgrass. The efficiency of the IL pretreatment of corn stover and eucalyptus was also probed using the same instrumentation and technique, and unveiled similar results [92,119]. FTIR was employed to study the molecular structure and spatial arrangement of lignin when fabricated into monomolecular Langmuirian films, not only in an effort to understand fundamental structural details, but also evaluate using these films as transducers in sensing devices [129]. FTIR spectroscopy

showed that the aromatic rings were predominantly oriented parallel to the surface of a solid substrate. Further analysis indicated some interaction between lignin films and cadmium ions; therefore, the authors concluded the viability of these lignin films as potential transducers. Lastly, hydrogen bonding in lignin model compounds was probed using FTIR [139]. Aliphatic hydroxyl moieties established more resilient hydrogen bonding juxtaposed to phenolic hydroxyl functionalities. Dimeric model compounds fashioned more robust hydrogen bonds than monomeric species. This evaluation was employed to explain differences in hard- and softwood lignin hydrogen bonding.

2.5. Nuclear magnetic resonance

No single analytical technique has been more comprehensively employed for the cognitive advancement of lignin structure than NMR [13,44,54,59–61,64,67,78–81,91,110,119,121,123,127,128,132–135,137,140–171]. This analytical tool, in all of its varieties, has enabled unparalleled structural features of lignin to be elucidated. While a complete review of this body of work could easily be endeavored, this manuscript will illustrate assorted recent, cutting-edge uses of NMR spectroscopy that resulted in novel lignin structural insights. The research of John Ralph and co-authors has bestowed a significant trove of lignin structural data [141,149, 153,162,168,172]. Lignin, extracted from kiwi fruit, pear, rhubarb, and wheat bran fiber, was characterized using heteronuclear single quantum correlation (HSQC) 2D-NMR [141]. The authors were able to authenticate the lignin in pear, kiwi, and rhubarb, but conclude that wheat bran lignin has been overestimated by the standard analytical techniques, necessitating methods possessing greater accuracy. A variety of molecules were identified from the ^{13}C–^{1}H spectra, including G and S moieties and a benzodioxane structure unique to kiwi. HSQC difference spectra enabled the evaluation of ^{13}C-enriched and unmodified protolignin of Gingko biloba [162]. Protolignin is a heterogeneous polymeric combination of monolignols in the polysaccharide matrix. Enriching the biomass with ^{13}C resulted in higher spectral resolution. Following acetylation of the dissolved protolignins, the spectra of un-enriched G. biloba was subtracted from the ^{13}C-enriched spectra, successfully removing carbohydrate interferents, providing lignin-specific structural data. This technique does not require lignin isolation, and permits the monitoring of specific C-H connections during any potentially lignin-modifying process. Solution-state HSQC 2D-NMR was employed for the structural analysis of poplar lignin [149]. In this study, the authors elegantly combined the structurally detailed NMR spectra with multivariate analysis to avoid having to interpret unresolved spectral peaks. Evaluation of the 2D loadings plots enabled the determination of the most relevant spectral features for classification. This technique provides a novel approach to understanding cell wall structural differences in normal and tension wood, as well as elucidating subtle lignin compositional variations following the down-regulation of pectin methylesterase. In 2012, the methodology enabling the solution-state 2D-NMR analysis of whole plant cell walls was contrasted with a variety of degradative techniques for obtaining structural detail [153]. This manuscript systematically detailed the cell wall isolation and preparation, solubilization, and 2D-NMR analysis, and juxtaposes this novel technique with nitrobenzene oxidation (NBO) and DFRC.

Rencoret and co-authors have also utilized NMR for developing a detailed understanding of agave, coconut coir, and eucalypt lignin [156–159]. The lignin structure of young versus adult E. globulus trees was analyzed using HSQC 2D-NMR [156]. Spirodienone-β-1 structures increased with growth, while phenylcoumaran groups decreased. No change in resinol structures was measured; however significant differences in the lignin monomer composition with increased growth were detected (see

lignin monomer composition section). *E. globulus*, spruce, and agave samples swelled in deuterated dimethylsulfoxide (DMSO-d_6) were analyzed using HSQC 2D-NMR [158]. The spectra of whole plant samples and their respective milled-wood lignins were compared. The major lignin peaks, including S and G content, the main lignin substructures, and the acylation of the side chains were found to closely resemble those measured in the MWL, eliminating the need to extract lignin from plant cell walls. The MWLs of *E. globulus*, *E. nitens*, *E. maidenii*, *E. grandis*, and *E. dunnii* have also been characterized using HSQC 2D-NMR [157].

HSQC 2D-NMR was used to characterize different preparations of corn stover lignin [91]. Variations of the AFEX pretreatment, such as low or high ammonia loading, enabled the formation of different extracted lignins. Measurement of L-AFEX lignin revealed augmentation in syringyl groups. The NMR analysis also showed that abundant *p*-coumarate esters were severed during the pretreatment, leaving 10–15% of these groups in the biomass. The structural assessment of wheat straw lignin, using 2D-NMR, revealed the main lignin substructures as being predominantly β-*O*-4 ethers (75%) and phenylcoumarans (11%) [59]. The analysis of the NMR spectra also showed about 10% γ-acylated lignin, as well as the presence of *p*-coumarates and ferulates. A novel high-throughput technique for the enrichment of ^{13}C in corn stover cell walls coupled with dissolution in perdeuterated pyridinium molten salt and DMSO-d_6 enabled reductions in 1D, 2D, and ^{13}C cross-polarization/magic-angle spinning (CP/MAS) solid-state NMR analysis time by 220, 39, and 10 times, respectively [146]. This technique enabled the lignin from whole plant cell walls to be evaluated without isolating the lignin. Another study unveiled the development of a different bi-solvent dissolution system employing [Emim]OAc and DMSO-d_6, enabling the complete dissolution of *Miscanthus* biomass [143]. This solvent combination was juxtaposed with various solvents including (perdeuterated DMSO)/pyridine-d_5, DMSO-d_6/tetrabutylammonium fluoride, and DMSO-d_6/deuterated pyridinium chloride. The authors note that the 4 main lignin peaks were all discernible when DMSO-d_6/[Emim]OAc was employed as the solvent, while the other solvent systems did not lead to complete detection. Although spectral peaks arising from DMSO-d_6/[Emim]OAc did not overlap with those from the analytes, strong signals were nevertheless detected. The authors synthesized deuterated [Emim]OAc to reduce this interference. ^{13}C and HSQC 2D-NMR have been used to evaluate a novel phosphoric acid/steam pretreatment strategy on various sugarcane bagasse lignin preparations [167]. The structures of ball-milled, ethanol and dioxane-dissolved, and water-soluble lignin were contrasted, whereupon it was determined that ethanol-extracted lignin effectively preserved the basic lignin composition. The structural changes induced by the extraction were lower β-*O*-4 linkages, S/G ratios, and *p*-coumarate/ferulate ratios. The ethanol extraction also removed approximately 8% of the total mass. Lastly, the ability of a novel vanadium catalyst to facilitate lignin depolymerization was monitored using 2D-NMR [171]. NMR spectra revealed that β-*O*-4 linkages in both lignin model dimers and in *Miscanthus* lignin were efficiently deconstructed.

Another technique commonly employed to study solid biomass is ^{13}C CP/MAS solid-state NMR [152,170]. The analysis of corn stover following a dilute H_2SO_4 pretreatment revealed an association between ^{13}C-enriched sugars and lignin [152]. After the pretreatment, these sugars, as well as other small molecule extractives, polymerized, adding to the collected residue. This additional polymeric material resulted in a higher mass balance closure for Klason lignin than what was present in the cell wall. The down-regulation of *p*-coumarate 3-hydroxylase (C3H) or HCT led to two transgenic alfalfa lines lower in lignin compared to the native plant [170]. ^{13}C CP/MAS NMR analysis of the transgenic alfalfa, relative to the unmodified control, revealed a decrease in

the aromatic region of the spectrum, typically assigned to lignin. The modified alfalfa plants also showed a significant increase in H lignin with concomitant decreases in S and G lignin. The extractability of the wild-type and transgenic lignins were gauged by measuring the NMR spectra following treatment with 0.1 and 2.0 M NaOH. Analysis of the spectral data showed increased extractability of the modified lignins, in part due to the decrease in molecular weight with the loss of the methoxy groups in transforming from S or G to H lignin.

Lignin from *Acacia mangium* was isolated and characterized using ^{1}H and ^{13}C NMR [155]. Proton NMR allowed the analysis of CH_2 and CH_3 groups, aliphatic and phenolic hydroxyl functionalities, β-β and β-*O*-4 substructures. ^{13}C NMR was used to evaluate methoxyl, aromatic-O, C, or H structures, CHO groups in benzaldehydes and cinnamaldehydes, ketones, and β-*O*-4 substructures. In sum, these methods revealed a low syringyl content, high percentage of condensation, and a low quantity of β-*O*-4 substructures.

^{31}P NMR is often used for the quantitation of specific functionalities in lignin, such as hydroxyl groups. Three commercially obtained pine kraft lignins were partitioned into smaller fractions using an incremental addition of hexanes into acetone [169]. Aliphatic, non-condensed and condensed phenolic, total phenolic, and carboxylic acid hydroxyl moieties were quantified in the different lignin fractions. The measurement of these lignin preparations revealed a reduction in the aliphatic hydroxyl content, and an increase in the total phenolic hydroxyl groups relative to the acetone-insoluble kraft lignin. This finding has precedent in the literature when probing the chemistry of the kraft process, which is known to form new phenolic hydroxyl groups while removing aliphatic hydroxyl functionalities as the lignin fragments into smaller species. Quantitative ^{13}C NMR spectroscopy was used to measure the MWL of *E. globulus*, *E. nitens*, *E. urograndis*, birch, red alder, *Acacia*, and cottonwood hardwoods [161]. The authors compared acetylated and non-acetylated lignins. A linear correlation was measured when the C_9-normalized methoxy contents, obtained via wet chemical techniques, were plotted against the S/G ratios, β-*O*-4 per 100 aromatics, and methoxy per 100 aromatics, measured using NMR. Ball-milled switchgrass lignin was evaluated before and after a dilute H_2SO_4 pretreatment using ^{1}H, ^{13}C, 2D-NMR, and ^{31}P NMR [160]. Quantitative ^{13}C NMR elucidated considerable differences when untreated and pretreated switchgrass were compared. The ball-milled lignin was not free of carbohydrates, and the S lignin content decreased following pretreatment as did β-β, β-5, and β-*O*-4 substructures. 2D-NMR detected cinnamates derived from coumarates and ferulates while ^{31}P NMR was used to quantify aliphatic, condensed phenolic, G phenolic, *p*-hydroxyphenyl, and carboxylic hydroxyl functionalities. Pretreated switchgrass showed an increase in all hydroxyl groups except aliphatic hydroxyls. Quantitative ^{13}C NMR was used to characterize the chemical structure of kraft and nitrosated lignins extracted from softwood black liquor [151]. Carbon containing functionalities such as aldehyde, carbonyl, carboxyl, and methoxy groups were quantified for each of the lignin preparations. The lignin was determined to be derived from softwood biomass only, as only G lignin subunits were measured. Methoxy and carbonyl groups decreased, while the number of carboxyl groups increased, when the evaluation of mechanical grinding lignins were juxtaposed to kraft lignin. Nitration, using sodium nitrate, resulted in the loss of methoxyl groups and the formation of carboxyl units. Nitrosation was found to demethylate approximately 15% of G lignin rings and eliminate the side chains, forming a higher proportion of carbonyl and carboxyl groups. Butanol was found to preferentially extract low molecular-weight groups of the nitrosated lignin. Lastly, proton NMR was employed to study Organosolv lignins isolated from prairie cordgrass, switchgrass, and corn stover [144].

2.6. Electronic spectroscopy

UV spectrophotometry provides another analytical tool for lignin structural analysis, as lignin absorbs light in this region of the electromagnetic spectrum [44,128,129,133,173–175].Phenolic hydroxyl groups were quantified using differential UV spectrophotometry by evaluating technical lignins using wavelengths at 300 and 360 nm [44]. The change in molar absorptivity ($\Delta\varepsilon$) of the unknowns was compared with that of model compounds. Carbonyl structures, including aldehydes and ketones, were also quantified using differential UV spectrophotometry. UV microspectrophotometry was used to topochemically measure sugarcane lignin in a variety of cell wall structures [175]. Spectra of untreated sugarcane revealed an absorption maximum at 278 nm, indicative of G lignin units, and another, more pronounced band at 315 nm, due to hydroxycinnamic acids connected to lignin. The strongest signal stemmed from analysis of the vessel secondary wall from rind and pith. The secondary wall of parenchyma cells showed the lowest absorption. Pretreatment of the rind and pith, with an acetic acid/sodium chlorite aqueous solution, resulted in 12% delignification in the rind after four hours of incubation, and 5% lignin removal in the pith following the two hour incubation. UV spectra of the secondary cell wall showed lignin remained in the CCs and CML following the four hour pretreatment. The band at 315 nm decreased first, indicative of the removal of hydroxycinnamic acids in the beginning stages of delignification. Lignin detection in the cell walls of brown-rotted Scots pine was evaluated using scanning UV microspectrophotometry [173]. Sapwood samples were incubated for 6, 8, 10, 30 and 50 days with the fungus *Coniophora puteana*. As the polysaccharides degraded, the absorption at 280 nm increased with time for both early and latewood. Lignin absorbance values were higher when the CCs were measured, relative to the secondary wall. 2D and 3D UV images were constructed by scanning the sample at 280 nm with a spatial resolution of 0.25 μm × 0.25 μm. CCs and the CML were found to contain the greatest lignin content. This technique enabled the *in situ* monitoring of the fungal degradation of polysaccharides, and concomitant lignin absorbance.

Fluorescence spectroscopy provides another electronic spectroscopic tool for lignin structural analysis [102,103,120,131,176,177]. Fluorescence lifetime imaging (FLIM) enabled the analysis of normal and compression pine wood [177]. Fluorescence lifetime refers to the amount of time that elapses between excitation of the fluorophore, and when the relaxation results in photon emission. The differences in the FLIM measurements between normal and compression wood coincided with the identified alterations in lignin composition and distribution in tracheid cell walls. Many lignin intrinsic fluorophores were measured to have differing lifetimes. Comparisons in the total fluorescence lifetimes revealed a short-lifetime fluorophore, identified in the outer secondary walls of the tracheids of compression wood, while no such molecule was measured in normal wood. This technique proved superior to routine fluorescence intensity spectroscopy for elucidating key cell wall differences, such as between the secondary wall and middle lamella. Coletta and co-authors also used FLIM to elegantly map lignin distribution in sugarcane bagasse [176]. Acidic and alkaline pretreatment effects on lignin were studied using fluorescence decay. A direct relationship between the rate of decay and the amount of lignin was identified: the lower the lignin contents, the slower the decay measured. Shifts in the decay time distributions resulted from increased NaOH pretreatment, meaning the shift was interrelated with the delignification extent. Broadening of the decay peaks was indicative of lignin structural rearrangements to more disordered conformations. Domains within the plant cell with differing lignin concentrations were measured. The low-lignin regions of the cell wall were efficiently delignified with NaOH, whereas the high-lignin

portions could only be delignified using the highest alkalinity used. Using this methodology, the authors concluded that lignin is preferentially removed from inside the cell wall first, while the other lignin portion aggregates on the cell wall exterior, following the alkaline treatment. Using FLIM, the untreated sugarcane bagasse was found to have weak lignin–lignin interactions. Acid treatment resulted in the accretion of the non-solubilized lignin fraction. Fluorescence microscopy has been utilized to probe compositional and structural variations in Siberian dogwood [103] and lignin distribution in the compression wood tracheids of Yunnan pine [102].

2.7. Atomic force and electron microscopy

Atomic force (AFM) and electron microscopy have enabled researchers to visually characterize the ultrastructure and molecular configuration of lignin in plant cell walls, evaluate morphological changes during lignin pretreatments, and survey lignin surface characteristics such as morphology and roughness [71,75, 103,178,179]. Gidh et al. developed a novel technique for using AFM to visualize the molecular conformation of lignin isolated from black liquor [178]. The measured molecular size was in agreement with results obtained via a light scattering method. The surface morphology of an Indulin AT film, a commercial softwood Kraft lignin, was explored using AFM [179]. The AFM images revealed a smooth surface, although a rougher surface was measured when juxtaposed to glucomannan films. Scanning electron microscopy (SEM) was used to gauge sugarcane bagasse lignin deconstruction during ozonation [75]. The untreated biomass revealed homogeneity in the parenchyma. Following four hours of ozonation, surface morphological changes could be seen. Epidermal changes in surface roughness were also captured, indicative that the ozonation treatment was oxidizing the bagasse surface. Field-emission SEM was employed to gauge the efficiency of pretreating milled birch and pine wood using hydrothermal, hydrotropic, and IL pretreatment strategies [71]. No significant structural changes were witnessed following a 30 or 120 min hydrothermal treatment. Higher magnification revealed formation of spherical droplets of pseudo-lignin. The images captured after IL incubation displayed a more swollen structure, with higher surface degradation when compared to the hot water extraction. The authors note that the IL pretreatment was more effective on pine compared to birch. Neither swelling nor surface degradative changes were witnessed following the sodium xylenesulphonate, hydrotropic treatment. Transmission electron microscopy (TEM) was used to characterize the ultrastructure of *Cornus alba* L. (dogwood) cell walls [103]. The CML exhibited lignin heterogeneity, revealing a blotchy, electron dense region. The variations in electron density were found to be representative of lignin deposition, which was directly proportional to concentration. The interfiber pit membranes, followed by the fiber and parenchyma, were measured to have the highest lignin concentration, while the lowest concentration was measured in the pit membrane between the fiber and vessel.

2.8. Miscellaneous analytical methods

A variety of other methods have been explored and developed to pursue a more vigorous comprehension of lignin structure. The techniques include differential scanning calorimetry for the determination of the glass transition temperature of industrial lignins [60], ellipsometry for the measurement of lignin dielectric properties [179], optical absorption spectroscopy to assess the ozonation treatment of sugarcane bagasse [75], potentiometry for quantitation of carboxylic and phenolic hydroxyl functionalities [44], and the use of DFT calculations to probe lignin valence band structure

Table 5
Quantitation of lignin–lignin and lignin–carbohydrate linkages in various lignin fractions.

Plant	Benzyl ether	β-O-4	Resinol (β-β)	Phenyl-coumaran (β-5)	γ-esters	Phenyl glycoside	Spiro-dienone	Reference
Agave Fiber		100[a]	0[a]	0[a]			0[a]	[158]
Agave MWL		85[a]	4[a]	2[a]			7[a]	[158]
Birch CEL	2.5[b]	48.1[b]	9.4[b]	3.0[b]	3.5[b]	0.8[b]		[193]
Birch MWL	1.4[b]	38.4[b]	9.4[b]	2.2[b]	5.3[b]	3.5[b]		[193]
Coconut Coir		82[a]	4[a]	13[a]				[159]
E. dunnii		65.9[a]	19.0[a]	4.0[a]			4.2[a]	[157]
E. globulus		69.3[a]	18.2[a]	2.9[a]			2.8[a]	[157]
E. grandis		66.9[a]	16.5[a]	6.8[a]			2.9[a]	[157]
E. maidenii		69.7[a]	16.4[a]	3.6[a]			3.6[a]	[157]
E. nitens		71.7[a]	16.1[a]	4.0[a]			1.3[a]	[157]
Eucalyptus wood		80[a]	14[a]	2[a]			2[a]	[158]
Eucalyptus MWL		76[a]	17[a]	2[a]			2[a]	[158]
Miscanthus **Formsolv lignin**		63[a]	0[a]	37[a]				[135]
Miscanthus **acetosolv lignin**		73[a]	4[a]	23[a]				[135]
Miscanthus **MWL**		93[a]	4[a]	3[a]				[135]
Pine CEL	5.8[b]	35.1[b]	4.8[b]	10.7[b]	2.2[b]	0.6[b]		[193]
Pine MWL	3.9[b]	27.5[b]	4.4[b]	9.8[b]	1.8[b]	2.0[b]		[193]
Poplar MAL	5.8[b]	43.3[b]	4.0[b]	12.7[b]	1.3[b]	4.5[b]	0[b]	[192]
Poplar MWL	2.1[b]	41.5[b]	3.7[b]	14.6[b]	3.4[b]	4.1[b]	0.7[b]	[192]
Spruce glucan-lignin		72[a]	1[a]	11[a]			0[a]	[190]
Spruce glucomannan- lignin	3.8	62[a]	6[a]	14[a]		4.4	1[a]	[190]
Spruce MWL		56[a]	9[a]	17[a]			1[a]	[190]
Spruce MWL		65[a]	11[a]	18[a]			0[a]	[158]
Spruce wood		69[a]	10[a]	18[a]			0[a]	[158]
Spruce xylan-lignin	6.1	53[a]	11[a]	13[a]			1[a]	[190]
Sugarcane EL		17.7[b]	0[b]	4.8[b]			0[b]	[167]
Sugarcane MBL		31.7[b]	1.7[b]	3.3[b]			1.4[b]	[167]
Wheat Straw CEL	n.d.	77.1[a]	1.9[a]	13.3[a]		n.d.	n.d.	[166]
Wheat Straw ML	1.8[a]	79.3[a]	3.5[a]	14.4[a]		n.d.	1.1[a]	[166]
Wheat Straw ML		24.2[a]	2.7[a]	1.67[a]				[137]
Wheat Straw MWL		75[a]	4[a]	11[a]			3[a]	[59]
Wheat Straw Soda AQ Lignin		0.36[a]	0.15[a]	0.03[a]				[137]

[a] Percent of the total side chains.
[b] Amounts of linkages per 100 aromatics.

[180] as well as develop theoretical Raman spectra vibrational mode assignments for model lignin compounds [88]. Lastly, although NIR spectroscopy has not conventionally been employed to gauge lignin structure, Mitsui et al. used the vibrational mode at 6913 cm^{-1} to probe the degradation of phenolic hydroxyl groups during a steam treatment of Sitka spruce [181].

3. Lignin-carbohydrate and lignin-lignin linkages

One of the hottest topics in contemporary lignin research is the evaluation of lignin linkages, both to carbohydrates and to other lignin molecules. Understanding how these cell wall components are interlaced can provide paramount insights into forming strategies to efficiently decompose plants for biofuel and bio-based chemical applications. A distinguished overview has explored the mechanisms responsible for the incorporation of hydroxycinnamates in the lignification of biomass [172]. For example, it has become apparent that ferulate, dehydrodiferulates, and other oligomers of ferulate, actively participate in cross-linking reactions between carbohydrates and lignin. This cross-linking reduces the ease with which lignocellulosic biomass deconstructs, thus requiring more stringent pretreatment strategies. Table 5 summarizes the quantitation of lignin–lignin and lignin–carbohydrate linkages in various lignin fractions.

3.1. Wet chemistry and chromatography

Thioacidolysis coupled with size-exclusion chromatography (SEC) enabled analysis of lignin–carbohydrate complexes (LCCs) in spruce [182]. Arylglycerol-β-aryl ether linkages were cleaved using the thioacidolysis protocol, resulting in monomeric and oligomeric species that were gauged using SEC. Monomers and dimers comprised the

majority of the thioacidolysis-fragments, and relatively few condensed structures. Thioacidolysis-GC of glucan-lignin (GL), glucomannan-lignin (GML), and xylan-lignin (XL), from pulps that were incubated with laccase-mediator systems, revealed that only XL contained uncondensed monomeric groups [183]. Pulps treated with laccase-1-hydroxybenzotriazole exhibited stronger delignification. SEC showed that the laccase-mediator systems effectively deconstructed lignin to smaller fragments.

SEC, following acetobromination, enabled the molecular mass distribution of novel preparations of LCCs that varied in the severity of pH [184]. Increased alkalinity resulted in lower molecular masses, due to the breaking of specific linkages. Despite this trend, further escalations in alkalinity did not result in the production of free lignin. Xylanase, mannase, and pectinase were applied to the four LCC fractions. Pectinase affected the molecular weight of one of the preparations, resulting in a shift to a higher mass. The author proposed that pectin forms a globular network interlaced with lignin. The pectinase treatment, in turn, increased the hydrodynamic volume of the LCC. Analysis of another fraction revealed that mannase and xylanase treatment resulted in a shift to lower molecular weight, indicative of GML and XL complexes. SEC analysis of thioacidolysis products was used as a gauge of molecular weight differences before and after delignification [185]. Two dominant fractions could be discerned from the chromatograms: a glucomannan-lignin-xylan and a xylan-lignin-glucomannan complex. The latter complex possessed a linear arrangement of β-O-4 linkages, while the glucomannan-lignin-xylan fraction resembled configurations observed in wood. The effects of ball-milling on the LCCs of *E. globulus* were characterized using thioacidolysis, SEC, GC, and NMR [186]. The thioacidolysis-SEC data showed that 12 h of ball-milling had no effect on the separation whereas 24 h rigorously altered lignin structure, creating non-hydrolyzable lignin linkages. Monomeric

thioacidolysis products were not affected by 12 h of milling time giving credence to the nomination of this duration as optimal. In the quest for a universal dissolution technique for pulps and wood, a variety of solvent systems were evaluated. DMSO plus tetrabutylammonium hydroxide was found to provide complete dissolution of biomass. Two LCC fractions were determined using SEC, commensurate with the theory that two types of lignin occur in wood: lignin linked to glucomannan or xylan and cellulose.

Hydroxycinnamic acids, involved in ester and ether linkages between carbohydrates and lignin, were isolated from barley, maize, oil palm, rice, rye, and wheat feedstocks, and quantified using HPLC [187]. Extraction with hot 4 M NaOH cleaves ester and ether bonds, but an additional, milder alkaline extraction was required to more efficiently isolate hydroxycinnamic acids. With the exception of maize, the plants were found to have higher ferulic than *p*-coumaric acid yields. Ferulic acid (FA) mainly formed ester and ether complexes with hemicellulose and/or lignin, while *p*-coumaric acid was predominantly involved in ester-linkages with lignin. A similar analysis of cell wall ester and ether-linked phenolics using HPLC was performed on various *Miscanthus* feedstocks [188]. An analytical method employing GC for cell wall phenolic analysis enabled investigations of how FA was bound to the cell walls of dicotyledonous biomass such as buckwheat, flax, and soybean [189]. After oxidizing the cell walls with a copper sulfate-NaOH solution, the GC analysis revealed that 60–80% of the FA was bound to cell-wall constituents via ether linkages. This study concluded that hydroxycinnamic acids can compose 0.01–0.19% of the dry weight of dicot cell walls.

3.2. Thermochemical methods

pyGCMS has aided researchers in assessing LCCs and lignin–lignin linkages [182,183,190]. pyGCMS supplemented the NMR analysis of GL, GML, and XL LCCs [182]. Since the signals from the LCCs were quite low in the NMR spectra, lignin-polysaccharide bonding was not entirely apparent. When pyrolyzed, GML cleaved into glucomannan and lignin. The majority of phenolic monomers had their side-chains detached completely, or at least shortened. The most abundant fragments produced by pyrolysis were vanillin (15.7%), 4-methylguaiacol (18.2%) and 4-vinylguaiacol (22.5%) for GL, GML, and XL respectively. Analysis of GL, GML, and XL before and after enzymatic hydrolysis unveiled noteworthy differences in 19 detectable compounds using pyGCMS. Coniferyl alcohol content, originally quite low in the LCCs, increased significantly following the enzymatic treatment, resulting in levels typically quantified in MWL. The authors note that this clearly exposes the effects carbohydrates have on the pyrolysis of lignin, since the presence of lignin–carbohydrate linkages may prevent decomposition reactions resulting in little to no coniferyl alcohol.

Another thermochemical method used for lignin linkage analysis is pyrolysis in the presence of tetramethylammonium hydroxide (pyTMAH), as a transesterification and methylation agent [59,65]. Importantly, this method circumvents the problems associated with measuring *p*-hydroxycinnamic acids that form cross-links between lignin and carbohydrates. When pyrolyzed, these molecules can result in products similar to that of lignin. The utilization of TMAH results in the measurement of methylated, intact *p*-hydroxycinnamic acids. This method breaks β-*O*-4 ether linkages in lignin, resulting in methylated aldehydes, ketones, and acids, as well as transesterification of *p*-hydroxycinnamic esters. pyTMAH data revealed that ferulates are predominantly linked with carbohydrates while *p*-coumarate is mostly connected with lignin in wheat straw [59]. Abaca and sisal lignins were found to contain high levels of *p*-coumaric and FAs. The ratio of coumaric/ferulic acid was lower in isolated lignins (with broken ester bonds) that in the whole plant (with intact ester bonds), indicative that

coumaric acid was involved in ester-linkages to lignin and carbohydrates, whereas FA is involved in ether bonds with lignin.

LCCs isolated from three unbleached kraft pulps of spruce and beech wood were characterized by GC and GCMS following oxidation with 2,3-dichloro-5,6-dicyanobenzoquinone, and methylation [191]. Benzyl ethers were found to provide the linkage between carbohydrates and lignin, with galactose and mannose (in spruce), and galactose and xylose (in beech) primarily furnishing this bridge. The principal bonding position in hexoses was the C_6, while the C_2 and C_3 in xylose also were paramount in forming LCCs. The authors established that cellulose could be linked to lignin in residual lignin preparations, perhaps providing the source of carbohydrates often measured in isolated lignins.

Other analytical methods used for assessing lignin–lignin and lignin–carbohydrates linkages include: the evaluation of extracted herbaceous lignins using MALDI-ToF [73], the detection of erythro and threo forms of the β-*O*-4 linkages of hardwood lignins using ozonation [161], and the use of permanganate oxidation to evaluate the inter-unit linkages of three industrial lignin fractions [60].

3.3. Nuclear magnetic resonance

A quick survey of the literature will delineate NMR as the most commonly employed analytical tool for probing lignin–carbohydrate complexes (LCCs) and lignin–lignin linkages [54,59,61,132,135,137,157–161,165–167,172,182–184,186,190,192–195]. Du and co-authors have recently employed various NMR methodologies to elucidate how lignin is linked to other cell wall constituents [182,183,190]. An ubiquitous approach to LCC isolation and the subsequent analysis of lignin in the complex was proposed using spruce wood to demonstrate the validity of the established technique [182]. The authors improved upon a previously developed hardwood and non-wood fractionation technique by adding an additional preparatory step incorporating barium hydroxide precipitation to sequester the GML complex, extending the method to softwoods. GL, GML, and XL complexes were found to contain high levels of lignin (19.3–42.7%), owing to the success of the fractionation procedure. Using a 400 MHz HSQC 2D-NMR instrument, no lignin signals were detected for either the GL or GML complexes, but were evident in the XL fraction. Solid-state CP/MAS NMR was used to evaluate GML since solubilizing this high molecular-mass complex proved problematic. Aromatic moieties were clearly discernible in GML, but spectral resolution prevented elucidation of further structural features. Use of a cryo-platform and probe enabled higher resolution 2D-NMR of GML. Analysis of these complexes with traditional NMR was not possible due to the bondage of lignin to carbohydrates, thereby creating the high molecular-mass assemblage. GL, GML, and XL complexes were treated with xylanase or endoglucanase/β-glucosidase and evaluated with 2D-NMR [190]. Removal of the polysaccharides allowed the enhancement of the NMR analysis of the lignin fraction of the LCC as lignin comprised 92.6–98.8% of the remaining complex. Although phenyl glycoside, uronic γ-ester, and benzyl ether lignin–carbohydrate linkages have been reported to be detectable using 2D-NMR, these bonds were not discernible until the polysaccharides had been enzymatically deconstructed. Linkages, attributed to phenyl glycosides, were evident in GML following enzymatic treatment. While these linkages had been envisaged, but not directly measured in spruce, this work quantified three separate types of this complex in GML, which the authors attribute to different sugar moieties linked to the phenolic hydroxyls of lignin. Due to signal overlap with spirodienones, only one benzyl ether structure, hypothesized to represent the lignin C_α conjoined to primary hydroxyl of a sugar unit, was identifiable in spruce LCCs. Galactose side-chains were postulated to play a major role in the complexation of lignin to carbohydrates, due to the increased quantity of this sugar compared to glucose, mannose, and xylose. Inter-lignin linkages were also elucidated following the

enzymatic removal of polysaccharides. In all, five lignin–lignin linkages were detected in GML and XL, namely, β-O-4′, phenylcoumaran, dibenzodioxocin, pinoresinol, and spirodienone groups. The low solubility and resultant limited spectral resolution in the GL analysis only allowed the detection of β-O-4′ and phenylcoumaran linkages, and lignin methoxyl moieties. Following acetylation of this sample, the solubility increased, resulting in the identical linkage detection as the GML and XL. The relative percentage of the diverse lignin substructures was calculated by peak integration. The most abundant structures in spruce were β-O-4′ ethers (53–72%) and phenylcoumaran (11–17%). GL lignin emerged as the most atypical, possessing 72% β-O-4′ ethers, very low pinoresinols, and no spirodienones.

LCCs, from laccase-mediator treated eucalyptus kraft pulp, were partitioned into GL and XL fractions and analyzed with ^{1}H–NMR [183]. GL complexes represented 80% of the isolated fractions, containing between 0.4% and 2.4% lignin, while XL fractions (20% yield) had higher quantities of lignin (2.7–7.3%). The GL complex was acetylated to promote solubility. No lignin was detected in the aromatic proton region of the NMR spectrum due to the low lignin contents of these fractions. XL fractions were dissolved in DMSO-d_6, and following signal amplification in the aromatic region of the spectra, a broad peak could be perceived, confirming that the lignin was entangled with xylan.

Analytical ^{31}P NMR was used to assess different novel preparations of LCCs, classified by their severity of pH, and dissolved in an IL [184]. The lowest guaiacyl phenolic contents were found in pectin–lignin (PL) and XL complexes. Condensation in the phenolic units was highest, however in the PL fraction. Xylan-rich LCCs contained the lowest levels of condensation of phenolics and ethers.
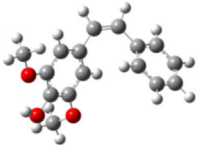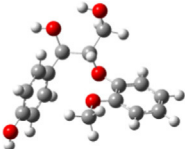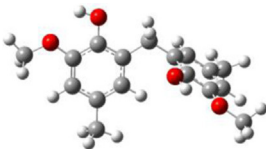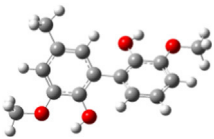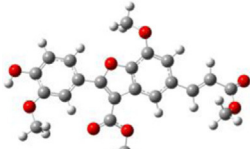
Solution-state 2D-NMR was used to demonstrate the cleavage of lignin and xylan in wheat straw following a hydrothermal pretreatment and enzymatic saccharification [165]. Using ^{13}C–^{1}H NMR spectra, it was ascertained that β-aryl ether linkages decreased by 60% while acetyl linkages diminished by 81%. Aromatic functionalities in lignin remained unaltered from the pretreatment strategy. This study established that the hydrothermal pretreatment ruptured the linkages between hemicellulose and lignin, leaving lignin and cellulose inside the plant cell wall.

HSQC 2D-NMR has also been utilized in the analysis of lignin linkages in the MWLs of various eucalypts [157]. The dominant linkages were measured to be β-O-4 ether (66–72%) followed by β-β-resinol-type (16–19%), and β-5′-phenylcoumaran linkages. The HSQC spectra enabled the β-β structures to be classified as predominantly syringaresinol moie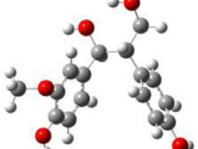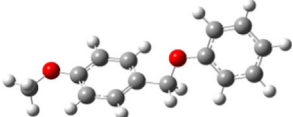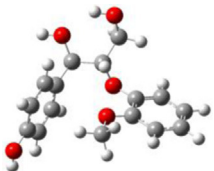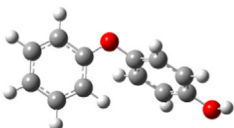ties. This instrumentation was also applied to the analysis of lignin linkages in coconut coir [159]. These linkages were measured to follow the trend: β-O-4 ether > phenylcoumaran > resinol > dibenzodioxocin. Linkages in ball-milled eucalypt, spruce, and agave were assessed in a deuterated DMSO gel using HSQC 2D-NMR [158]. β-O-4 ethers were the most copious linkages, comprising 76, 65, and 85% of eucalyptus, spruce, and agave MWL, respectively. β-β-resinols (17%) were the second-most prevalent linkage for eucalyptus, while β-5′-phenylcoumarans (18%) and β-1′ spirodienones (7%) were the next most abundant linkages for spruce and agave, respectively. HSQC 2D-NMR has also been used to characterize the lignin linkages in wheat straw [59].

HSQC, heteronuclear multiple bond coherence (HMBC), and quantitative ^{13}C NMR were employed in the analysis of LCCs isolated from loblolly pine [194].The fractions contained nearly equivalent carbohydrates and lignin, and were much higher in their arabinose and galactose contents. HSQC spectra revealed the presence phenyl glycoside bonds. Multiple signals indicated that different carbohydrates were attached to lignin. Benzyl ether and γ-ester lignin–carbohydrate bonds could also be detected. LCC linkages were quantified in MWL and CEL preparations from loblolly pine and white birch woods using ^{13}C NMR and HSQC 2D-NMR [193]. A

previous study revealed that extracting MWL with acetic acid resulted in LCC-rich preparations. Phenyl glycoside, benzyl ether, and γ-ester linkages were detected in both the acid-extracted MWL-LCC and the CEL-LCC. NMR signals between 103–96 (phenyl glycoside), 90–78 (benzyl ether), and 65–58 (γ-ester) ppm from the corresponding ^{13}C NMR spectra were used as internal reference standards such that the relative amounts of the various linkages could be quantified using HSQC 2D-NMR. These values were then associated with the signal from the aromatic carbons between 163 and 103 ppm, enabling the calculation of specific linkages per 100 aromatic groups. This work presents the first direct method for quantifying these linkages in LCC fractions. The pine CEL-LCC was found to contain higher quantities of benzyl ethers, β-O-4, β-β, and β-5′ linkages, compared to the acetic acid-extracted MWL-LCC. Phenyl glycosides were found to be much lower in the CEL fraction (0.7/100 aromatic groups) compared to MWL-LCC (7.2/100 aromatic groups). A similar trend was measured with white birch, except β-β content was lower in the CEL-LCC. These results indicate that the CEL method of preparation leaves the lignin less degraded. Using a 950 MHz NMR spectrometer equipped with a CryoProbe™, the spectral signals from γ-esters were resolved to γ-acetyl and γ-uronosil groups. In sum, the authors found that CEL preparations are best suited for studying benzyl ether linkages, but that birch MWL and pine LCC acetic acid fractions provide better analytes for detection of phenyl glycosides and γ-ester linkages. A similar study of LCCs has been performed using MWL and mild acidolysis lignin (MAL) from poplar [192]. Using a combination of ^{13}C NMR and HSQC 2D-NMR, the authors determined that 4-O-methylgluconoxylan is the main carbohydrate coupled to lignin. The main linkages quantified in either LCC preparation were β-O-4′ aryl ethers representing 60.9 and 70.4% of MWL and MAL side chains, respectively. The other dominant linkages in both preparations were resinol and phenylcoumaran structures. The XL fraction of E. globulus LCCs was then partitioned into soluble and insoluble preparations [195]. The insoluble fraction was further extracted into a soluble and insoluble portion using DMSO. This soluble preparation was predominantly xylan with some syringyl lignin, potentially enriched in phenyl glycoside linkages, while the insoluble portion was predominantly lignin with little xylan, and was quite similar structurally to MWL with α-ether-type LCC linkages. Milled-straw lignin (MSL) and CEL from wheat straw were contrasted using quantitative ^{13}C NMR and HSQC 2D-NMR [166]. CEL contained much higher quantities of polysaccharides as well as ferulate. Thus, the authors concluded that the isolation of CEL is paramount to effectively evaluating ferulate content. As a whole, the hydroxycinnamates comprised a higher proportion of the CEL compared to MSL. The analysis of inter-lignin linkages revealed that 77.1 and 79.3% of the bonds were β-O-4 for CEL and MSL, respectively. No LCC linkages were determined for the CEL preparation, and only benzyl esters and ethers were detected for the MSL fraction. The authors hypothesized that these results give credence to LCCs in wheat straw being primarily comprised of ferulate linkages. This technique was recently extended to a variety of sugarcane bagasse lignin preparations to gauge the effectiveness of a phosphoric acid/steam pretreatment protocol [167]. Ball-milled bagasse, ethanol-dissolved, water-soluble, and dioxane-dissolved lignin samples were evaluated for hydroxycinnamates. The water-soluble lignin fraction contained nearly four times as much ferulate compared to the other preparations, indicative that sugarcane bagasse LCCs were linked via ferulate molecules. The p-coumarate content was highest in the ball-milled and dioxane-dissolved lignins, and lowest in the water-soluble sample. No β-O-4 linkages were detected in the water-soluble fraction, signifying a monomeric and not a polymeric lignin, as was later confirmed using gel permeation chromatography (GPC). Overall, the phosphoric acid/steam pretreatment cleaved the β-O-4 linkages in lignin, resulting in elevated syringyl content. ^{13}C NMR and HSQC 2D-NMR have been

Table 6
Bond distances and dissociation energies for the ether and the C–C linkages of lignin model compounds with a representative optimized structure.

		Bond distance (A')	Bond energy (kcal/mol)
	C–C linkages [217]		
$\beta = 1$		1.34	163.5
β-O-4		1.52	76.84
α-1		1.51	91.1
5-5		1.48	116.8
ß-5		1.46	126.4
ß-1		1.54	67.68
	C–O linkages [217]		
α-O-4		1.43	52.41
β-O-4		1.43	63.79
4-O-5		1.38	80.08

employed in the analysis of lignin and LCC linkages in wheat straw following a ^{13}C isotopic labeling of xylose [137]. The lignin-[13]xylose complexes were extracted and ball-milled prior to soda-anthraquinone (AQ) pulping. ^{13}C NMR analysis suggested that the C_2 position in xylose is connected to lignin via γ-ester linkages, and that the C_5 position of xylan is possibly coupled to lignin via benzyl ether bonds. The predominant lignin inter-unit linkages were β-O-4, β-β′, β-5′, and β-1; however, all were found to be significantly lessened following the pulping process. Carbohydrate association in *Miscanthus x giganteus* with different lignin preparation was gauged using HSQC 2D-NMR [196]. The predominant polysaccharides in ethanol Organosolv lignin were α-and β-arabinofuranose, which were conjoined to lignin via *p*-coumarate linkages.

Other studies employing NMR techniques applied to lignin–lignin and lignin–carbohydrate linkages include an assessment of inter-unit and LCC linkages of MWL and lignin preparations produced by fractionation with either acetic or formic acid, extracted from *Miscanthus x giganteus* [135], the evaluation of ball-milled switch-grass lignin linkages, before and after a dilute H_2SO_4 pretreatment using a combination of ^{13}C, HSQC, and ^{31}P NMR methods [160], and the assessment of inter-unit linkages in MWLs from beech, pine, and spruce using ^{13}C NMR and HSQC 2D-NMR [61].

3.4. Computational aspects of lignin linkages

Quantification of structural features and chemical properties of lignin is crucial for understanding the recalcitrance of biomass. Besides experimental techniques, computational chemistry tools such as quantum chemistry calculations and molecular dynamics (MD) simulations are useful for characterizing the structural and energetic properties of the model lignin compounds and macro-models of lignin. Theoretical approaches provide accurate struc-tures, energies, and molecular electronic properties and have been described as "Molecular Orbital Spectrometers" [197]. As noted in Section 2.8, theoretical methods were utilized for lignin analysis and aided in validation of vibrational spectra and conformations. Boltzmann-averaged, multi-standard NMR calculations were used for evaluating the ^{13}C gauge including atomic orbital (GIAO) and ^{1}H chemical shifts with experimental data for the four stereoi-somers of the β-O-4 dimer, as well as the 5-5, β-5, and β-β dimers of coniferyl alcohol [198]. The ^{13}C results show an excellent correlation with experiment ($R^2 > 0.99$). DFT based methods offered the possibility of qualifying the assignment of Raman bands of lignin and lignin models (below 1600 cm^{-1}), thereby helping to avoid inaccurate spectral band assignments [88].

Various quantum chemical methods and MD simulations have been explored in understanding structure, [199,200] lignin biosynth-esis, [201] lignin pyrolysis, [202] and force-field based modeling of lignin macromolecular assembly [203,204]. Quantum chemical calcu-lations provide insight into molecular information that is inaccessible to conventional experimental techniques. In a recent review, Elder summarized computational efforts, such as Hückel calculations, hybrid DFT methods, and force-field based MD simulations, carried out for the development of a better understanding of lignin struc-ture [205]. The association between lignin and cellulose has been modeled using molecular mechanics tools [206–208]. DFT calcula-tions were carried out to characterize radical–radical coupling reac-tions involved in monolignol dimerization of six major linkages observed in natural lignin and to compute reaction enthalpies for the initial self- and cross-coupling reactions [201]. This work sug-gested that 8-O-4, 8-8, and 8-5 couplings were more favorable than the 5-O-4, 5-5, and 8-1 linkages. Quantum chemical calculations and MD methods for understanding lignin synthesis and structure were highlighted by Sangha et al. [209]. Extensive experimental and theoretical studies were conducted on phenethyl phenyl ether (PPE), a model for the lignin β-O-4 linkage [210,211]. Beste and co-

workers have illustrated the substitution effects of homolysis on PPE [211] and β-5 model compounds [212]. Homolytic cleavage reactions and chain-propagating steps in the thermal degradation of substi-tuted β-O-4 linked dilignols and the concerted pyrolysis mechanisms for fully substituted G, S, and H type lignin compounds were investigated using quantum chemical calculations [213]. More recently, acid-catalyzed reactions [214,215] and IL interactions with lignin model compounds [216] were studied. For the first time, bond dissociation energies (BDEs) of the ether and carbon–carbon (C–C) bond linkages in diverse lignin model compounds were reported [217]. These molecules had different substituents on the arene rings and aliphatic carbons connecting the rings, thereby covering the dominant linkages found in polymeric lignin. The calculated bond distances and BDEs from the optimized geometries of lignin model compounds are reported in Table 6. As mentioned above, the lignin linkages can be classified into two broad categories: ether linkages and C–C bond linkages. Within the ether classification, 4-O-5 com-pounds contain the shorter linkages (shortest, 1.375 Å) while the β-O-4 (1.44 Å), and α-O-4 (1.43 Å) compounds tend to have longer ether bond lengths. C–C linkages, including the β-1 linkage, generally comprise the larger bond lengths (1.55 Å). The exceptions occur for the double-bonded stilbene type of β-1 compounds. The C–C bond lengths observed in the β-5 linkage subtypes are shorter, with a bond distance around 1.46 Å. In general, the linkages with ether bonds are comparatively shorter than those with C–C linkages except for those with C꞊C double bonds in the β-1 linkage subtype compounds.

The bond dissociation energies at 298 °K (Zero Point Energy corrected) for the ether and the C–C linkages of the lignin compounds are also shown in Table 6. Overall, except 4-O-5 type, the β-O-4 and α-O-4 ether bonds were found to be weaker than the C–C linkages. Ether bonds in 4-O-5 type linkages are the strongest and also exhibit the shortest bond lengths, as expected. In the $C_α$–$C_β$ linkage category, β-1 type bonds are the weakest. They are followed by the β-O-4 linkages. It is quite likely that the fragmentation in these β-O-4 linkages, one of the highly abundant linkages in nature, is facilitated by the weaker ether bonds instead of the $C_α$–$C_β$ cleavage. α-1 linkages show higher C–C BDEs com-pared to β-O-4 and β-1 linkages.

Within the α-O-4 linkage category, methoxy group substitutions at the di-*ortho* position in the arene ring, adjacent to the ether bond, gives rise to the lowest BDEs. Single methoxy substitutions at *ortho* positions result in higher BDEs, while even higher BDEs are seen in α-O-4 linked compounds when there are no *ortho* substitutions. A strong relationship between the calculated bond length of a C–C bond and its bond strength indicate that the longer the bond, the easier it is to break. However, no similar correlation was found for ether bonds. The weakening of ether linkages can be attributed to steric hindrance induced by the *ortho*-methoxy groups. The lowest BDEs for C–C linkages have been calculated are seen in the β-1 $C_α$–$C_β$ bond types. Naturally, β-1 type linkages with $C_α$–$C_β$ double bonds exhibit the highest BDEs among all model compounds containing C–C bond linkages. A similar study on lignin model compounds showed that oxidation of primary and secondary alcohol groups on the alkyl substituents of lignin resulted in lower BDEs [218]. LCC linkages comparing hydrogen and covalent bonds in cellulose-hemicellulose and lignin-hemicellulose complexes were assessed using DFT calcu-lations [219].The authors concluded that the ether bonds in LCCs were less stable in pretreatment, though a more comprehensive understanding of the nature of bonding between sugars and lignin covering different categories will be necessary for targeting these linkages. DFT calculations on lignin model compounds not only were successful in predicting the BDEs and reactivity trend on experimen-tally observed product selectivities but also emphasized the roles of electron delocalization and methoxy group effects on the radical cation formation [220]. Also, the dissociating linkages can have different adjacent substituents, such as the methoxy functionality

on arene rings and hydrocarbon, methyl, and hydroxyl group substitutions on aliphatic carbon atoms. These substituents affect the ease of dissociation of lignin linkages and can be used to develop predictive models for delignification.

4. Lignin molecular weight

A key metric for studying lignin physicochemical properties, reactivity, and deconstruction whether through biochemical (i.e., lignin-degrading enzymes, pretreatments) or instrumental means (i.e., pyrolysis) is the measurement of the molecular weight [61,64,73,77,78, 81,128,129,134,135,147,150,163,167,169,170,178,183,184,196,221–224]. Analytical techniques capable of accurately quantifying lignin's molecular weight have been elusive due to the complexity of the lignin three-dimensional structure and disparities in both polarity and solubility.

4.1. Chromatography

Gel-permeation and size exclusion chromatography (GPC and SEC, respectively) are two of the most common methods employed for the determination of lignin molecular weight (MW). While a variety of studies utilize these techniques to evaluate the molar mass of lignin, only novel, contemporary results will be showcased in this section. Although there have not been abundant advances in the methodology of GPC, a few applications highlight how researchers have recently employed its use. One conventional usage is for gauging lignin degradation from various delignification strategies. A novel "expansion" pretreatment method was evaluated for its ability to delignify rice husk and straw [163]. GPC enabled the comparison of different lignin preparations that were partitioned according to variations in the water content of the pretreatment. GPC analysis of the fractionation of kraft lignin to more narrow fractions for commercial application disclosed the reduction in polydispersity with increasing aliquots of hexanes [169]. The authors hypothesize that this polydispersity diminution could be achieved due to the stepwise addition of hexanes allowing a more gradual polarity modification. The polydispersity index, calculated from the analysis of the GPC data, decreased rapidly with hexanes addition. In another study, lignins, isolated from ball-milled wild-type and transgenic alfalfa, were measured using GPC to determine whether significant differences in MW resulted from the modification [170].The transgenic lignins had smaller MWs when juxtaposed to the isolated wild-type lignin. Lower degrees of down-regulation resulted in lignins that were congruent to the native plant. GPC also aided in evaluating the MW of lignin isolated from: binderless boards produced from thermomechanical pulp [134], milled pine, MWL, and residual enzyme lignin [150], industrial black liquor [61], and the effect of a dilute phosphoric acid/steam explosion pretreatment on sugarcane bagasse lignin [167].

Baumberger et al. addressed the demand for standardized SEC measurements [222]. SEC is advantageous since it provides a wide mass range, but comparing results from different laboratories has proven challenging, in part to the differences in selecting appropriate calibration standards such as polystyrene, lignin model compounds, or pure lignin. Kraft, soda bagasse, steam explosion, and Alcell lignins, as well as lignosulfonates were evaluated using various column configurations, and eluents. In all cases, the number average molecular weight (M_n) proved to be more reproducible between labs than the weight average (M_w). Linear calibration curves (coefficient of determination, $R^2 = 0.99$) were produced for the specific mass ranges considered, depending on the eluent. The authors also probed the best data processing techniques for integration of chromatographic peaks. Separation configurations that resulted in the most reproducible data were outlined for both aqueous and organic matrices.

A derivitization scheme using acetobromination allowed the preparation of tetrahydrofuran (THF)-soluble lignin derivatives for use in SEC [221]. Non-polar and polar associative reactions between lignin and a variety of solvents impede accurate MW measurements. In the interest of developing a standardized protocol for reliable assessments of various lignin MWs, the authors employed acetyl bromide in excess glacial acetic acid to curtail associative reactions. In addition to two kraft lignins, MWL was used due to its known structural similarity to native lignin. Acetobromination required as little as 30 min reaction time compared to using acetic anhydride in pyridine, which required six days to react. Dissolved lignin samples, in THF were found to be stable for at least one week.

Multi-angle laser light scattering (MALLS) coupled with SEC has enabled a more detailed analysis of lignin MW and its aggregates [178,224]. MALLS utilizes detectors placed around a flow cell at 18 different locations to efficiently capture light scattering. The intensities measured are directly proportional to the molecular morphology. Traditional SEC was compared with MALLS through the use of sodium polystyrene sulfonate MW standards. Good agreement was found between manufacturer specifications and MALLS. Overall, use of MALLS led to a significant reduction in data acquisition time, and in addition to determining variations in MW, MALLS also enables differences in hydrodynamic and gyration radii to be monitored. The authors identify the main advantage of this technique as its ability to characterize large lignin aggregates, which were undetected using refractive index (RI) or UV detectors [224]. The absence of these aggregates in traditional RI or UV detection could be misinterpreted as a reduction in lignin MW, when in reality, these species are present. This technique was applied to the study of kraft lignin in various solvents [178].

SEC has been recently used for characterization of eucalyptus lignin MW during various alkaline delignification reactions [64], to probe the effectiveness of organic bases for delignification of acidified and hardwood lignin [77], for the evaluation of H_2SO_4 and alkaline H_2O_2 extractions [81], for the characterization of lignins for use in lignin-film fabrication [129], for monitoring acetylated Miscanthus x giganteus lignin before and after the cleavage of β-O-4 linkages using thioacidolysis [135], and finally, to compare MWL, CEL, and enzymatic MAL preparations isolated from Douglas and White fir, Eucalyptus, redwood, and pine [147].

4.2. Thermochemical methods

MALDI-ToF-MS has been employed for lignin MW determination (with mixed results) since the m/z of the ions produced is directly proportional to the analyte molar mass [73,78]. Matrix interference, however, can occur at the low mass region of the spectrum. A MALDI MW measurement of herbaceous lignins only detected a mass range between 100 and 600 Da, while high-performance SEC revealed a molecular weight of 2000 or 2800 for non-acetylated or acetylated lignin respectively [73]. The authors hypothesized that laser-induced degradation of the lignin into smaller fragments was possible. However, when alkaline-extracted switchgrass lignin was measured, the HPSEC and MALDI measurements exhibited good agreement, indicating the potential of this technique for MW determination. MALDI-ToF-MS was also used to evaluate the MW distribution of hard- and softwood kraft lignins [78]. Each preparation produced similar mass spectral results, but did not provide the higher MW distributions of lignin.

Another relatively new technique for gauging lignin molecular weight is Fourier-transform ion cyclotron resonance mass spectrometry (FT–ICR–MS) [223]. This technique, however, led to significant differences in detected molecular mass compared to GPC. Peaks with m/z larger than 2000 could not be detected, however, the peaks that were measured revealed a correlation with each other, as they were separated by identical amounts (44.026 m/z). Sugarcane bagasse lignin, therefore, exhibited a more ordered, less random structure.

5. Total lignin content

Measuring the amount of lignin in biomass remains one of the most crucial aspects of developing lignocellulosic biomass for biofuels and bio-based chemicals. Knowing the amount of lignin in plant cell walls facilitates partitioning interesting feedstocks according to anticipated recalcitrance and aids researchers in developing effective pretreatment strategies. However, the challenges researchers have encountered in comparing the lignin content of samples with different lignin composition and the ability to determine absolute levels of lignin have prompted the proficiency to quantify only relative lignin concentrations. For example, Klason lignin analysis quantifies insoluble residues after a dilute H_2SO_4 hydrolysis. Often, owing to the minute biomass aliquot used, ash content cannot be directly measured, resulting in a Klason lignin measurement that may also incorporate some ash. Additionally, isolation methods, like the Klason analysis, are known to chemically alter lignin. Some lignin becomes solubilized during the acid hydrolysis. The conventional quantification method of acid soluble lignin is UV spectrophotometry. If the biomass has not been sufficiently extracted, however, the extraneous extractive materials can obfuscate the analysis.

5.1. Wet chemistry

The most conventional wet chemical techniques employed to gauge lignin content are the acetyl bromide [225–227], Klason or acid-insoluble lignin (AIL) [228–234], and Van Soest methods [227,235]. While these pervasive protocols have provided researchers with tools for obtaining the magnitude of total lignin in a plant, they also have a variety of shortcomings, such as the use of caustic/toxic reagents (H_2SO_4, acetyl bromide) and time-consuming preparations. DeMartini et al. addressed the low-throughput nature of AIL quantitation by developing an automated process that employed a liquid and powder dispensing robot equipped with an analytical balance for weighing individual vials before and after heating in a reactor block [233]. This downscaled protocol did not allow for ash determination, therefore, the acid-insoluble residue was a combination of lignin and ash.

These techniques can produce widely different results due to the mechanism of each method [225]. For instance, portions of the lignin may become solubilized during the reaction, causing the measurement to reveal less total lignin, such as in the acid-detergent lignin analysis [225,236]. During oxidative reactions, other biomass constituents may be targeted by the reagents, embellishing the total lignin measurements [237]. One of the key concerns with the Klason analysis is whether or not the carbohydrates have been completely hydrolyzed [228]. Additionally, hydrolysis products from acidic carbohydrate degradation, such as furfural and hydroxymethylfurfural, can condense with lignin producing erroneously high lignin values in AIL measurements, and the presence of these molecules, by themselves, can interfere with acid-soluble lignin evaluation at 280 nm. Switching to 205 nm has been used to correct this interference. Any UV spectrophotometric method must address the question of what value to employ for the lignin extinction coefficient [228].

5.2. Thermochemical methods

5.2.1. Pyrolysis

Thermochemical techniques have occasionally been utilized for the measurement of total lignin content [66,238–240]. Alves and co-authors utilized analytical pyrolysis and GC-FID to measure the lignin content of a variety of hard- and softwoods [66,238,239]. The authors first investigated how their technique compared to the standard Klason analysis [239]. The precision of the pyrolytic method (0.43% for pine, 0.34% for spruce) was close to that of the reference technique (0.34%). A correlation coefficient (r) of 0.95 was measured. This technique was then extended to larch species and compression wood [238]. A calibration equation was produced that encompassed the previously measured softwoods with the hardwood and compression wood with a R^2 of 0.95. Finally, PCA was employed to classify softwoods according to species- and tissue-specific variance [66]. The authors concluded that vanillin, isoeugenol, dihydroconiferyl alcohol, and G-C=C=C structures that separate spruce and larch from pine. *E. globulus* total lignin content was measured using pyGC-FID [240]. This study measured a strong linear correlation ($R^2 = 0.979$) between wet chemistry total lignin and pyGC-FID, regardless of the pulping conditions.

Pyrolysis molecular beam mass spectrometry (pyMBMS) has been advanced by the National Renewable Energy Laboratory as a high-throughput analytical tool capable of lignin quantitation [241–243]. Application of a correction factor calculated by measuring the Klason lignin value for a standard biomass sample (*i.e.*, National Institute of Standards and Technology sample 8492, *Populus deltoids*) resulted in a strong linear correlation [242]. pyMBMS spectra were coupled with Klason lignin values to generate PLS predictive models incorporating a diverse selection of feedstocks, such as agave, coconut coir, cotton, flax, hemp, and kenaf bast, to name a few [241]. In all, 41 plant samples were used in the calibration and subsequent cross-validation with a validation r of 0.77. Within tree variability of lignin content between seven different poplar trees was measured using pyMBMS [243]. The authors concluded that there was greater ring to ring variance in total lignin content, than when sampling a tree from different heights.

5.2.2. Thermogravimetric analysis

Another high-throughput, thermochemical technique used more frequently for lignin analysis is TGA [244–247]. Mixtures of cellulose and lignin were successfully quantified to within 7–18% of the measured value using a mathematical treatment of pyrolytic unit thermographs [247]. Two models were developed to predict the relative amounts of cellulose and lignin by using linear correlation between cellulose and lignin content and peak decomposition rate, or a system of linear equations. The future objective of this work is to move from cellulose and lignin standards to whole biomass samples. A mathematical treatment was applied to the TGA data of eight different corn stover samples [245]. A multiple linear regression equation, using biomass degradation temperatures as well as the cellulose, hemicellulose, and lignin contents measured by standard wet chemical analysis, enabled lignin to be predicted within 0.74% of the reference results. Serapiglia et al. achieved the high-throughput measurement of total lignin content in 95 shrub willow clones [246]. The TGA results were statistically analyzed using multivariate analysis. The authors note that further refinements in the method may decrease the error in the measurements, as well as the analysis time of 90 min/sample and 16 samples/day. TGA has not produced highly correlated results in all attempts to predict total lignin content, however [244]. In this example, the lack of correlation between the TGA predictions and the reference method was hypothesized to stem from the use of the Klason lignin analysis, which is not representative of all lignin present.

5.3. Vibrational spectroscopy

5.3.1. Raman spectroscopy

Raman spectroscopy has not been routinely employed for lignin content analysis, perhaps due to significant spectral interference by intrinsic sample fluorescence, even at NIR excitation wavelengths [96]. Although the Raman analysis of individual lignin monomers

Table 7
Near-infrared vibrational mode band and speculative band assignments.

Vibrational mode	Assignment
4014	CH and CC stretch [38]
4195	Not yet assigned, but confirmed w/MWL [351]
4280	CH stretch [38]
4411	OH stretch [38]
4546	CH and C~O stretch [352]
4686	CH and C~C stretch [351]
5522	Not yet assigned, but confirmed w/MWL [38]
5583	1st overtone CH stretch [38]
5795	1st overtone CH stretch [38]
5890	1st overtone CH stretch [38]
5935	1st overtone aromatic CH stretch [335,351,352]
5963	1st overtone aromatic CH stretch [38,352]
5974	1st overtone aromatic CH stretch [352]
5978	1st overtone aromatic CH stretch [38,352]
5980	1st overtone aromatic CH stretch [352]
6874	1st overtone OH stretch [38]
6913	1st overtone OH stretch [181]
6944	1st overtone CH and CH deformation [335]
7057	1st overtone CH and CH bend [335,352]
7092	1st overtone OH stretch [335]
8547	2nd overtone asymmetric CH stretch, HC~CH [352]
8749	2nd overtone aromatic CH stretch; 2nd overtone CH stretch of CH_3 [353]

reveal slight variation in the location and intensity of the main vibrational modes near 1600 cm^{-1} [95,96], Agarwal and co-authors found this band to linearly correlate with kappa number [248,249]. Evaluation of peak heights or areas resulted in R^2 values of 0.95 and 0.93, respectively. A follow-up study explored three lignin modification techniques (alkaline H_2O_2, diimide, sodium borohydride treatments) for reducing other factors, besides concentration, that can contribute to band intensity [248].

Ona et al. have also explored the use of FT-Raman spectroscopy coupled with PLS to predict lignin content in *Eucalyptus* species [250,251]. Using six principal components (PCs), the authors were able to generate a predictive model with a r of 0.792 and standard error of prediction (SEP)=1.85 using 2nd derivative Raman spectra [250]. A follow-up study using 1st derivative spectral data resulted in a more robust model for lignin content analysis, requiring only four PCs with a $r=0.903$, SEP=1.3 [251].

UVRR spectroscopy has enabled lignin analysis due to the electronic absorption in this wavelength region [226]. Due to the intensity associated with this transition, UVRR spectroscopy can selectively enhance the spectral features of lignin, while reducing spectral contributions from cellulose. A rapid, quantitative method for determining lignin in bleached hardwood kraft pulps was generated by Jääskeläinen and co-authors [107]. Following the standard addition of known concentrations of a hardwood kraft lignin solution, lignin contents from 0.5% to 5.0% were accurately measured using the peak height of the 1604.5 cm^{-1} vibrational mode. Use of 244 or 257 nm excitation did not alter linear correlation ($R^2=0.987$).

5.3.2. Mid-infrared spectroscopy

MIR spectroscopy has also been used to gauge total lignin content [252–255]. Diffuse reflectance MIR Fourier transform (DRIFT) spectroscopy coupled with PLS modeling enabled the evaluation of lignin content in 491 Sitka spruce from 50 different clones, 24 tropical hardwoods, and 20 softwoods [254]. Individual and ranges of wavenumbers were evaluated to gauge which strengthened model performance. The authors note that reducing the number of wavelengths did not have a significant effect on model performance; however, the number of factors was reduced from three to two when fewer wavelengths were used. The calibration R^2 was 0.78 when all wood samples were in the model, and the root mean standard error of prediction (RMSEP) was 1.6.

Kraft pulps from *Pinus radiata* were evaluated using photoacoustic rapid scan FT-MIR (PA-FTMIR) spectroscopy and PLS [253]. PA-FTMIR requires little to no sample preparation, significantly increasing analysis throughput, is not morphologically sensitive, and probes larger sample quantities. Comparisons between actual and predicted kappa number showed good correlation ($R^2=0.96$). Allison et al. used FT-MIR and PLS to predict lignin content in *Dactylis* (orchard grass), *Festuca*, *Lolium* (ryegrass), reed canary grass, and switchgrass [252]. Application of a 1st derivative spectral transformation was found to provide the best compromise between reducing the number of latent variables (LVs) used to explain the variance in the model, and reductions in RMSEP. For example, three LVs successfully explained the variance in the 1st derivative model with RMSEP values of 0.33, while 10 LVs were required to yield a similar RMSEP (0.32) after a 2nd derivative transformation. Lignin content in triticale and wheat straw was predicted using FT-MIR and PLS [255]. Models encompassing both plants resulted in intermediate RMSEP and R^2 values, compared to using each feedstock by itself (RMSEP=0.27-both plants, 0.305-triticale, 0.163-wheat straw, $R^2=0.952$-both plants, 0.935-triticale, and 0.985-wheat straw).

5.3.3. Near-infrared spectroscopy

NIR spectroscopy, coupled with multivariate analysis, has been the predominant vibrational technique for assessing total lignin content [93,178,241,256–279]. A list of predominant lignin vibrational mode assignments can be found in Table 7. The studies combine NIR spectra with a reference technique, such as Klason lignin analysis, to produce multivariate analysis models capable of predicting the total lignin content. The reference technique is performed on a subset of samples, ideally covering the complete range of expected results. The use of robust, thoroughly evaluated multivariate models alleviates the need to perform labor-intensive reference techniques for all samples, significantly increasing the throughput while decreasing experimental and analytical time and expense. Wolfrum and Sluiter illustrated the use of NIR spectroscopy coupled with untreated and dilute-acid, pretreated, corn stover Klason lignin results [271]. The authors provided a thorough analysis of how different mathematical pretreatments and calibration algorithms affected predictive models. PLS-1 was found to result in the lowest RMSEP (1.49) and highest R^2 (0.85) compared to a four-constituent (RMSEP=1.81, $R^2=0.75$) or 13-constituent PLS-2 (RMSEP=1.92, $R^2=0.75$) for lignin content predictions.

Table 8
Pyrolysis fragments for lignin and lignin monomer quantitation.

Molecule	m/z	Monomer assignment
Phenol	94/66/65	H [59,299]
2-Methylphenol	108/107/79	H [59,299]
4-Methylphenol	107/108	H [59,299]
Guaiacol	124/109/81	G [59,298,299]
Dimethylphenol	107/122/121	H [59,299]
4-Ethylphenol	107/122/77	H [299]
4-Methylguaiacol	138/123/95	G [59,298,299]
4-Allylphenol	134	H [59]
4-Vinylphenol	120/91/119	H [59,299]
3-Methylcatechol	124	G [354]
3-Methoxycatechol	140/125/97	MWL [298,301,354]
4-Ethylguaiacol	137/152	G [59,298,299]
4-Vinylguaiacol	150/135/77/107	G [59,298,299]
4-allylphenol	134/133	H [299]
Syringol	154/139/96	S [59,298,299]
cis-4-propenylphenol	134	H [59,354]
4-Propylguaiacol	137/166/122	G [299]
Eugenol	164/77/149	G [59,298,299]
4-Hydroxybenzaldehyde	121/122/93	H [299]
4-trans-propenylphenol	134	H [59,354]
Vanillin	151/152/81	G [59,298,299]
cis-Isoeugenol	164/149/131	G [59,298,299]
4-Methylsyringol	168/153/125	S [59,298,299]
trans-Isoeugenol	164/149/131	G [59,298,299]
Homovanillin	137/166/122	G [298,299]
Guaiacol derivative (G-C3H3), 4-propenylguaiacol	162/147	G [59,298,299]
Guaiacol derivative (G-C3H3), 4-allenylguaiacol	162/147	G [59,298,299]
trans-p-coumaryl alcohol	150	H [354]
Acetoguaiacone	151/166/123	G [59,298,299]
propioguaiacone	151/178	G [239]
4-Ethylsyringol	167/182/107	S [59,298,299]
Guaiacyl acetone	137/180/122	G [59,298,299]
4-Vinylsyringol	180/165/137	S [59,298,299]
4-Allyl-syringol	194/91/119	S [59,298,299]
4-allylsyringol	196/167/123	S [298]
4-Propylsyringol	167/196	S [59,298,299]
Propenylsyringol	194/91/119	S [59,299]
cis-4-Propenylsyringol	194/91/119	S [59,298,299]
Syringaldehyde	182/181/167	S [59,298,299]
Syringol derivative (S-C3H3). 4-propenylsyringol	192/131/177	S [59,298,299]
Syringol derivative (S-C3H3), 4-allenylsyringol	192/131/177	S [59,299]
trans-p-coumaraldehyde	148	H [354]
trans-4-Propenylsyringol	194/91/119/179	S [59,298,299]
Homosyringaldehyde	167/196/123	S [298,299]
Acetosyringone	181/196/178/153	S [59,298,299]
Coniferyl alcohol	137/91/180	G [299]
trans-coniferaldehyde	178	G [59]
Syringyl acetone	167/210	S [59,298,299]
Propiosyringone	181/182/210	S [59,298,299]
4-propanalsyringol	210/182/167	S [298]
Trans-sinapaldehyde	208	S [59,298]

NIR spectroscopy and pyMBMS were coupled with wet chemical data to produce PLS models for assessing total lignin content in a variety of agricultural feedstocks including coconut coir, cotton, hemp, kenaf bast, and sugarcane, to name a few [241]. pyMBMS models resulted in a lower RMSEP (5.50) and higher validation correlation coefficient (0.77) than those produced using NIR spectroscopy (RMSEP=6.10, r=0.71). Extractives in sugarcane bagasse were found to adversely affect calibrations using extractive-free NIR spectral data [258]. Application of a direct orthogonal signal correction alleviated the need to physical extract these materials prior to analysis. Following this mathematical treatment, independent validation resulted in a RMSEP of 0.879 and a R^2 of 0.93, and a reduction in the number of latent variables (LVs).

Other applications of NIR spectroscopy coupled with multivariate analysis for determining total lignin content extend to *Acacia* [259,273], aspen [276], *E. globulus* [264], larch [259], poplar [259], and southern [261] and Turkish pine [270], to name a few.

5.4. Electronic spectroscopy

Fluorescence spectroscopy coupled with PLS was used to predict lignin contents in yellow poplar [277] and northern red oak [278]. Using a wavelength region of 295–872 cm^{-1}, the authors developed an eight PC calibration model with a validation R^2 of 0.62, and a RMSEP of 0.0889 for the total lignin content of poplar. The results using northern red oak were more accurate (seven PCs, R^2val=0.88, RMSEP=0.0436). Comparisons with models generated using NIR spectra revealed the latter to be more robust for analyzing poplar lignin (four PCs, R^2=0.66, RMSEP=0.0885), while the metrics produced from the oak analysis using NIR spectra were less accurate, although the models also required fewer PCs to explain the data (five PCs, R^2val=0.70, RMSEP=0.0531).

UV/vis spectrophotometry has been routinely employed for lignin analysis, as it remains a standard analytical tool for measuring acid-soluble lignin and acetyl bromide lignin [108,125,142,225,232,

280–285]. In order to measure lignin spectrophotometrically using Beer's Law, an accurate extinction coefficient is required. A lack of homogeneity in diverse lignin preparations perturbs standardizing UV/vis measurements. Fukushima and Kerley investigated the use of extracted lignins from hard- and softwoods, and herbaceous plants as standards in acetyl bromide lignin detection [282]. Standard calibration curves were generated, and using the slopes and intercepts, a global mean extinction coefficient was calculated that could be used regardless of botanical origin. This technique alleviates the need to extract and isolate lignin from biomass.

UV/vis spectrophotometry enabled the quantification of lignin in whole biomass after dissolution in an IL [125]. Absorbance measurements were recorded at 440 nm for a variety of hard- and softwoods. A similar process was carried out using a variety of UV wavelengths to quantify dissolved lignin after a single-shot steam process [283]. Lastly, UV/vis photoacoustic (PA) spectroscopy enabled lignin quantification in synthetic mixtures of xylan and cellulose [286]. While the PA spectra contain no discernible peaks, the amplitude of the signal intensified as the lignin concentration increased.

5.5. Nuclear magnetic resonance

Another powerful technique utilized in measuring total lignin content is NMR [80,140,146,152,169,287,288]. ^{13}C CP/MAS NMR was used to quantitate loblolly pine lignin residues following an acid hydrolysis [288]. The analysis time was reduced to three hours using this technique, as opposed to over 24 h using standard wet chemical analyses. The quantitative results were contrasted for 13 different biomass treatments, and were found to be in good agreement with standard TAPPI methods. In another study investigating rapid NMR analysis, isolated poplar and switchgrass lignins, dissolved in a perdeuterated pyridinium IL, [Hpyr]Cl-d6/[D_6]-DMSO, were quantified with ^{1}H–NMR using the ratio of integration of peaks between 6.0–8.0 ppm and the DMSO standard [287]. Ball and Wiley milled biomass were used, and the results were compared with Klason lignin results. Overestimation of corn stover lignin content using ^{13}C CP/MAS NMR resulted from a H_2SO_4 hydrolysis [152]. The interfering analytes were found to be extractives, including carbohydrates like fructose, which polymerized forming solids, during pretreatment.

5.6. Color image analysis

Lastly, color image analysis was used to quantify the lignification of maize tissue [289]. This method provides a rough approximation of the total lignification in a plant tissue by using Safranin and Alcian blue staining. Lignified tissues are stained red, while non-lignified tissues are stained blue. A more rigorous calculation can be achieved by the computation of intensity profiles that monitor the ratio of red to blue stained regions as a function of distance from the epidermis.

6. Lignin monomer composition

The measurement of S, G, and H lignin monomers enables classification of plants as gymnosperm (G-lignin), angiosperm (S-G lignin), or herbaceous (S-G-H lignin), with some exceptions, such as eucalypts, which are classified as angiosperms, but are known to contain H lignin [1,154,290]. S/G lignin ratios have proven to be important parameters for gauging the recalcitrance of lignin, although no clear trend has been established as to whether or not a high S content results in increased monomeric sugar release following an enzymatic hydrolysis. The traditional methods for measuring lignin monomer composition include NMR, pyGCMS,

pyMBMS, and various wet chemical methods such as nitrobenzene oxidation (NBO) and thioacidolysis [4,5,13,56,58,59,61–66,68,70, 126,135,157,159,183,240,242,291–307]. Common pyrolysis and mass spectral fragments are listed in Table 8, and illustrated in Fig. 3. Table 9 lists the S, G, H percentages and S/G ratios for a diverse selection of biomass feedstocks.

6.1. Wet chemistry

The conventional wet chemical techniques used for quantifying lignin monomers are acidolysis, cupric oxide, NBO, permanganate oxidation and thioacidolysis [22,292,294,296,297,302,304,307]. While there have not been abundant recent advances in wet chemical techniques for lignin monomer analysis, except for the scaling down of the standard thioacidolysis protocol to achieve higher throughput and diminutions in reagent consumption [304,307], the prevalence of these techniques in the literature warrants their discussion. Lapierre provided a thorough review on the applicability, benefits, and pitfalls of these methods [22]. Although well-studied, these techniques have drawbacks. For example, NBO targets C_6C_3 bonds, and converts them to C_6C_1 monomers and dimers. The reaction products are then acidified, and following the extraction of the analytes, the specific monomers are quantified with LC or GC. NBO tends to yield higher S/G ratios that what is actually present due to the fact that S lignin is not as interlaced in inter-unit bonds as G lignin. Additionally, NBO suffers from a lack of specificity. If other, non-lignin phenolics are present in the plant cell wall that can undergo the same transformation during the NBO reaction, the data can be obscured.

Thioacidolysis specifically cleaves β-O-4 bonds into C_6C_3 species. Depending on the degree to which these bonds are prevalent in a specific classification of biomass, monomeric yields can be vastly different. Hardwoods, for instance, have a higher abundance of S lignin than softwoods, and therefore, reveal a higher proportion of β-O-4 linkages. The monomeric products, quantified by GCMS, require derivatization to promote volatility, making this procedure another labor-intensive protocol.

In summary, the wet chemical techniques are labor-intensive, require the usage of toxic reagents such as nitrobenzene or boron trifluoride etherate, and are bond-specific, and therefore, may not provide a "true" measurement of lignin monomers. These techniques are, however, quite prevalent in the literature, given the knowledge of what they can do and what limitations they have. Lapierre addressed the need for higher-throughput methods [22], and many researchers have begun to pair wet chemical techniques with other instrumental tools, such as spectroscopy.

6.2. Thermochemical methods

6.2.1. Pyrolysis
Thermochemical evaluations of lignin monomers have become increasing prevalent [4,5,13,59,61–66,68,70,126,157,159,183,240,242, 293,295,298–301,303,305,306,308]. When heated, lignin linkages are cleaved, permitting the identification of individual monomeric moieties. Sykes et al. addressed the potential overestimation of S/G ratios, resultant from a possible preferential liberation of S lignin moieties, since previous experimental data showed sinapyl alcohol to be released from lignin during the primary stages of the pyrolytic degradation [243,309]. Pyrolysis GC-FID or pyGCMS, previously outlined by Meier and Faix [300], has provided a robust alternative to wet chemical degradations for the analysis of lignin monomers, and specifically for the measurement of lignin S/G ratios [13,59,61–66,126,156,157,159,183, 240,293,295,298,299,301,303,305]. Del Rio and co-authors have analyzed a diverse variety of non-woody plant materials using pyGCMS, including kenaf, jute, sisal, abaca, hemp, flax, and wheat straw [59,65,293]. Using the GC retention times, coupled with the mass
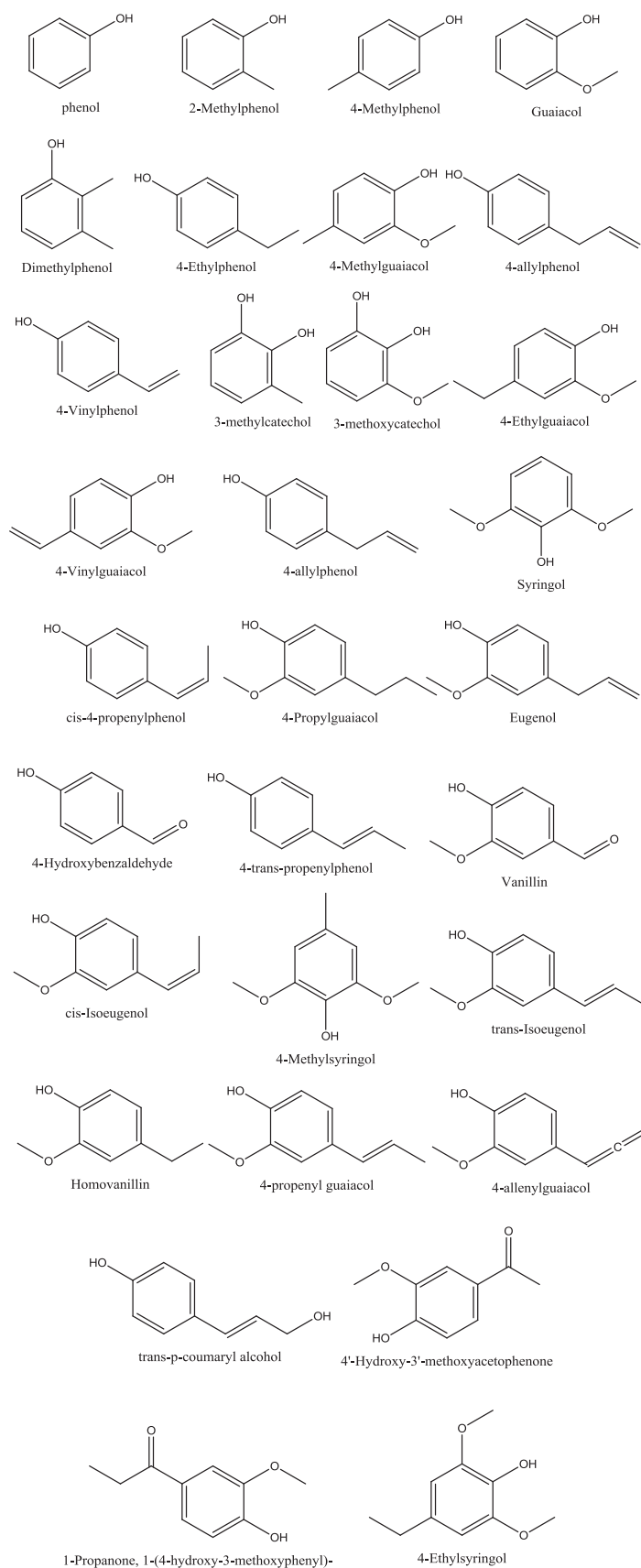
Fig. 3. Common fragments of lignin measured after pyrolysis.

1-(4-hydroxy-3-methoxyphenyl)propan-2-one

4-Vinylsyringol

4-Allyl-syringol

4-Propylsyringol

Propenylsyringol

cis-4-Propenylsyringol

Syringaldehyde

4-propenylsyringol

4-allenylsyringol

trans-p-coumaraldehyde

trans-4-Propenylsyringol

Acetosyringone

Coniferyl alcohol

trans-coniferaldehyde

Syringyl acetone

Propiophenone, 4'-hydroxy-3',5'-dimethoxy
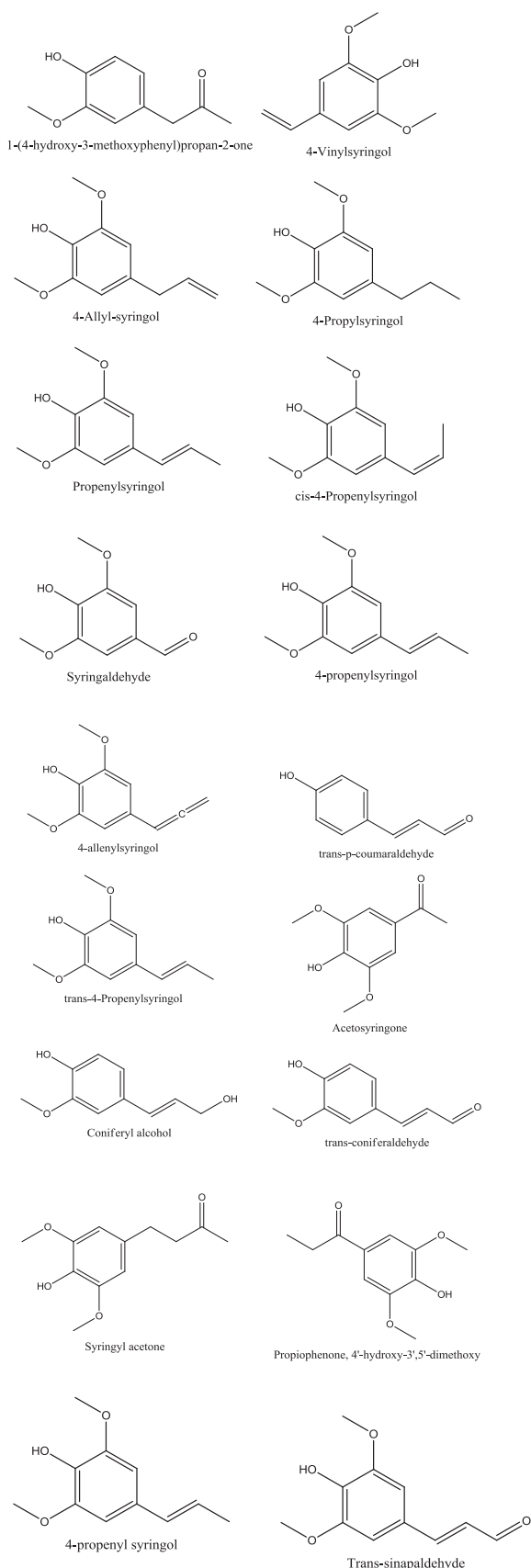
4-propenyl syringol

Trans-sinapaldehyde

Fig. 3. (continued)

spectra, the identification of phenylpropanoid structures representative of S, G, and H lignin is possible. Hemp, flax, and wheat straw were measured to be predominantly G lignin, while kenaf, jute, sisal, and

abaca were comprised of mostly S lignin. One of the paramount necessities in using pyGC-FID or pyGCMS is standardization in data analysis, specifically, identifying which peaks should be utilized in S/G/H calculations. Del Rio et al. have deduced that 4-vinylphenol and 4-vinylguaiacol should be left out of lignin monomer calculations for herbaceous feedstocks, since a proportion of these molecules arise from p-hydroxycinnamates, and are not part of the core lignin structure [59]. Using these species in monomer evaluations will result in erroneously high G and H lignin.

pyGCMS has also been employed to study of variety of eucalypts including *E. globulus*, *E. nitens*, *E. maidenii*, *E. grandis*, and *E. dunnii* [63,156,157,301,303,305]. The lignin S/G ratios of the eucalypts ranged from 2.7 (*E. grandis*) to 4.1 (*E. globulus*) [303]. Analysis of young and adult trees revealed that G and H lignin units are deposited during the early stages of development while S lignin forms later in the lignification of the plant [156]. The S/G/H ratio of one month old *E. globulus* was 52.1/38.5/9.4 while at nine years of age, the ratio had transformed to 77.6/20.4/1.9. A follow-up study of the milled-wood lignins of these feedstocks compared pyGCMS, 2D-NMR, and thioacidolysis evaluations of S/G ratios [157]. The thioacidolysis and pyGCMS results were quite similar, signifying the suitability of the latter technique to supplant wet chemical degradation techniques. Environmental variability, such as geographical location, has been shown to significantly affect S and G lignin content in *E. globulus* [305]. The S/G ratios of wild-type *E. grandis* and hybridized *E. grandis x E. urophylla* were determined using NBO and pyGCMS [301]. There was no statistical variance between the methods again conveying the power of this technique to replace wet chemical analyses. pyGCMS also enabled the quantitation of the S/G ratio for a variety of *Eucalyptus* hybrids [63]. The authors used PCA to attempt to classify the different hybrids based upon lignin structure. Importantly, this study concluded that all S and G lignin decomposition products should be used in S/G ratio calculations, and not simply specific selected products, since analysis of the PCA loadings plot revealed a positive correlation between G and S phenolic compounds possessing similar side chains. Lastly, pyGC-FID data and PCA were used to partition larch, pine, and spruce into distinct groups [66]. Differences in vanillin, isoeugenol, dihydroconiferyl alcohol, and G–C=C–C structures enabled the segregation of larch and spruce from pine. Normal and reaction wood and site-specific variance were also studied using PCA.

pyMBMS has been developed as a high-throughput analytical tool for gauging lignin monomer content [4,5,242,243]. The instrument is capable of measuring 42 samples per hour, resulting in the ability to screen large arrays of feedstocks for biofuel traits such as S/G ratios. Lignin peaks were identified with $m/z = 120$, 124, 137, 138, 150, 152, 154, 164, 167, 178, 180, 181, 182, 194, 210 with representative S peaks at $m/z = 154$, 167, 168, 182, 194, 208, 210 and G peaks at $m/z = 124$, 137, 138, 150, 164, and 178. As of 2009, this instrument had been employed for the analysis of over 1500 biomass samples including eucalypts, maize, and poplar species. In contrast to many studies, Davison and co-authors used pyMBMS to show that a decrease in the S/G ratio of poplar variants led to improvements in the rate of hydrolysis using dilute H_2SO_4 [5]. The authors hypothesized that the acid may cleave G units more readily, a theory witnessed in forage maize digestibility research, where less S lignin was shown to provide enhanced digestibility [310]. These studies hypothesize that S lignin is more prevalent in younger, less lignified biomass, a finding in parallel to the aforementioned analysis of young and mature eucalyptus trees [156].

6.2.2. Mass spectrometry

Recently, MALDI imaging MS was employed to evaluate *E. globulus* and *E. grandis* [68]. Using this technique, 22 of 24 known soluble lignin monomer compounds were detected and located in the plant cell walls, and the S/G ratios were calculated. The authors

Table 9
Lignin S/G/H composition and S/G ratios of various potential biofuel feedstocks.

Feedstock	S	G	H	S/G	References
Abaca	55	19	26	2.9	[65]
Acacia	48	49	3	1.0	[155,314]
				1.2	[161]
Acacia microbotrya	–	–	–	1.3	[317]
A. saligna	–	–	–	1.7	[317]
Agave	76	22	2	3.4	[65]
	–	–	–	3.6	[158]
Alfalfa	30	70	n.d.	0.4	[95]
Arabodopsis	–	–	–	0.3	[316]
Aspen	–	–	–	1.5	[130]
Banana Leaf sheath	63	25	12	2.5	[128]
Big Bluestem	–	–	–	1.1	[54]
Birch	69	29	2	2.4	[314]
	–	–	–	3.1	[161]
	–	–	–	1.3	[58]
Black Locust	–	–	–	0.9	[130]
Bromegrass	–	–	–	3.4	[54]
Cherry	–	–	–	1.5	[58]
Coconut Coir	25	68	7	0.3	[159]
Corymbia citriodora subsp. *Citriodora*	–	–	–	2.4	[317]
C. citriodora variegata	–	–	–	2.3	[317]
Corymbia hybrids	–	–	–	2.3	[317]
C. torelliana	–	–	–	2.1	[317]
C. citriodora subsp.*variegata*	–	–	–	2.6	[317]
Cottonwood	–	–	–	1.4	[161]
Curaua	41	29	30	1.4	[308]
Douglas fir cork	1	97	2	0.0	[126]
Eucalyptus argophloia	–	–	–	2.1	[317]
E. cladocalyx	–	–	–	2.5	[317]
E. cloeziana	–	–	–	1.9	[317]
E. crebra	–	–	–	1.6	[317]
E. dunnii	–	–	–	2.3–2.7	[157]
	–	–	–	2.5	[317]
E. globulus	84	14	1	6.0	[314]
	–	–	–	2.7, 2.8	[158,161]
	–	–	–	2.5–2.9	[157]
	–	–	–	2.6	[317]
E. globulus Heartwood	76	22	2	3.4	[240]
E. globulus Sapwood	76	21	3	3.6	[240]
E. globulus, 1 month old	52	38	9	1.4	[156]
E. globulus, 18 months old	77	21	2	3.7	[156]
E. globulus, 9 years old	78	20	2	3.9	[156]
E. globulus, 0 h milling	–	–	–	4.1	[186]
E. globulus, 3 h milling	–	–	–	4.2	[186]
E. globulus, 12 h milling	–	–	–	4.3	[186]
E. globulus, 24 h milling	–	–	–	4.9	[186]
E. grandis	69	27	4	2.5	[314]
	–	–	–	1.6–1.9	[157]
	–	–	–	2.0	[317]
E. kochii	–	–	–	2.2	[317]
E. longirostrata	–	–	–	2.2	[317]
E. loxophleba	–	–	–	2.4	[317]
E. maidenii	–	–	–	1.8–2.4	[157]
E. moluccana	–	–	–	2.2	[317]
E. nitens	–	–	–	2.6	[161]
	–	–	–	2.1–2.7	[157]
E. occidentalis	–	–	–	2.4	[317]
E. polybractea	–	–	–	2.3	[317]
E. urograndis	66	30	4	2.2	[314]
	–	–	–	1.8	[161]
Elephant grass	–	–	–	1.2	[145]
Fescue	42	55	3	0.8	[355]
	–	–	–	0.8	[54]
Flax	29	67	4	0.4	[65]
Hemp	40	51	9	0.8	[65]
Jute	62	36	2	1.7	[65]
Kenaf–Bast	89	11	n.d	8.1	[95]
	79	19	2	4.1	[324]
Kenaf–Core	24	76	n.d	3.2	[95]
	58	41	1	1.4	[324]
Little Bluestem	–	–	–	1.7	[54]
Loblolly pine	0	87	13	0	[147]
Maize	–	–	–	0.5	[316]
	–	–	–	0.5	[130]
	–	–	–	1.4	[54]

Table 9 (*continued*)

Feedstock	S	G	H	S/G	References
Maple	–	–	–	1.3	[161]
	–	–	–	1.2	[58]
Miscanthus × giganteus	39	61	n.d.	0.6	[95]
	–	–	–	0.5, 0.6	[196]
	–	–	–	0.7	[135]
Newsprint	–	–	–	0.0	[130]
Oat	–	–	–	1.6	[54]
Orchard grass	31	68	n.d.	0.4	[95]
	–	–	–	1.3	[54]
Pampas grass	43	57	n.d.	0.75	[95]
Pine	1	99	n.d	0.0, 0.0	[95,316]
Poplar	83	17	n.d	4.9	[95]
Poplar	68	31	0	2.2	[304]
Red alder	–	–	–	1.4	[161]
	–	–	–	1.3	[58]
Red oak	72	28	n.d	2.6	[95]
	–	–	–	1.4	[58]
	–	–	–	2.6, 2.9	[130]
	–	–	–	2.1	[161]
Reed canarygrass	–	–	–	2.0	[54]
Rice straw	–	–	–	0.6	[163]
Rice husk	–	–	–	0.6	[163]
Sorghum	–	–	–	0.3	[316]
	–	–	–	2.5	[54]
Spruce	–	–	–	0.0	[158]
Sugarcane bagasse	–	–	–	1.4	[167]
	–	–	–	1.1	[130]
Sweet gum	–	–	–	1.6	[161]
Switchgrass	17	83	n.d	0.2	[95]
	–	–	–	0.3	[316]
	–	–	–	0.4	[130]
	–	–	–	1.2	[54]
Tulip poplar	–	–	–	4.2, 5.2	[130]
Wheat straw	26	41	2	0.6	[166]
	–	–	–	0.5	[59]
	–	–	–	1.2	[54]
	–	–	–	1.3	[137]

used silica rather than routine desorption/ionization matrices, as silica has been previously proposed in mapping small analytes in biological tissues, and can reduce background noise in the measurement of low-mass species. Other recent developments in thermo-chemical analyses include a ToF-SIMS analysis of a mixed hardwood pulp containing birch, aspen, beech, and spruce [70], and the study of pine pyrolysis products using synchrotron vacuum ultraviolet photoionization mass spectrometry [306].

6.3. Chromatography

Chromatographic methods for lignin monomer analysis are typically used in conjunction with a wet chemical method such as DFRC, NBO or thioacidolysis. Headspace solid-phase microextraction and GC were used to evaluate six phenolic model compounds (acetophenone, acetosyringone, *p*-coumaric acid, guaiacol, 4-hydroxy-3-methoxyphenylacetone, and vanillin) found in the supernatant of liquid hot water pretreated biomass [56]. Once this stage was successfully optimized, the novel high-throughput method was applied to wheat straw. The effects of various storage conditions on the different phenolic compounds were also appraised. The authors conclude that freezing the sample may be the most ideal treatment, as variation in temperature led to the most significant alterations in concentration. Lastly, ultra-ahigh performance LC-tandem MS was used to assess sugarcane soluble lignin [311]. The authors developed an extensive mass spectral database containing 25 enzymatically synthesized monomers, dimers, and oligomers. Products resulting from an ethyl acetate extraction of sugarcane lignin were evaluated using this library.

6.4. Vibrational spectroscopy

6.4.1. Raman spectroscopy

Vibrational spectroscopy can be employed to measure lignin S/G ratios directly and indirectly by using multivariate analysis [65,95,96,111,112,124,130,134,163,304,312–317]. Sun et al. generated a rapid method for measuring S/G ratios in diverse feedstocks including *Eucalyptus* and *Arabidopsis* using FT-Raman spectroscopy. Vibrational modes corresponding to S and G lignin were established from model compounds, and then used in deconvoluting Raman spectra. A calibration equation comparing Raman and pyGCMS S/G ratios provided good correlation ($R^2 = 0.983$). The authors note that cellulose contributions were problematic in the spectral regions used for S and G lignin quantitation which could have led to the higher ratios calculated from the Raman spectra. Ona et al. have also surveyed the use of FT-Raman spectroscopy for the quantitation of the S/G ratio in *Eucalyptus* using 2nd derivative Raman spectra coupled with thioacidolysis results to construct a PLS regression model with a prediction R^2 of 0.935 [315]. A recent study evaluated the potential of high-throughput FT-Raman spectroscopy (compared with MIR and NIR spectroscopies), coupled with pyMBMS, for the development of multivariate, predictive models capable of screening hundreds of *Acacia* and eucalypt plants based on lignin S/G ratios [317]. Various spectral processing techniques were assessed, including 1st and 2nd derivative transformations, standard normal variate, multiplicative and extended multiplicative scatter correction, to gauge which methodology led to the most robust PLS models. The authors constructed three independent, randomly-generated calibration and validation matrices for the evaluation of

each type of spectral processing. RMSEPs were comparable between the Raman (0.13–0.16) and MIR models, but led to more accurate predictions when contrasted with NIR models (RMSEP=0.18–0.21). The spectral regions identified using the regression coefficients were assigned to respective lignin S, G, or H vibrational modes.

NIR, dispersive Raman spectroscopy innovations have illuminated ideal features for biomass analysis. A home-built, NIR, dispersive, multichannel, Raman spectrometer enabled an investigation of a variety of feedstocks with emphasis on herbaceous plants such as switchgrass and *Miscanthus* [95]. The 1600 cm^{-1} wavenumber region was identified as being free from polysaccharide contributions, therefore, the authors concluded, analyses focusing on lignin monomer content should concentrate on this spectral region. Raman spectra were conjoined with S and G lignin content measured by thioacidolysis/GCMS. A principal component regression model allowed for the rapid, accurate prediction of S and G lignin for most feedstocks (R^2=0.985–0.986).

UVRR spectroscopy was used to determine vibrational modes characteristic of S, G, and H lignin model compounds through employment of 229, 244, and 257 nm excitation [112]. The intensity of H structures was highest when excited with a 244 nm wavelength, and revealed features at 1167–1179 and 1214–1217 cm^{-1}. G compounds resulted in highest intensity when 257 nm excitation was used, with peaks at 704–791, 1155–1158, 1185–1187, and 1279–1289 cm^{-1}, while spectra of S model structures excited with 244 or 257 nm laser wavelengths revealed comparable intensities at 962–981, 1330–1333, and 1506–1514 cm^{-1}. Polysaccharide modes, which would overlay many of these spectral regions using visible or NIR excitation, were trivial, allowing application of these spectral regions to whole wood samples. Key vibrational modes for various lignin model compounds, including condensed, conjugated, and stilbene model compounds were elucidated using PLS modeling [111].

6.4.2. Mid-infrared spectroscopy

MIR spectroscopy was employed to measure the S lignin ratio (S/S+G) of 17 softwoods and 48 hardwoods [124]. Peak area ratios including 1595/1509, 1509/1460, 1275/1220, 1130/1032, and 835/(855+815) cm^{-1} were calculated, and after plotting on a logarithmic scale, the 1595/1509 and 1275/1220 cm^{-1} ratios were found to have the highest correlation coefficients (r=0.98) when compared to NBO results. The ratio of the 1325 and 1268 vibrational modes in the MIR spectra of 32 Organosolv-fractionated lignins was used to quantify the S/G ratio [130]. A comparison with another standard technique was not made. High-throughput MIR spectroscopy and pyMBMS were also employed in the development of PLS predictive models for the screening of *Acacia* and eucalypt plants based on lignin S/G ratios [317]. This instrument was compared with high-throughput Raman and NIR instruments, and was found to provide analogous RMSEPs as the Raman predictive models (MIR=0.13–0.15, Raman=0.13–0.16), but slightly higher accuracy than those constructed from NIR spectral data (RMSEP=0.18–0.21).

6.4.3. Near-infrared spectroscopy

NIR spectroscopy and analytical pyrolysis were employed to measure the H/G ratio of 68 maritime pine samples [312]. A validation set of 34 spectra, used to test the 34 sample calibration model, revealed good correlation (R^2=86%). NIR spectroscopy and analytical pyrolysis were also used to develop PLS models capable of predicting lignin S/G ratios from *E. globulus* [313]. Combinations of spectral preprocessing techniques were evaluated including 1st and 2nd derivative, vector normalization, multiplicative scatter correction, and straight-line subtraction. Regardless of the 1st derivative spectral processing technique, the correlation of determination was 0.96 with RMSEPs between 0.024–0.027. Second

derivative spectral data provided slightly less correlation (R^2=0.92) and higher error (RMSEP=0.036). NIR spectral data coupled with pyMBMS lignin S/G ratios allowed the formation of PLS predictive models for the high-throughput screening of *Acacia* and eucalypt plants [317]. The diminished structural features and spectral variance illustrated in the NIR spectral data were identified as the likely reasons that the NIR predictions were less accurate than those calculated using the MIR and Raman models.

6.5. Nuclear magnetic resonance

The unparalleled structural detail obtained using NMR has prompted researchers to routinely utilize this method in lignin monomer analysis, and S/G ratio determination [61,64,78,81,128, 134,137,141–143,146,154,156,158,161,166,167,196,318]. HSQC 2D-NMR was used to probe lignin monomer composition in young and adult eucalyptus trees [156]. The calculated S/G/H contents and S/G ratios were in close agreement with results obtained using pyGCMS, and indicated an increase of S lignin moieties with time. MSL and CEL isolated from wheat straw were assessed using HSQC and ^{13}C NMR [166]. The authors endeavored to develop a rapid and quantitative NMR method capable of spectrally resolving the crowded aromatic region of the NMR spectra prevalent in complex herbaceous lignin samples. The S/G ratio of the MSL and CEL was 0.63 and 0.69, respectively, whereas wet chemical degradative methods measured relatively even S and G contributions. The authors suggest that this NMR technique may be more suitable for depicting lignin monomer composition. Rencoret and co-authors developed a technique enabling the *in situ* analysis of *Agave*, eucalypt, and spruce lignins [158]. Swelling of the ball-milled samples was achieved using DMSO-d$_6$, resulting in a gel. MWL spectra allowed the identification of representative lignin peaks in the spectra of whole plant samples. Comparison of the S/G ratio of MWL to whole fiber revealed good agreement, thereby indicating that this technique could be employed to quantify key lignin moieties without requiring the tedious isolation of the lignin fraction. *Miscanthus* was thoroughly dissolved in DMSO-d$_6$ containing [Emim]Oac for analysis with HSQC 2D-NMR [143]. Other solvent systems reported in the literature such as DMSO-d$_6$/pyridine-d$_5$ or DMSO-d$_6$/NMI-d$_6$ (perdeuterated N-methylimidazole) do not completely dissolve the biomass. Application of a time-zero extrapolation to correct for differential relaxation resulted in more accurate measurements of phenotypic parameters including the lignin S/G ratio (0.67). The S/G ratios of *Miscanthus x giganteus* lignins, isolated using different solvents and reflux times, were quantified using HSQC 2D-NMR and these results were compared with those calculated from thioacidolysis/GCMS [196]. The S/G ratio did not significantly vary with increasing ethanol concentration or reflux time (0.54–0.61), but increased to 1.08 when dioxane was used as the reflux solvent (S/G=2.18, when GCMS quantitation was used). This alteration has not yet been determined to stem from the properties of the extraction solvents or from the modification of the isolated lignin. The analysis of the lignin monomer composition of ^{13}C-enriched corn stover dissolved in perdeuterated pyridinium chloride–DMSO-d$_6$ [146], lignin isolated from industrial black liquor [61], and changes in eucalypt lignin structure following alkaline delignification by kraft, AQ, and soda-AQ processed [64] further illustrate the advances and applications of HSQC 2D-NMR for the measurement of lignin monomer composition in complex environments for diverse feedstocks.

Xia et al. used ^{13}C and ^{31}P–NMR to quantitate hydroxyl and methoxyl functionalities in model compounds as well as Round-Robin standard lignins including Indulin kraft pulping, steam explosion yellow poplar, and steam explosion aspen lignins [318]. 1,3,5-trioxane and pentafluorobenzene were employed as internal standards to facilitate comparison with the results of other laboratories. NMR spectroscopy has been utilized for the

analysis of lignin monomer composition in other diverse ligno-cellulosic feedstocks including acacia [142,154], banana leaves [128], *Corymbia* [142], *Eucalyptus* [142,154], fruit and vegetable fiber [141], giant reed [81], *Miscanthus* [81], sugarcane [167], and wheat straw [137], to name a few.

7. Conclusions

This review provides a broad synopsis of recent, cutting-edge, research in the effort to cultivate a more thorough comprehension of lignin, qualitatively and quantitatively. Although no single method may stand alone as the superlative analytical method, techniques involving, for example, advances in NMR, imaging, mass spectrometry, and vibrational spectroscopy, during the last decade, have facilitated the construction of a more expansive toolbox to consult for a variety of lignin applications. While many laborious wet chemical techniques are still employed, and perhaps necessary for certain purposes, the development of high-through-put, multivariate analysis modeling as a way to efficiently screen biomass for key biofuel traits, such as low lignin content, or high S/G ratios, has enabled more plants to be surveyed with shorter analysis time, and decreased consumable usage. Advances in pyMBMS have provided another innovative, high-throughput technique for probing lignin monomer content. 2D-NMR is one of the most prevalent techniques developed during the last decade for probing lignin structure, linkages to carbohydrates, and quantifying specific functionalities and linkages present in lignin. Further advancements in these analytical tools, as well as in future methods yet to be conceived, can only build upon the foundation laid by the research described in this review.

Acknowledgements

References

[1] Sarkanen KV, Hergert HL. Classification and distribution. In: Sarkanen KV, Ludwig CH, editors. Lignins: occurrence and formation, structure, chemical and macromolecular properties, and utilization. New York (NY): John Wiley & Sons; 1971. p. 43–94.

[2] Tsutsumi Y, Kondo R, Sakai K, Imamura H. The difference of reactivity between syringyl lignin and guaiacyl lignin in alkaline systems. Holzforschung 1995;49:423–8.

[3] Li X, Ximenes E, Kim Y, Slininger M, Meilan R, Ladisch M, et al. Lignin monomer composition affects *Arabidopsis* cell-wall degradability after liquid hot water pretreatment. Biotechnol Biofuels 2010;3:27–33.

[4] Studer MH, DeMartini JD, Davis MF, Sykes RW, Davison B, Keller M, et al. Lignin content in natural *Populus* variants affects sugar release. Proc Natl Acad Sci USA 2011;108:6300–5 S/1–S/6.

[5] Davison BH, Drescher SR, Tuskan GA, Davis MF, Nghiem NP. Variation of S/G ratio and lignin content in a *Populus* family influences the release of xylose by dilute acid hydrolysis. Appl Biochem Biotechnol. 2006;129–132:427–35.

[6] Chen M, Zhao J, Xia L. Comparison of four different chemical pretreatments of corn stover for enhancing enzymatic digestibility. Biomass Bioenergy 2009;33:1381–5.

[7] Nakagame S, Chandra RP, Saddler JN. The effect of isolated lignins, obtained from a range of pretreated lignocellulosic substrates, on enzymatic hydrolysis. Biotechnol Bioeng 2009;105:871–9.

[8] Nakagame S, Chandra RP, Saddler JN. The influence of lignin on enzymatic hydrolysis of pretreated biomass substrates. ACS Symp Ser 2011;1067:145–67.

[9] Yu Z, Jameel H, Chang H-m, Park S. The effect of delignification of forest biomass on enzymatic hydrolysis. Bioresour Technol 2011;102:9083–9.

[10] Blanch HW, Simmons BA, Klein-Marcuschamer D. Biomass deconstruction to sugars. Biotechnol J 2011;6:1086–102.

[11] Sathitsuksanoh N, Holtman KM, Yelle DJ, Morgan T, Stavila V, Pelton J, et al. Lignin fate and characterization during ionic liquid biomass pretreatment for renewable chemicals and fuels production. Green Chem 2014;16:1236–47.

[12] Shi J, Gladden JM, Sathitsuksanoh N, Kambam P, Sandoval L, Mitra D, et al. One-pot ionic liquid pretreatment and saccharification of switchgrass. Green Chem 2013;15:2579–89.

[13] Bule MV, Gao AH, Hiscox B, Chen S. Structural modification of lignin and characterization of pretreated wheat straw by ozonation. J Agric Food Chem 2013;61:3916–25.

[14] Chiaramonti D, Prussi M, Ferrero S, Oriani L, Ottonello P, Torre P, et al. Review of pretreatment processes for lignocellulosic ethanol production, and development of an innovative method. Biomass Bioenergy 2012;46:25–35.

[15] Gargulak JD, Lebo SE. Commercial use of lignin-based materials. ACS Symp Ser 2000;742:304–20.

[16] Hu TQ., editor. Chemical modification, properties, and usage of lignin; 2002.

[17] Pourhashem G, Adler PR, McAloon AJ, Spatari S. Cost and greenhouse gas emission tradeoffs of alternative uses of lignin for second generation ethanol. Environ Res Lett 2013;8:025021/1–13.

[18] Varanasi P, Singh P, Auer M, Adams PD, Simmons BA, Singh S. Survey of renewable chemicals produced from lignocellulosic biomass during ionic liquid pretreatment. Biotechnol Biofuels 2013;6:14.

[19] Zakzeski J, Bruijnincx PCA, Jongerius AL, Weckhuysen BM. The catalytic valorization of lignin for the production of renewable chemicals. Chem Rev (Washington, DC, United States) 2010;110:3552–99.

[20] Hatfield R, Fukushima RS. Can lignin be accurately measured? Crop Sci 2005;45:832–9.

[21] Brunow G. Methods to reveal the structure of lignin. Biopolymers 2001;1:89–116.

[22] Lapierre C. Determining lignin structure by chemical degradations. In: Heitner C, Dimmel DR, Schmidt JA, editors. Lignin and lignans: advances in chemistry. Boca Raton (FL): CRC Press; 2010. p. 11–48.

[23] Reale S, di Tullio A, Spreti N, de Angelis F. Mass spectrometry in the biosynthetic and structural investigation of lignins. Mass Spectrom Rev 2004;23:87–126.

[24] Laskar DD, Ke J, Zeng J, Gao X, Chen S. Py-GC/MS as a powerful and rapid tool for determining lignin compositional and structural changes in biological processes. Curr Anal Chem 2013;9:335–51.

[25] Amen-Chen C, Pakdel H, Roy C. Production of monomeric phenols by thermochemical conversion of biomass: a review. Bioresour Technol 2001;79:277–99.

[26] Ghaffar SH, Fan M. Structural analysis for lignin characteristics in biomass straw. Biomass Bioenergy 2013;57:264–79.

[27] Ralph J, Landucci Larry L. NMR of lignins. In: Heitner C, Dimmel DR, Schmidt JA, editors. Lignin and lignans: advances in chemistry. Boca Raton (FL): CRC Press; 2010. p. 137–244.

[28] Argyropoulos DS. Heteronuclear NMR spectroscopy of lignins. In: Heitner C, Dimmel DR, Schmidt JA, editors. Lignin and lignans: advances in chemistry. Boca Raton, FL: CRC Press; 2010. p. 245–65.

[29] Lupoi JS, Singh S, Simmons BA, Henry RJ. Assessment of lignocellulosic biomass using analytical spectroscopy: an evolution to high-throughput techniques. Bioenergy Res 2013.

[30] Balakshin MY, Capanema EA, Chang H-m. Recent advances in the isolation and analysis of lignins and lignin–carbohydrate complexes. Charact Lignocell Mater 2008:148–70.

[31] Maunu SL. 13C CPMAS NMR studies of wood, cellulose fibers, and derivatives. Charact Lignocell Mater 2008:227–48.

[32] Agarwal UP. An overview of Raman spectroscopy as applied to lignocellulosic materials. Adv Lignocellul Charact 1999:201–25.

[33] Agarwal UP, Atalla, Rajai H. Vibrational spectroscopy. In: Heitner C, Dimmel DR, Schmidt JA, editors. Lignin and lignans: advances in chemistry. Boca Raton, FL: CRC Press; 2010. p. 103–36.

[34] Moore AK, Owen NL. Infrared spectroscopic studies of solid wood. Appl Spectrosc Rev 2001;36:65–86.

[35] Tsuchikawa S. A review of recent near infrared research for wood and paper. Appl Spectrosc Rev 2007;42:43–71.

[36] Workman Jr. JJ. Infrared and Raman spectroscopy in paper and pulp analysis. Appl Spectrosc Rev 2001;36:139–68.

[37] Schmidt JA. Electronic spectroscopy of lignins. In: Heitner C, Dimmel DR, Schmidt JA, editors. Lignin and lignans: advances in chemistry. Boca Raton (FL): CRC Press; 2010. p. 49–102.

[38] Schwanninger M, Rodrigues JC, Fackler K. A review of band assignments in near infrared spectra of wood and wood components. J Near Infrared Spectrosc 2011;19:287–308.

[39] Brunow G, Lundquist K. Functional groups and bonding patterns in lignin (including the lignin–carbohydrate complexes). In: Heitner C, Dimmel DR, Schmidt JA, editors. Lignin and lignans: advances in chemistry. Boca Raton (FL): CRC Press; 2010. p. 267–99.

[40] Chen CL. Determination of carbonyl groups [in lignin]. In: Lin SY, Dence CW, editors. Methods in lignin chemistry. Berlin (DE): Springer-Verlag; 1992. p. 446–57.

[41] Chen CL. Determination of methoxyl groups [in lignin]. In: Lin SY, Dence CW, editors. Methods in lignin chemistry. Berlin (DE): Springer-Verlag; 1992. p. 465–72.

[42] Chen CL. Determination of total and aliphatic hydroxyl groups [in lignin]. In: Lin SY, Dence, CW, editors. Methods in lignin chemistry; 1992. p. 409–22.

[43] Dence CW. Determination of carboxyl groups [in lignin]. In: Lin SY, Dence CW, editors. Methods in lignin chemistry. Berlin (DE): Springer-Verlag; 1992. p. 458–64.

[44] El Mansouri N-E, Salvado J. Analytical methods for determining functional groups in various technical lignins. Ind Crops Prod 2007;26:116–24.

[45] Eshkiki RB, Mortha G, Lachenal D. A new method for the titration of free phenolic groups in pulps. Holzforschung 2007;61:242–6.

[46] Faix O, Andersons B, Zakis G. Determination of carbonyl groups of six round robin lignins by modified oximation and FTIR spectroscopy. Holzforschung 1998;52:268–74.

[47] Gosselink RJA, Abacherli A, Semke H, Malherbe R, Kauper P, Nadif A, et al. Analytical protocols for characterisation of sulphur-free lignin. Ind Crops Prod 2004;19:271–81.

[48] Lai YZ. Determination of phenolic hydroxyl groups [in lignin]. In: Lin SY, Dence CW, editors. Methods in lignin chemistry. Berlin (DE): Springer-Verlag; 1992. p. 423–34.

[49] Lai YZ, Xu H, Yang R. An overview of chemical degradation methods for determining lignin condensed units. ACS Symp Ser 2000;742:239–49.

[50] Zakis G.F. Functional analysis of lignins and their derivatives 1994.

[51] Milne TA, Chum HL, Agblevor F, Johnson DK. Standardized analytical methods. Biomass Bioenergy 1992;2:341–66.

[52] Dupont A-L, Egasse C, Morin A, Vasseur F. Comprehensive characterization of cellulose- and lignocellulose degradation products in aged papers: capillary zone electrophoresis of low-molar mass organic acids, carbohydrates, and aromatic lignin derivatives. Carbohydr Polym 2007;68:1–16.

[53] Gora R, Hutta M, Vrska M, Katuscak S, Jablonsky M. Characterization of Klason lignins by reversed phase high-performance liquid chromatography using wide-pore octadecylsilica and stepwise gradients of dimethylforma-mide in water. J Sep Sci 2006;29:2179–89.

[54] Hatfield RD, Marita JM, Frost K, Grabber J, Ralph J, Lu F, et al. Grass lignin acylation: p-Coumaroyl transferase activity and cell wall characteristics of C3 and C4 grasses. Planta 2009;229:1253–67.

[55] Li H, Chai X-S, Liu M, Deng Y. Novel method for the determination of the methoxyl content in lignin by headspace gas chromatography. J Agric Food Chem 2012;60:5307–10.

[56] Kolb M, Schieder D, Faulstich M, Sieber V. Analysis of lignocellulose derived phenolic monomers by headspace solid-phase microextraction and gas chromatography. J Chromatogr A 2013;1307:144–57.

[57] Lu F, Ralph J. Derivatization followed by reductive cleavage (DFRC method), a new method for lignin analysis: protocol for analysis of DFRC monomers. J Agric Food Chem 1997;45:2590–2.

[58] Matsui N, Ohira T. Analysis of broad leaf lignin of Japanese angiospermous trees by DFRC (derivatization followed by reductive cleavage) method. Plant Physiol Biochem (Issy-les-Moulineaux, France) 2013;72:112–5.

[59] del Rio JC, Rencoret J, Prinsen P, Martinez AT, Ralph J, Gutierrez A. Structural characterization of wheat straw lignin as revealed by analytical pyrolysis, 2D-NMR, and reductive cleavage methods. J Agric Food Chem 2012;60:5922–35.

[60] Fox SC, McDonald AG. Chemical and thermal characterization of three industrial lignins and their corresponding lignin esters. BioResources 2010;5:990–1009.

[61] Hu J, Shen D, Xiao R, Wu S, Zhang H. Free-radical analysis on thermochemical transformation of lignin to phenolic compounds. Energy Fuels 2013;27:285–93.

[62] Modugno F, Ribechini E, Calderisi M, Giachi G, Colombini MP. Analysis of lignin from archaeological waterlogged wood by direct exposure mass spectrometry (DE-MS) and PCA evaluation of mass spectral data. Microchem J 2008;88:186–93.

[63] Ohra-aho T, Gomes FJB, Colodette JL, Tamminen T. S/G ratio and lignin structure among Eucalyptus hybrids determined by Py-GC/MS and nitro-benzene oxidation. J Anal Appl Pyrolysis 2013;101:166–71.

[64] Prinsen P, Rencoret J, Gutierrez A, Liitia T, Tamminen T, Colodette JL, et al. Modification of the lignin structure during alkaline delignification of Eucalyptus Wood by Kraft, Soda-AQ, and Soda-O2 cooking. Ind Eng Chem Res 2013;52:15702–12.

[65] del Rio JC, Gutierrez A, Rodriguez IM, Ibarra D, Martinez AT. Composition of non-woody plant lignins and cinnamic acids by Py-GC/MS, Py/TMAH and FT-IR. J Anal Appl Pyrolysis 2007;79:39–46.

[66] Alves A, Gierlinger N, Schwanninger M, Rodrigues J. Analytical pyrolysis as a direct method to determine the lignin content in wood. J Anal Appl Pyrolysis 2009;85:30–7.

[67] Banoub JH, Benjelloun-Mlayah B, Ziarelli F, Joly N, Delmas M. Elucidation of the complex molecular structure of wheat straw lignin polymer by atmospheric pressure photoionization quadrupole time-of-flight tandem mass spectrometry. Rapid Commun Mass Spectrom 2007;21:2867–88.

[68] Araújo P, Ferreira MS, deOliveira DN, Pereira L, Sawaya AC, Catharino RR, Mazzafera P. Mass spectrometry imaging: an expeditious and powerful technique for fast in situ lignin assessment in Eucalyptus. Anal Chem. 2014;86(7):3415–9 (ISSN: 1520-6882) http://dx.doi.org/10.1021/ac500220r.

[69] Goacher RE, Jeremic D, Master ER. Expanding the library of secondary ions that distinguish lignin and polysaccharides in time-of-flight secondary ion mass spectrometry analysis of wood. Anal Chem (Washington, DC, United States) 2011;83:804–12.

[70] Kleen M. Surface lignin and extractives on hardwood RDH kraft pulp chemically characterized by ToF-SIMS. Holzforschung 2005;59:481–7.

[71] Mou H-Y, Orblin E, Kruus K, Fardim P. Topochemical pretreatment of wood biomass to enhance enzymatic hydrolysis of polysaccharides to sugars. Bioresour Technol 2013;142:540–5.

[72] Mukarakate C, Scheer AM, Robichaud DJ, Jarvis MW, David DE, Ellison GB, et al. Laser ablation with resonance-enhanced multiphoton ionization time-of-flight mass spectrometry for determining aromatic lignin volatilization products from biomass. Rev Sci Instrum 2011;82:033104/1–10.

[73] Richel A, Vanderghem C, Simon M, Wathelet B, Paquot M. Evaluation of matrix-assisted laser desorption/ionization mass spectrometry for second-generation lignin analysis. Anal Chem Insights 2012;7:79–89.

[74] Saito K, Kato T, Takamori H, Kishimoto T, Yamamoto A, Fukushima K. A new analysis of the depolymerized fragments of lignin polymer in the plant cell walls using ToF-SIMS. Appl Surf Sci 2006;252:6734–7.

[75] Souza-Correa JA, Ridenti MA, Oliveira C, Araujo SR, Amorim J. Decomposition of lignin from sugar cane bagasse during ozonation process monitored by optical and mass spectrometries. J Phys Chem B 2013;117:3110–9.

[76] Tokareva EN, Fardim P, Pranovich AV, Fagerholm HP, Daniel G, Holmbom B. Imaging of wood tissue by ToF-SIMS: Critical evaluation and development of sample preparation techniques. Appl Surf Sci 2007;253:7569–77.

[77] Xia G-G, Chen B, Zhang R, Zhang ZC. Catalytic hydrolytic cleavage and oxy-cleavage of lignin linkages. J Mol Catal A Chem 2014;388-389(July):35–40. http://dx.doi.org/10.1016/j.molcata.2013.08.016 in press.

[78] Awal A, Sain M. Spectroscopic studies and evaluation of thermorheological properties of softwood and hardwood lignin. J Appl Polym Sci 2011;122:956–63.

[79] Casas A, Oliet M, Alonso MV, Rodriguez F. Dissolution of Pinus radiata and Eucalyptus globulus woods in ionic liquids under microwave radiation: lignin regeneration and characterization. Sep Purif Technol 2012;97:115–22.

[80] Martin-Sampedro R, Capanema EA, Hoeger I, Villar JC, Rojas OJ. Lignin changes after steam explosion and laccase-mediator treatment of eucalyptus wood chips. J Agric Food Chem 2011;59:8761–9.

[81] Savy D, Piccolo A. Physical-chemical characteristics of lignins separated from biomasses for second-generation ethanol. Biomass Bioenergy 2014 in press.

[82] Sebio-Punal T, Naya S, Lopez-Beceiro J, Tarrio-Saavedra J, Artiaga R. Thermo-gravimetric analysis of wood, holocellulose, and lignin from five wood species. J Therm Anal Calorimetry 2012;109:1163–7.

[83] Zhang J, Feng L, Wang D, Zhang R, Liu G, Cheng G. Thermogravimetric analysis of lignocellulosic biomass with ionic liquid pretreatment. Bioresour Technol 2014;153:379–82.

[84] Agarwal UP. Raman spectroscopic characterization of wood and pulp fibers. Charact Lignocellul. Mater 2008:17–35.

[85] Agarwal UP, McSweeny JD, Ralph SA. FT-Raman investigation of milled-wood lignins: softwood, hardwood, and chemically modified black spruce lignins. J Wood Chem Technol 2011;31:324–44.

[86] Agarwal UP, Ralph SA. Determination of ethylenic residues in wood and TMP of spruce by FT-Raman spectroscopy. Holzforschung 2008;62:667–75.

[87] Agarwal UP, Ralph SA. FT-Raman spectroscopy of wood: identifying con-tributions of lignin and carbohydrate polymers in the spectrum of black spruce (Picea mariana). Appl Spectrosc 1997;51:1648–55.

[88] Larsen KL, Barsberg S. Theoretical and Raman spectroscopic studies of phenolic lignin model monomers. J Phys Chem B 2010;114:8009–21.

[89] Larsen KL, Barsberg S. Environmental effects on the lignin model monomer, vanillyl alcohol, studied by raman spectroscopy. J Phys Chem B 2011;115:11470–80.

[90] Kihara M, Takayama M, Wariishi H, Tanaka H. Determination of the carbonyl groups in native lignin utilizing Fourier transform Raman spectroscopy. Spectrochim Acta, Part A Mol Biomol Spectrosc 2002;58A:2213–21.

[91] Chundawat SPS, Donohoe BS, Sousa LdC, Elder T, Agarwal UP, Lu F, et al. Multi-scale visualization and characterization of lignocellulosic plant cell wall deconstruction during thermochemical pretreatment. Energy Environ Sci 2011;4:973–84.

[92] Li C, Cheng G, Balan V, Kent MS, Ong M, Chundawat SPS, et al. Influence of physico-chemical changes on enzymatic digestibility of ionic liquid and AFEX pretreated corn stover. Bioresour Technol 2011;102:6928–36.

[93] Liu L, Ye XP, Womac AR, Sokhansanj S. Variability of biomass chemical composition and rapid analysis using FT-NIR techniques. Carbohydr Polym 2010;81:820–9.

[94] Li C, Sun L, Simmons BA, Singh S. Comparing the recalcitrance of eucalyptus, pine, and switchgrass using ionic liquid and dilute acid pretreatments. BioEnergy Res 2013;6:14–23.

[95] Lupoi JS, Smith EA. Characterization of woody and herbaceous biomasses lignin composition with 1064 nm dispersive multichannel Raman spectro-scopy. Appl Spectrosc 2012;66:903–10.

[96] Meyer MW, Lupoi JS, Smith EA. 1064 nm dispersive multichannel Raman spectroscopy for the analysis of plant lignin. Anal Chim Acta 2011;706:164–70.

[97] Sun L, Li C, Xue Z, Simmons BA, Singh S. Unveiling high-resolution, tissue specific dynamic changes in corn stover during ionic liquid pretreatment. RSC Adv 2013;3:2017–27.

[98] Sun L, Simmons BA, Singh S. Understanding tissue specific compositions of bioenergy feedstocks through hyperspectral Raman imaging. Biotechnol Bioeng 2010;108:286–95.

[99] Agarwal UP. Raman imaging to investigate ultrastructure and composition of plant cell walls: distribution of lignin and cellulose in black spruce wood (Picea mariana). Planta 2006;224:1141–53.

[100] Chu L-Q, Masyuko R, Sweedler JV, Bohn PW. Base-induced delignification of Miscanthus x giganteus studied by three-dimensional confocal raman imaging. Bioresour Technol 2010;101:4919–25.

[101] Gierlinger N, Schwanninger M. Chemical imaging of poplar wood cell walls by confocal Raman microscopy. Plant Physiol 2006;140:1246–54.

[102] Ji Z, Ma J-F, Zhang Z-H, Xu F, Sun R-C. Distribution of lignin and cellulose in compression wood tracheids of Pinus yunnanensis determined by fluorescence microscopy and confocal Raman microscopy. Ind Crops Prod 2013;47: 212–7.

[103] Ma J, Ji Z, Zhou X, Zhang Z, Xu F. Transmission electron microscopy, fluorescence microscopy, and confocal Raman microscopic analysis of ultrastructural and compositional heterogeneity of Cornus alba L. wood cell wall. Microsc Microanal 2013;19:243–53.

[104] Saar BG, Zeng Y, Freudiger CW, Liu Y-S, Himmel ME, Xie XS, et al. Label-free, real-time monitoring of biomass processing with stimulated raman scattering microscopy. Angew Chem, Int Ed. 2010;49:5476–9 S1–S/5.

[105] Barsberg S, Matousek P, Towrie M. Structural analysis of lignin by resonance Raman spectroscopy. Macromol Biosci 2005;5:743–52.

[106] Barsberg S, Matousek P, Towrie M, Joergensen H, Felby C. Lignin radicals in the plant cell wall probed by Kerr-gated resonance Raman spectroscopy. Biophys J 2006;90:2978–86.

[107] Jaaskelaeinen A-S, Saariaho A-M, Vuorinen T. Quantification of lignin and hexenuronic acid in bleached hardwood kraft pulps: a new calibration method for UVRR spectroscopy and evaluation of the conventional methods. J Wood Chem Technol 2005;25:51–65.

[108] Jaaskelainen A-S, Saariaho A-M, Vyorykka J, Vuorinen T, Matousek P, Parker AW. Application of UV–vis and resonance Raman spectroscopy to study bleaching and photoyellowing of thermomechanical pulps. Holzforschung 2006;60:231–8.

[109] Nuopponen M, Vuorinen T, Jaemsae S, Viitaniemi P. Thermal modifications in softwood studied by FT-IR and UV resonance Raman spectroscopies. J Wood Chem Technol 2004;24:13–26.

[110] Nuopponen MH, Wikberg HI, Birch GM, Jaaskelainen A-S, Maunu SL, Vuorinen T, et al. Characterization of 25 tropical hardwoods with Fourier transform infrared, ultraviolet resonance Raman, and 13C NMR cross-polarization/magic-angle spinning spectroscopy. J Appl Polym Sci 2006;102:810–9.

[111] Saariaho A-M, Argyropoulos DS, Jaeaeskelaeinen A-S, Vuorinen T. Development of the partial least squares models for the interpretation of the UV resonance Raman spectra of lignin model compounds. Vib Spectrosc 2005;37:111–21.

[112] Saariaho A-M, Jaaskelainen A-S, Nuopponen M, Vuorinen T. Ultraviolet resonance Raman spectroscopy in lignin analysis: determination of characteristic vibrations of p-hydroxyphenyl, guaiacyl, and syringyl lignin structures. Appl Spectrosc 2003;57:58–66.

[113] Saariaho A-M, Jaeaeskelaeinen A-S, Matousek P, Towrie M, Parker AW, Vuorinen T. Resonance Raman spectroscopy of highly fluorescing lignin containing chemical pulps: suppression of fluorescence with an optical Kerr gate. Holzforschung 2004;58:82–90.

[114] Warsta E, Lahdetie A, Jaaskelainen A-S, Vuorinen T. Effect of pH on lignin analysis by Raman spectroscopy. Holzforschung 2012;66:451–7.

[115] Pandey KK, Vuorinen T. UV resonance Raman spectroscopic study of photodegradation of hardwood and softwood lignins by UV laser. Holzforschung 2008;62:183–8.

[116] Pohling C, Brackmann C, Duarte A, Buckup T, Enejder A, Motzkus M. Chemical imaging of lignocellulosic biomass by CARS microscopy. J Biophoton 2014;7: 126–34.

[117] Zeng Y, Himmel ME, Ding S-Y. Coherent Raman microscopy analysis of plant cell walls. Methods Mol Biol (New York, NY, United States) 2012;908: 49–60.

[118] Brebu M, Tamminen T, Spiridon I. Thermal degradation of various lignins by TG-MS/FTIR and Py-GC–MS. J Anal Appl Pyrol 2013;104:531–9.

[119] Cetinkol OP, Dibble DC, Cheng G, Kent MS, Knierim B, Auer M, et al. Understanding the impact of ionic liquid pretreatment on eucalyptus. Biofuels 2010;1:33–46.

[120] Djikanovic D, Kalauzi A, Radotic K, Lapierre C, Jeremic M. Deconvolution of lignin fluorescence spectra: a contribution to the comparative structural studies of lignins. Russ J Phys Chem A 2007;81:1425–8.

[121] Hoareau W, Trindade WG, Siegmund B, Castellan A, Frollini E. Sugar cane bagasse and curaua lignins oxidized by chlorine dioxide and reacted with furfuryl alcohol: characterization and stability. Polym Degrad Stab 2004;86: 567–76.

[122] Hu J, Xiao R, Shen D, Zhang H. Structural analysis of lignin residue from black liquor and its thermal performance in thermogravimetric-Fourier transform infrared spectroscopy. Bioresour Technol 2013;128:633–9.

[123] Huang F, Singh PM, Ragauskas AJ. Characterization of Milled Wood Lignin (MWL) in Loblolly Pine Stem Wood, Residue, and Bark. J Agric Food Chem 2011;59:12910–6.

[124] Huang Y, Wang L, Chao Y, Nawawi DS, Akiyama T, Yokoyama T, et al. Analysis of lignin aromatic structure in wood based on the IR spectrum. J Wood Chem Technol 2012;32:294–303.

[125] Kline LM, Hayes DG, Womac AR, Labbe N. Simplified determination of lignin content in hard and soft woods via UV-spectrophotometric analysis of biomass dissolved in ionic liquids. BioResources 2010;5:1366–83.

[126] Marques AV, Pereira H, Rodrigues J, Meier D, Faix O. Isolation and comparative characterization of a Bjoerkman lignin from the saponified cork of Douglas-fir bark. J Anal Appl Pyrolysis 2006;77:169–76.

[127] Notley SM, Norgren M. Surface energy and wettability of spin-coated thin films of lignin isolated from wood. Langmuir 2010;26:5484–90.

[128] Oliveira L, Evtuguin DV, Cordeiro N, Silvestre AJD, Silva AMS, Torres IC. Structural characterization of lignin from leaf sheaths of dwarf cavendish banana plant. J Agric Food Chem 2006;54:2598–605.

[129] Pereira AA, Martins GF, Antunes PA, Conrrado R, Pasquini D, Job AE, et al. Lignin from sugar cane bagasse: extraction, fabrication of nanostructured films, and application. Langmuir 2007;23:6652–9.

[130] Sammons RJ, Harper DP, Labbe N, Bozell JJ, Elder T, Rials TG. Characterization of organosolv lignins using thermal and FT-IR spectroscopic analysis. BioResources 2013;8:2752–67 16 pp.

[131] Singh S, Simmons BA, Vogel KP. Visualization of biomass solubilization and cellulose regeneration during ionic liquid pretreatment of switchgrass. Biotechnol Bioeng 2009;104:68–75.

[132] Sun R, Tomkinson J, Wang S, Zhu W. Characterization of lignins from wheat straw by alkaline peroxide treatment. Polym Degrad Stab 1999;67:101–7.

[133] Sun X-F, Wang H, Zhang G, Fowler P, Rajaratnam M. Extraction and characterization of lignins from maize stem and sugarcane bagasse. J Appl Polym Sci 2011;120:3587–95.

[134] Sun Y-C, Lin Z, Peng W-X, Yuan T-Q, Xu F, Wu Y-Q, et al. Chemical changes of raw materials and manufactured binderless boards during hot pressing: lignin isolation and characterization. BioResources 2014;9:1055–71 17 pp.

[135] Villaverde JJ, Li J, Ek M, Ligero P, de Vega A. Native lignin structure of Miscanthus × giganteus and its changes during acetic and formic acid fractionation. J Agric Food Chem 2009;57:6262–70.

[136] Xu G, Wang L, Liu J, Wu J. FTIR and XPS analysis of the changes in bamboo chemical structure decayed by white-rot and brown-rot fungi. Appl Surf Sci 2013;280:799–805.

[137] Yang H, Zheng X, Yao L, Xie Y. Structural changes of lignin in the soda-AQ pulping process studied using the carbon-13 tracer method. BioResources 2014;9:176–90.

[138] Zhang Y, Wang Q, Fan X, Yuan J. Structural changes of lignin in the jute fiber treated by laccase and mediator system. J Mol Catal B Enzymatic 2014;101:133–6.

[139] Kubo S, Kadla JF. Hydrogen bonding in lignin: a Fourier transform infrared model compound study. Biomacromolecules 2005;6:2815–21.

[140] Bardet M, Gerbaud G, Giffard M, Doan C, Hediger S, Pape LL. 13C high-resolution solid-state NMR for structural elucidation of archaeological woods. Prog Nucl Magn Reson Spectrosc 2009;55:199–214.

[141] Bunzel M, Ralph J. NMR characterization of lignins isolated from fruit and vegetable insoluble dietary fiber. J Agric Food Chem 2006;54:8352–61.

[142] Cetinkol OP, Smith-Moritz AM, Cheng G, Lao J, George A, Hong K, et al. Structural and chemical characterization of hardwood from tree species with applications as bioenergy feedstocks. PLoS One 2012;7:e52820.

[143] Cheng K, Sorek H, Zimmermann H, Wemmer DE, Pauly M. Solution-state 2D NMR spectroscopy of plant cell walls enabled by a dimethylsulfoxide-d6/1-ethyl-3-methylimidazolium acetate solvent. Anal Chem (Washington, DC, United States) 2013;85:3213–21.

[144] Cybulska I, Brudecki G, Rosentrater K, Julson JL, Lei H. Comparative study of organosolv lignin extracted from prairie cordgrass, switchgrass and corn stover. Bioresour Technol 2012;118:30–6.

[145] del Rio JC, Prinsen P, Rencoret J, Nieto L, Jimenez-Barbero J, Ralph J, et al. Structural characterization of the lignin in the cortex and pith of elephant grass (Pennisetum purpureum) stems. J Agric Food Chem 2012;60: 3619–34.

[146] Foston M, Samuel R, Ragauskas AJ. 13C cell wall enrichment and ionic liquid NMR analysis: progress towards a high-throughput detailed chemical analysis of the whole plant cell wall. Analyst (Cambridge, United Kingdom) 2012;137:3904–9.

[147] Guerra A, Filpponen I, Lucia LA, Argyropoulos DS. Comparative evaluation of three lignin isolation protocols for various wood species. J Agric Food Chem 2006;54:9696–705.

[148] Hallac BB, Sannigrahi P, Pu Y, Ray M, Murphy RJ, Ragauskas AJ. Biomass characterization of Buddleja davidii: a potential feedstock for biofuel production. J Agric Food Chem 2009;57:1275–81.

[149] Hedenstroem M, Wiklund-Lindstroem S, Oeman T, Lu F, Gerber L, Schatz P, et al. Identification of lignin and polysaccharide modifications in Populus wood by chemometric analysis of 2D NMR spectra from dissolved cell walls. Mol Plant 2009;2:933–42.

[150] Holtman KM, Chang H-M, Kadla JF. An NMR comparison of the whole lignin from milled wood, MWL, and REL dissolved by the DMSO/NMI procedure. J Wood Chem Technol 2007;27:179–200.

[151] Kanitskaya LV, Gogotov AF, Khai DTT, Rokhin AV. Quantitative 13C NMR spectroscopy. Chemical structure of kraft and nitrosated lignins. Russ J Bioorg Chem 2012;38:720–5.

[152] Katahira R, Sluiter JB, Schell DJ, Davis MF. Degradation of carbohydrates during dilute sulfuric acid pretreatment can interfere with lignin measurements in solid residues. J Agric Food Chem 2013;61:3286–92.

[153] Mansfield SD, Kim H, Lu F, Ralph J. Whole plant cell wall characterization using solution-state 2D NMR. Nat Protoc 2012;7:1579–89.

[154] Pinto PC, Evtuguin DV, Pascoal Neto C. Effect of structural features of wood biopolymers on hardwood pulping and bleaching performance. Ind Eng Chem Res 2005;44:9777–84.

[155] Pinto PC, Evtuguin DV, Pascoal Neto C. Chemical composition and structural features of the macromolecular components of plantation Acacia mangium wood. J Agric Food Chem 2005;53:7856–62.

[156] Rencoret J, Gutierrez A, Nieto L, Jimenez-Barbero J, Faulds CB, Kim H, et al. Lignin composition and structure in young versus adult *Eucalyptus globulus* plants. Plant Physiol 2011;155:667–82.

[157] Rencoret J, Marques G, Gutierrez A, Ibarra D, Li J, Gellerstedt G, et al. Structural characterization of milled wood lignins from different eucalypt species. Holzforschung 2008;62:514–26.

[158] Rencoret J, Marques G, Gutierrez A, Nieto L, Santos JI, Jimenez-Barbero J, et al. HSQC-NMR analysis of lignin in woody (*Eucalyptus globulus* and *Picea abies*) and non-woody (*Agave sisalana*) ball-milled plant materials at the gel state. Holzforschung 2009;63:691–8.

[159] Rencoret J, Ralph J, Marques G, Gutierrez A, Martinez AT, del Rio JC. Structural characterization of lignin isolated from coconut (*Cocos nucifera*) coir fibers. J Agric Food Chem 2013;61:2434–45.

[160] Samuel R, Pu Y, Raman B, Ragauskas AJ. Structural characterization and comparison of switchgrass ball-milled lignin before and after dilute acid pretreatment. Appl Biochem Biotechnol 2010;162:62–74.

[161] Santos RB, Capanema EA, Balakshin MY, Chang H-m, Jameel H. Lignin structural variation in hardwood species. J Agric Food Chem 2012;60:4923–30.

[162] Terashima N, Akiyama T, Ralph S, Evtuguin D, Pascoal Neto C, Parkas J, et al. 2D-NMR (HSQC) difference spectra between specifically 13C-enriched and unenriched protolignin of Ginkgo biloba obtained in the solution state of whole cell wall material. Holzforschung 2009;63:379–84.

[163] Wu M, Pang J, Lu F, Zhang X, Che L, Xu F, et al. Application of new expansion pretreatment method on agricultural waste. Part I: influence of pretreatment on the properties of lignin. Ind Crops Prod 2013;50:887–95.

[164] Yan J, Hu Z, Pu Y, Charles Brummer E, Ragauskas AJ. Chemical compositions of four switchgrass populations. Biomass Bioenergy 2010;34:48–53.

[165] Yelle DJ, Kaparaju P, Hunt CG, Hirth K, Kim H, Ralph J, et al. Two-dimensional NMR evidence for cleavage of lignin and xylan substituents in wheat straw through hydrothermal pretreatment and enzymatic hydrolysis. BioEnergy Res 2013;6:211–21.

[166] Zeng J, Helms GL, Gao X, Chen S. Quantification of wheat straw lignin structure by comprehensive NMR analysis. J Agric Food Chem 2013;61: 10848–57.

[167] Zeng J, Tong Z, Wang L, Zhu JY, Ingram L. Isolation and structural characterization of sugarcane bagasse lignin after dilute phosphoric acid plus steam explosion pretreatment and its effect on cellulose hydrolysis. Bioresour Technol 2014;154:274–81.

[168] Zhang A, Lu F, Sun R, Ralph J. Ferulate-coniferyl alcohol cross-coupled products formed by radical coupling reactions. Planta 2009;229:1099–108.

[169] Cui C, Sun R, Argyropoulos DS. Fractional precipitation of softwood kraft lignin: isolation of narrow fractions common to a variety of lignins. ACS Sustain Chem Eng 2014;2(4):959–68. http://dx.doi.org/10.1021/sc400545d in press.

[170] Ziebell A, Gracom K, Katahira R, Chen F, Pu Y, Ragauskas A, et al. Increase in 4-Coumaryl alcohol units during lignification in Alfalfa (*Medicago sativa*) alters the extractability and molecular weight of lignin. J Biol Chem 2010;285:38961–8.

[171] Chan JMW, Bauer S, Sorek H, Sreekumar S, Wang K, Toste FD. Studies on the vanadium-catalyzed nonoxidative depolymerization of *Miscanthus giganteus*-derived lignin. ACS Catal 2013;3:1369–77.

[172] Ralph J. Hydroxycinnamates in lignification. Phytochem Rev 2010;9:65–83.

[173] Irbe I, Noldt G, Koch G, Andersone I, Andersons B. Application of scanning UV microspectrophotometry for the topochemical detection of lignin within individual cell walls of brown-rotted scots pine (*Pinus sylvestris* L.) sapwood. Holzforschung 2006;60:601–7.

[174] Lozovik PA, Kaflyuk AE. Application of differential UV spectroscopy to the determination of lignin substances in polluted water. J Anal Chem 2005;60:833–7.

[175] Siqueira G, Milagres AMF, Carvalho W, Koch G, Ferraz A. Topochemical distribution of lignin and hydroxycinnamic acids in sugar-cane cell walls and its correlation with the enzymatic hydrolysis of polysaccharides. Biotechnol Biofuels 2011;4:7.

[176] Coletta VC, Rezende CA, Rodrigues da Conceicao F, Polikarpov I, Guimaraes FEG. Mapping the lignin distribution in pretreated sugarcane bagasse by confocal and fluorescence lifetime imaging microscopy. Biotechnol Biofuels 2013;6:43.

[177] Donaldson LA, Radotic K. Fluorescence lifetime imaging of lignin autofluorescence in normal and compression wood. J Microsc (Oxford, United Kingdom) 2013;251:178–87.

[178] Gidh AV, Decker SR, See CH, Himmel ME, Williford CW. Characterization of lignin using multi-angle laser light scattering and atomic force microscopy. Anal Chim Acta 2006;555:250–8.

[179] Hollertz R, Arwin H, Faure B, Zhang Y, Bergstroem L, Wagberg L. Dielectric properties of lignin and glucomannan as determined by spectroscopic ellipsometry and Lifshitz estimates of non-retarded Hamaker constants. Cellulose (Dordrecht, Netherlands) 2013;20:1639–48.

[180] Haensel T, Reinmoeller M, Lorenz P, Beenken WJD, Krischok S, Ahmed SI-U. Valence band structure of cellulose and lignin studied by XPS and DFT. Cellulose (Dordrecht, Netherlands) 2012;19:1005–11.

[181] Mitsui K, Inagaki T, Tsuchikawa S. Monitoring of hydroxyl groups in wood during heat treatment using NIR spectroscopy. Biomacromolecules 2008;9:286–8.

[182] Du X, Gellerstedt G, Li J. Universal fractionation of lignin–carbohydrate complexes (LCCs) from lignocellulosic biomass: an example using spruce wood. Plant J 2013;74:328–38.

[183] Du X, Li J, Gellerstedt G, Rencoret J, Del Rio JC, Martinez AT, et al. Understanding pulp delignification by laccase-mediator systems through isolation and characterization of lignin–carbohydrate complexes. Biomacromolecules 2013;14:3073–80.

[184] Lawoko M. Unveiling the structure and ultrastructure of lignin carbohydrate complexes in softwoods. Int J Biol Macromol 2013;62:705–13.

[185] Lawoko M, Henriksson G, Gellerstedt G. Structural differences between the lignin–carbohydrate complexes present in wood and in chemical pulps. Biomacromolecules 2005;6:3467–73.

[186] Li J, Martin-Sampedro R, Pedrazzi C, Gellerstedt G. Fractionation and characterization of lignin–carbohydrate complexes (LCCs) from eucalyptus fibers. Holzforschung 2011;65:43–50.

[187] Sun R-C, Sun X-F, Zhang S-H. Quantitative determination of hydroxycinnamic acids in wheat, rice, rye, and barley straws, maize stems, oil palm frond fiber, and fast-growing poplar wood. J AgricFood Chem 2001;49:5122–9.

[188] Lygin AV, Upton J, Dohleman FG, Juvik J, Zabotina OA, Widholm JM, et al. Composition of cell wall phenolics and polysaccharides of the potential bioenergy crop – Miscanthus. GCB Bioenergy 2011;3:333–45.

[189] Lozovaya VV, Gorshkova TA, Yablokova EV, Rumyantseva NI, Valieva A, Ulanov A, et al. Cold alkali can extract phenolic acids that are ether linked to cell wall components in dicotyledonous plants (buckwheat, soybean and flax). Phytochemistry 1998;50:395–400.

[190] Du X, Perez-Boada M, Fernandez C, Rencoret J, del Rio JC, Jimenez-Barbero J, et al. Analysis of lignin–carbohydrate and lignin–lignin linkages after hydrolase treatment of xylan–lignin, glucomannan–lignin and glucan–lignin complexes from spruce wood. Planta 2014(5):1079–90. http://dx.doi.org/10.1007/s00425-014-2037-y239 in press.

[191] Choi JW, Choi D-H, Faix O. Characterization of lignin–carbohydrate linkages in the residual lignins isolated from chemical pulps of spruce (*Picea abies*) and beech wood (*Fagus sylvatica*). J Wood Sci 2007;53:309–13.

[192] Yuan T-Q, Sun S-N, Xu F, Sun R-C. Characterization of lignin structures and lignin–carbohydrate complex (LCC) linkages by quantitative 13C and 2D HSQC NMR spectroscopy. J Agric Food Chem 2011;59:10604–14.

[193] Balakshin M, Capanema E, Gracz H, Chang H-m, Jameel H. Quantification of lignin–carbohydrate linkages with high-resolution NMR spectroscopy. Planta 2011;233:1097–110.

[194] Balakshin MY, Capanema EA, Chang H-m. MWL fraction with a high concentration of lignin–carbohydrate linkages: isolation and 2D NMR spectroscopic analysis. Holzforschung 2007;61:1–7.

[195] Miyagawa Y, Kamitakahara H, Takano T. Fractionation and characterization of lignin–carbohydrate complexes (LCCs) of Eucalyptus globulus in residues left after MWL isolation. Part II: analyses of xylan–lignin fraction (X–L). Holzforschung 2013;67:629–42.

[196] Bauer S, Sorek H, Mitchell VD, Ibanez AB, Wemmer DE. Characterization of *Miscanthus giganteus* lignin isolated by ethanol organosolv process under reflux condition. J Agric Food Chem 2012;60:8203–12.

[197] Clark VT. A handbook of computational chemistry. Angew Chem 1986;98:936.

[198] Watts HD, Mohamed MNA, Kubicki JD. Comparison of multistandard and TMS-standard calculated nmr shifts for coniferyl alcohol and application of the multistandard method to lignin dimers. J Phys Chem B 2011;115:1958–70.

[199] Lundquist K, Li S, Langer V. threo-2-(2,6-Dimethoxyphenoxy)-1-(4-hydroxy-3,5-dimethoxyphenyl)propane-1,3-diol: a conformational study. Acta Crystallogr Sect C 2005;61:o256–8.

[200] Mostaghni F, Teimouri A, Mirshokraei SA. Synthesis, spectroscopic characterization and DFT calculations of β-O-4 type lignin model compounds. Spectrochim Acta Part A: Mol Biomol Spectrosc 2013;110:430–6.

[201] Sangha AK, Parks JM, Standaert RF, Ziebell A, Davis M, Smith JC. Radical coupling reactions in lignin synthesis: a density functional theory study. J Phys Chem B 2012;116:4760–8.

[202] Elder T. A computational study of pyrolysis reactions of lignin model compounds. Holzforschung 2010;64:435–40.

[203] Petridis L, Schulz R, Smith JC. Simulation analysis of the temperature dependence of lignin structure and dynamics. J Am Chem Soc 2011;133:20277–87.

[204] Petridis L, Smith JC. A molecular mechanics force field for lignin. J Comput Chem 2009;30:457–67.

[205] Elder T, Fort RC. Reactivity of lignin – correlation with molecular orbital calculations. In: Heitner C, Dimmel DR, Schmidt JA, editors. Lignin and lignans: advances in chemistry. Boca raton (FL): CRC Press; 2010. p. 321–47.

[206] Charlier L, Mazeau K. Molecular modeling of the structural and dynamical properties of secondary plant cell walls: influence of lignin chemistry. J Phys Chem B 2012;116:4163–74.

[207] Besombes S, Mazeau K. The cellulose/lignin assembly assessed by molecular modeling. Part 1: adsorption of a threo guaiacyl β-O-4 dimer onto a Iβ cellulose whisker. Plant Physiol Biochem 2005;43:299–308.

[208] Besombes S, Mazeau K. The cellulose/lignin assembly assessed by molecular modeling. Part 2: seeking for evidence of organization of lignin molecules at the interface with cellulose. Plant Physiol Biochem 2005;43: 277–86.

[209] Sangha AK, Petridis L, Smith JC, Ziebell A, Parks JM. Molecular simulation as a tool for studying lignin. Environ Prog Sustain Energy 2012;31:47–54.

[210] Britt PF, Buchanan AC, Cooney MJ, Martineau DR. Flash vacuum pyrolysis of methoxy-substituted lignin model compounds. J Org Chem 2000;65:1376–89.

[211] Beste A, Buchanan AC. Computational study of bond dissociation enthalpies for lignin model compounds. substituent effects in phenethyl phenyl ethers. Plant Physiol Biochem 2009;74:2837–41.

[212] Younker JM, Beste A, Buchanan III AC. Computational study of bond dissociation enthalpies for lignin model compounds: beta-5 Arylcoumaran. Chem Phys Lett 2012;545:100–6.

[213] Elder T, Beste A. Density functional theory study of the concerted pyrolysis mechanism for lignin models. Energy Fuels 2014;28:5229–35.

[214] Janesko BG. Acid-catalyzed hydrolysis of lignin beta-O-4 linkages in ionic liquid solvents: a computational mechanistic study. Phys Chem Chem Phys 2014;16:5423–33.

[215] Janesko BG. Modeling interactions between lignocellulose and ionic liquids using DFT-D. Phys Chem Chem Phys 2011;13:11393–401.

[216] Sun N, Parthasarathi R, Socha AM, Shi J, Zhang S, Stavila V, et al. Understanding pretreatment efficacy of four cholinium and imidazolium ionic liquids by chemistry and computation. Green Chem 2014;16:2546–57.

[217] Parthasarathi R, Romero RA, Redondo A, Gnanakaran S. Theoretical study of the remarkably diverse linkages in lignin. J Phys Chem Lett 2011;2:2660–6.

[218] Kim S, Chmely SC, Nimlos MR, Bomble YJ, Foust TD, Paton RS, et al. Computational study of bond dissociation enthalpies for a large range of native and modified lignins. J Phys Chem Lett 2011;2:2846–52.

[219] Zhang X, Yang W, Blasiak W. Modeling study of woody biomass: interactions of cellulose, hemicellulose, and lignin. Energy Fuels 2011;25:4786–95.

[220] Cho DW, Parthasarathi R, Pimentel AS, Maestas GD, Park HJ, Yoon UC, et al. Nature and kinetic analysis of carbon–carbon bond fragmentation reactions of cation radicals derived from set-oxidation of lignin model compounds. J Org Chem 2010;75:6549–62.

[221] Asikkala J, Tamminen T, Argyropoulos DS. Accurate and reproducible determination of lignin molar mass by acetobromination. J Agric Food Chem 2012;60:8968–73.

[222] Baumberger S, Abaecherli A, Fasching M, Gellerstedt G, Gosselink R, Hortling B, et al. Molar mass determination of lignins by size-exclusion chromatography: towards standardisation of the method. Holzforschung 2007;61: 459–68.

[223] D'Auria M, Emanuele L, Racioppi R. FT-ICR-MS analysis of lignin. Nat Prod Res 2012;26:1368–74.

[224] Gidh AV, Decker SR, Vinzant TB, Himmel ME, Williford C. Determination of lignin by size exclusion chromatography using multi angle laser light scattering. J Chromatogr A 2006;1114:102–10.

[225] Fukushima RS, Hatfield RD. Comparison of the acetyl bromide spectrophotometric method with other analytical lignin methods for determining lignin concentration in forage samples. J Agric Food Chem 2004;52:3713–20.

[226] Johnson DB, Moore WE, Zank LC. The spectrophotometric determination of lignin in small wood samples. Tappi 1961;44:793–8.

[227] Gomes DI, Detmann E, Valadares Filho SdC, Fukushima RS, de Souza MA, Valente TNP, et al. Evaluation of lignin contents in tropical forages using different analytical methods and their correlations with degradation of insoluble fiber. Anim Feed Sci Technol 2011;168:206–22.

[228] Dence CW. The determination of lignin. In: Lin SY, Dence CW, editors. Methods in lignin chemistry. Berlin (DE): Springer-Verlag; 1992. p. 33–61.

[229] International A. Standard test method for acid-insoluble lignin in wood. West Conshohocken (PA): ASTM International; 2007.

[230] Ma XJ, Cao SL, Yang XF, Lin L, Chen LH, Huang LL. Lignin removal and benzene-alcohol extraction effects on lignin measurements of the hydrothermal pretreated bamboo substrate. Bioresour Technol 2014;151:244–8.

[231] Nicholson DJL, Aaron T, Francis, Raymond CA. THREE-stage Klason method for more accurate determinations of hardwood lignin conteNT. Cellul Chem Technol 2013;48:53–9.

[232] Sluiter Justin B, Ruiz Raymond O, Scarlata Christopher J, Sluiter Amie D, Templeton David W. Compositional analysis of lignocellulosic feedstocks. 1. Review and description of methods. J Agric Food Chem 2010;58:9043–53.

[233] DeMartini JD, Studer MH, Wyman CE. Small-scale and automatable high-throughput compositional analysis of biomass. Biotechnol Bioeng 2010;108:306–12.

[234] Aldaeus F, Schweinebarth H, Toerngren P, Jacobs A. Simplified determination of total lignin content in kraft lignin samples and black liquors. Holzforschung 2011;65:601–4.

[235] Van Soest PJ, Robertson JB, Lewis BA. Methods for dietary fiber, neutral detergent fiber, and nonstarch polysaccharides in relation to animal nutrition. J Dairy Sci 1991;74:3583–97.

[236] Van Soest PJ. Use of detergents in analysis of fibrous feeds. II. A rapid method for the determination of fiber and lignin. J Assoc Off Agric Chem 1963;46: 829–35.

[237] Van Soest PJ, Wine RH. Determination of lignin and cellulose in acid-detergent fiber with permanganate. J – Assoc Off Anal Chem 1968;51:780–5.

[238] Alves A, Rodrigues J, Wimmer R, Schwanninger M. Analytical pyrolysis as a direct method to determine the lignin content in wood: part 2: evaluation of the common model and the influence of compression wood. J Anal Appl Pyrolysis 2008;81:167–72.

[239] Alves A, Schwanninger M, Pereira H, Rodrigues J. Analytical pyrolysis as a direct method to determine the lignin content in wood. J Anal Appl Pyrolysis 2006;76:209–13.

[240] Lourenco A, Gominho J, Marques AV, Pereira H. Comparison of Py-GC/FID and wet chemistry analysis for lignin determination in wood and pulps from Eucalyptus globulus. BioResources 2013;8:2967–80 14 pp.

[241] Kelley SS, Rowell RM, Davis M, Jurich CK, Ibach R. Rapid analysis of the chemical composition of agricultural fibers using near infrared spectroscopy and pyrolysis molecular beam mass spectrometry. Biomass Bioenergy 2004;27:77–88.

[242] Sykes R, Yung M, Novaes E, Kirst M, Peter G, Davis M. High-throughput screening of plant cell-wall composition using pyrolysis molecular beam mass spectroscopy. Methods Mol Biol 2009:169–83.

[243] Sykes R, Kodrzycki B, Tuskan G, Foutz K, Davis M. Within tree variability of lignin composition in Populus. Wood Sci Technol 2008;42:649–61.

[244] Carrier M, Loppinet-Serani A, Denux D, Lasnier J-M, Ham-Pichavant F, Cansell F, et al. Thermogravimetric analysis as a new method to determine the lignocellulosic composition of biomass. Biomass Bioenergy 2011;35: 298–307.

[245] Freda C, Zimbardi F, Nanna F, Viola E. Mathematical tool from Corn Stover TGA to determine its composition. Appl Biochem Biotechnol 2012;167: 2283–94.

[246] Serapiglia MJ, Cameron KD, Stipanovic AJ, Smart LB. High-resolution thermo-gravimetric analysis for rapid characterization of biomass composition and selection of shrub willow varieties. Appl Biochem Biotechnol 2008;145:3–11.

[247] Singh K, Risse M, Das KC, Worley J. Determination of composition of cellulose and lignin mixtures using thermogravimetric analysis. J Energy Resour Technol 2009;131:022201/1–16.

[248] Agarwal U.P. Lignin quantitation by FT-Raman spectroscopy. In: Proceedings of the 16th international symposium on wood, fiber and pulping chemistry. Tianjin, China; 2011. p. 170–3.

[249] Agarwal UP, Weinstock IA, Atalla RH. FT-Raman spectroscopy for direct measurement of lignin concentrations in kraft pulps. Tappi J 2003;2:22–6.

[250] Ona T, Sonoda T, Ito K, Shibata M, Kato T, Ootake Y. Non-destructive determination of wood constituents by Fourier-transform Raman spectroscopy. J Wood Chem Technol 1997;17:399–417.

[251] Ona T, Sonoda T, Ohshima J, Yokota S, Yoshizawa N. A rapid quantitative method to assess eucalyptus wood properties for kraft pulp production by FT-Raman spectroscopy. J Pulp Pap Sci 2003;29:6–10.

[252] Allison GG, Thain SC, Morris P, Morris C, Hawkins S, Hauck B, et al. Quantification of hydroxycinnamic acids and lignin in perennial forage and energy grasses by Fourier-transform infrared spectroscopy and partial least squares regression. Bioresour Technol 2009;100:1252–61.

[253] Dang VQ, Bhardwaj NK, Hoang V, Nguyen KL. Determination of lignin content in high-yield kraft pulps using photoacoustic rapid scan Fourier transform infrared spectroscopy. Carbohydr Polym 2007;68:489–94.

[254] Nuopponen MH, Birch GM, Sykes RJ, Lee SJ, Stewart D. Estimation of wood density and chemical composition by means of diffuse reflectance mid-infrared fourier transform (DRIFT-MIR) spectroscopy. J Agric Food Chem 2006;54:34–40.

[255] Tamaki Y, Mazza G. Rapid determination of lignin content of straw using Fourier transform mid-infrared spectroscopy. J Agric Food Chem 2011;59: 504–12.

[256] Adler Paul R, Sanderson Matt A, Weimer Paul J, Vogel Kenneth P. Plant species composition and biofuel yields of conservation grasslands. Ecol Appl 2009;19:2202–9.

[257] Fackler K, Gradinger C, Hinterstoisser B, Messner K, Schwanninger M. Lignin degradation by white rot fungi on spruce wood shavings during short-time solid-state fermentations monitored by near infrared spectroscopy. Enzyme Microb Technol 2006;39:1476–83.

[258] Fong Chong B, Purcell DE, O'Shea MG. Diffuse reflectance, near-infrared spectroscopic estimation of sugarcane lignocellulose components—effect of sample preparation and calibration approach. BioEnergy Res 2013;6:153–65.

[259] He W, Hu H. Rapid prediction of different wood species extractives and lignin content using near infrared spectroscopy. J Wood Chem Technol 2013;33: 52–64.

[260] Hou S, Li L. Rapid characterization of woody biomass digestibility and chemical composition using near-infrared spectroscopy. J Integr Plant Biol 2011;53:166–75.

[261] Jiang W, Han G, Via BK, Tu M, Liu W, Fasina O. Rapid assessment of coniferous biomass lignin–carbohydrates with near-infrared spectroscopy. Wood Sci Technol 2014;48:109–22.

[262] Jin S, Chen H. Near-infrared analysis of the chemical composition of rice straw. Ind Crops Prod 2007;26:207–11.

[263] Poke FS, Raymond CA. Predicting extractives, lignin, and cellulose contents using near infrared spectroscopy on solid wood in Eucalyptus globulus. J Wood Chem Technol 2006;26:187–99.

[264] Poke FS, Wright JK, Raymond CA. Predicting extractives and lignin contents in Eucalyptus globulus using near infrared reflectance analysis. J Wood Chem Technol 2004;24:55–67.

[265] Pordesimo LO, Hames BR, Sokhansanj S, Edens WC. Variation in corn stover composition and energy content with crop maturity. Biomass Bioenergy 2005;28:366–74.

[266] Rambo MKD, Amorim EP, Ferreira MMC. Potential of visible-near infrared spectroscopy combined with chemometrics for analysis of some constituents of coffee and banana residues. Anal Chim Acta 2013;775:41–9.

[267] Smith-Moritz AM, Chern M, Lao J, Sze-To WH, Heazlewood JL, Ronald PC, et al. Combining multivariate analysis and monosaccharide composition modeling to identify plant cell wall variations by Fourier transform near infrared spectroscopy. Plant Methods 2011;7:26.

[268] Stackpole Desmond J, Vaillancourt Rene E, Alves A, Rodrigues J, Potts Brad M. Genetic variation in the chemical components of Eucalyptus globulus wood. G3 (Bethesda) 2011;1:151–9.

[269] Templeton DW, Sluiter AD, Hayward TK, Hames BR, Thomas SR. Assessing corn stover composition and sources of variability via NIRS. Cellulose (Dordrecht, Netherlands) 2009;16:621–39.

[270] Uner B, Karaman I, Tanriverdi H, Ozdemir D. Determination of lignin and extractive content of Turkish Pine (Pinus brutia Ten.) trees using near infrared spectroscopy and multivariate calibration. Wood Sci Technol 2011;45:121–34.

[271] Wolfrum EJ, Sluiter AD. Improved multivariate calibration models for corn stover feedstock and dilute-acid pretreated corn stover. Cellulose (Dordrecht, Netherlands) 2009;16:567–76.

[272] Yamada T, Yeh T-F, Chang H-M, Li L, Kadla JF, Chiang VL. Rapid analysis of transgenic trees using transmittance near-infrared spectroscopy (NIR). Holzforschung 2006;60:24–8.

[273] Yao S, Wu G, Xing M, Zhou S, Pu J. Determination of lignin content in Acacia spp. using near-infrared reflectance spectroscopy. BioResources 2010;5: 556–62.

[274] Ye XP, Liu L, Hayes D, Womac A, Hong K, Sokhansanj S. Fast classification and compositional analysis of cornstover fractions using Fourier transform near-infrared techniques. Bioresour Technol 2008;99:7323–32.

[275] Yeh T-F, Chang H-m, Kadla JF. Rapid prediction of solid wood lignin content using transmittance near-infrared spectroscopy. J Agric Food Chem 2004;52:1435–9.

[276] Yeh T-F, Yamada T, Capanema E, Chang H-M, Chiang V, Kadla JF. Rapid screening of wood chemical component variations using transmittance near-infrared spectroscopy. J Agric Food Chem 2005;53:3328–32.

[277] Nkansah K, Dawson-Andoh B. Rapid characterization of biomass using fluorescence spectroscopy coupled with multivariate data analysis. I. yellow poplar (*Liriodendron tulipifera* L.). J Renew Sustain Energy 2010;2:023103/ 1–023103/12.

[278] Nkansah K, Dawson-Andoh B. Rapid characterization of biomass using fluorescence spectroscopy coupled with multivariate data analysis. II. Northern red oak (*Quercus rubra*). J Renew Sustain Energy 2010;2:043101/1–10.

[279] Haffner FB, Mitchell VD, Arundale RA, Bauer S. Compositional analysis of *Miscanthus giganteus* by near infrared spectroscopy. Cellulose (Dordrecht, Netherlands) 2013;20:1629–37.

[280] Foster CE, Martin TM, Pauly M. Comprehensive compositional analysis of plant cell walls (lignocellulosic biomass) part I: lignin. J Visualized Exp 2010 no pp given.

[281] Fukushima RS, Hatfield RD. Extraction and isolation of lignin for utilization as a standard to determine lignin concentration using the acetyl bromide spectrophotometric method. J Agric Food Chem 2001;49:3133–9.

[282] Fukushima RS, Kerley MS. Use of lignin extracted from different plant sources as standards in the spectrophotometric acetyl bromide lignin method. J Agric Food Chem 2011;59:3505–9.

[283] Lee RA, Bedard C, Berberi V, Beauchet R, Lavoie J-M. UV–vis as quantification tool for solubilized lignin following a single-shot steam process. Bioresour Technol 2013;144:658–63.

[284] Lee SH, Doherty TV, Linhardt RJ, Dordick JS. Ionic liquid-mediated selective extraction of lignin from wood leading to enhanced enzymatic cellulose hydrolysis. Biotechnol Bioeng 2009;102:1368–76.

[285] Rabemanolontsoa H, Ayada S, Saka S. Quantitative method applicable for various biomass species to determine their chemical composition. Biomass Bioenergy 2011;35:4630–5.

[286] Doka O, Bicanic D, Bunzel M. Quantification of lignin in synthetic mixtures of xylan and cellulose powders by photoacoustic spectroscopy. Anal Chim Acta 2004;514:235–9.

[287] Jiang N, Pu Y, Ragauskas AJ. Rapid determination of lignin content via direct dissolution and 1H NMR analysis of plant cell walls. ChemSusChem 2010;3:1285–9.

[288] Sievers C, Marzialetti T, Hoskins TJC, Valenzuela Olarte MB, Agrawal PK, Jones CW. Quantitative solid state NMR analysis of residues from acid hydrolysis of loblolly pine wood. Bioresour Technol 2009;100:4758–65.

[289] Zhang Y, Legay S, Barriere Y, Mechin V, Legland D. Color quantification of stained maize stem section describes lignin spatial distribution within the whole stem. J Agric Food Chem 2013;61:3186–92.

[290] Browning BL. Wood lignins. In: Browning BL, editor. The chemistry of wood. New York: NY: Interscience Publishers (A Division of John Wiley & Sons); 1963. p. 249–311.

[291] Bose SK, Francis RC, Govender M, Bush T, Spark A. Lignin content versus syringyl to guaiacyl ratio amongst poplars. Bioresour Technol 2008;100: 1628–33.

[292] Chen CL. Nitrobenzene and cupric oxide oxidations [of lignin in solution]. In: Lin SY, Dence CW, editors. Methods in lignin chemistry. Berlin (DE): Springer-Verlag; 1992. p. 301–21.

[293] Del Rio JC, Gutierrez A, Martinez AT. Identifying acetylated lignin units in non-wood fibers using pyrolysis-gas chromatography/mass spectrometry. Rapid Commun Mass Spectrom 2004;18:1181–5.

[294] Hedges JI, Ertel JR. Characterization of lignin by gas capillary chromatography of cupric oxide oxidation products. Anal Chem 1982;54:174–8.

[295] Hou Y, Hu S, Lindstrom ME, Li J. Feasibility of monomer aromatic substances as calibration standards for lignin quantitative analyses in pyrolysis-GCMS. J Anal Appl Pyrolysis 2013;101:232–7.

[296] Lapierre C, Monties B, Rolando C. Thioacidolysis of lignin: comparison with acidolysis. J Wood Chem Technol 1985;5:277–92.

[297] Lapierre C, Rolando C, Monties B. Characterization of poplar lignins acidolysis products: capillary gas–liquid and liquid–liquid chromatography of monomeric compounds. Holzforschung 1983;37:189–98.

[298] Lima CF, Barbosa LCA, Marcelo CR, Silverio FO, Colodette JL. Comparison between analytical pyrolysis and nitrobenzene oxidation for determination

[299] of syringyl/guaiacyl ratio in Eucalyptus spp. lignin. BioResources 2008;3: 701–12.

[299] Lopes FF, Silverio FO, Baffa DCF, Loureiro ME, Barbosa MHP. Determination of sugarcane bagasse lignin S/G/H ratio by pyrolysis GC/MS. J Wood Chem Technol 2011;31:309–23.

[300] Meier D, Faix O. Pyrolysis-gas chromatography-mass spectrometry [of lignin in solid state]. In: Lin SY, Dence CW, editors. Methods in lignin chemistry. Berlin (DE): Springer-Verlag; 1992. p. 177–99.

[301] Nunes CA, Lima CF, Barbosa LCA, Colodette JL, Gouveia AFG, Silverio FO. Determination of Eucalyptus spp lignin S/G ratio: a comparison between methods. Bioresour Technol 2010;101:4056–61.

[302] Pepper JM, Baylis PET, Adler E. Isolation and properties of lignins obtained by the acidolysis of spruce and aspen woods in dioxane-water medium. Can J Chem 1959;37:1241–8.

[303] Rencoret J, Gutierrez A, del Rio JC. Lipid and lignin composition of woods from different eucalypt species. Holzforschung 2007;61:165–74.

[304] Robinson AR, Mansfield SD. Rapid analysis of poplar lignin monomer composition by a streamlined thioacidolysis procedure and near-infrared reflectance-based prediction modeling. Plant J 2009;58:706–14.

[305] Rodrigues J, Meier D, Faix O, Pereira H. Determination of tree-to-tree variation in syringyl/guaiacyl ratio of *Eucalyptus globulus* wood lignin by analytical pyrolysis. J Anal Appl Pyrolysis 1999;48:121–8.

[306] Weng J, Jia L, Sun S, Wang Y, Tang X, Zhou Z, et al. On-line product analysis of pine wood pyrolysis using synchrotron vacuum ultraviolet photoionization mass spectrometry. Anal Bioanal Chem 2013;405:7097–105.

[307] Yamamura M, Hattori T, Suzuki S, Shibata D, Umezawa T. Microscale thioacidolysis method for the rapid analysis of β-O-4 substructures in lignin. Plant Biotechnol (Tokyo, Japan) 2012;29:419–23.

[308] Marques G, Gutierrez A, del Rio JC. Chemical characterization of lignin and lipophilic fractions from leaf fibers of Curaua (*Ananas erectifolius*). J Agric Food Chem 2007;55:1327–36.

[309] Evans RJ, Milne TA, Soltys MN. Direct mass-spectrometric studies of the pyrolysis of carbonaceous fuels: III. Primary pyrolysis of lignin. J Anal Appl Pyrolysis 1986;9:207–36.

[310] Fontaine A-S, Bout S, Barriere Y, Vermerris W. Variation in cell wall composition among forage maize (Zea mays L.) inbred lines and its impact on digestibility: analysis of neutral detergent fiber composition by pyrolysis-gas chromatography-mass spectrometry. J Agric Food Chem 2003;51:8080–7.

[311] Kiyota E, Mazzafera P, Sawaya ACHF. Analysis of soluble lignin in sugarcane by ultrahigh performance liquid chromatography-tandem mass spectrometry with a do-it-yourself oligomer database. Anal Chem (Washington, DC, United States) 2012;84:7015–20.

[312] Alves A, Schwanninger M, Pereira H, Rodrigues J. Calibration of NIR to assess lignin composition (H/G ratio) in maritime pine wood using analytical pyrolysis as the reference method. Holzforschung 2006;60:29–31.

[313] Alves A, Simoes R, Stackpole DJ, Vaillancourt RE, Potts BM, Schwanninger M, et al. Determination of the syringyl/guaiacyl ratio of *Eucalyptus globulus* wood lignin by near infrared-based partial least squares regression models using analytical pyrolysis as the reference method. J Near Infrared Spectrosc 2011;19:343–8.

[314] Derkacheva OY. Estimation of aromatic structure contents in hardwood lignins from IR absorption spectra. J Appl Spectrosc 2013;80:670–6.

[315] Ona T, Sonoda T, Ito K, Shibata M, Katayama T, Kato T, et al. Non-destructive determination of lignin syringyl/guaiacyl monomeric composition in native wood by Fourier transform Raman spectroscopy. J Wood Chem Technol 1998;18:43–51.

[316] Sun L, Varanasi P, Yang F, Loque D, Simmons BA, Singh S. Rapid determination of syringyl:guaiacyl ratios using FT-Raman spectroscopy. Biotechnol Bioeng 2012;109:647–56.

[317] Lupoi JS, Singh S, Davis M, Lee DJ, Shepherd M, Simmons BA, et al. High-throughput prediction of eucalypt lignin syringyl/guaiacyl content using multivariate analysis: a comparison between mid-infrared, near-infrared, and Raman spectroscopies for model development. Biotechnol Biofuels 2014;7:93.

[318] Xia Z, Akim LG, Argyropoulos DS. Quantitative 13C NMR analysis of lignins with internal standards. J Agric Food Chem 2001;49:3573–8.

[319] Stewart D, Yahiaoui N, McDougall GJ, Myton K, Marque C, Boudet AM, et al. Fourier-transform infrared and Raman spectroscopic evidence for the incorporation of cinnamaldehydes into the lignin of transgenic tobacco (Nicotiana tabacum) plants with reduced expression of cinnamyl alcohol dehydrogenase. Planta 1997;201:311–8.

[320] Zhou G, Taylor G, Polle A. FTIR-ATR-based prediction and modelling of lignin and energy contents reveals independent intra-specific variation of these traits in bioenergy poplars. Plant Methods 2011;7:9.

[321] Keskar SS, Edye LA, Fellows CM, Doherty WOS. ATR-FTIR measurement of biomass components in phosphonium ionic liquids. J Wood Chem Technol 2012;32:175–86.

[322] White KE, Reeves III JB, Coale FJ. Mid-infrared diffuse reflectance spectroscopy for the rapid analysis of plant root composition. Geoderma 2011;167–168:197–203.

[323] Ishimaru K, Hata T, Bronsveld P, Meier D, Imamura Y. Spectroscopic analysis of carbonization behavior of wood, cellulose and lignin. J Mater Sci 2007;42:122–9.

[324] Kuroda K-i, Nakagawa-izumi A, Mazumder BB, Ohtani Y, Sameshima K. Evaluation of chemical composition of the core and bast lignins of variety Chinpi-3 kenaf (*Hibiscus cannabinus* L.) by pyrolysis-gas chromatography/

mass spectrometry and cupric oxide oxidation. Ind Crops Prod 2005;22: 223–32.

[325] Stewart JJ, Akiyama T, Chapple C, Ralph J, Mansfield SD. The effects on lignin structure of overexpression of ferulate 5-hydroxylase in hybrid poplar. Plant Physiol 2009;150:621–35.

[326] Harris DC. Gas chromatography. Quantitative chemical analysis. New York (NY): W.H. Freeman and Company; 2003. p. 578–606.

[327] Shih C-J, Smith EA. Determination of glucose and ethanol after enzymatic hydrolysis and fermentation of biomass using Raman spectroscopy. Anal Chim Acta 2009;653:200–6.

[328] Decker SR, Brunecky R, Tucker MP, Himmel ME, Selig MJ. High-throughput screening techniques for biomass conversion. BioEnergy Res 2009;2:179–92.

[329] Dolan JW, Snyder LR. Gradient elution chromatography. In: Meyers RA, editor. Encyclopedia of analytical chemistry. New York (NY): John Wiley & Sons; 2000. p. 11342–60.

[330] Dorsey JG. Column theory and resolution in liquid chromatography. In: Meyers RA, editor. Encyclopedia of analytical chemistry. New York (NY): John Wiley & Sons; 2000. p. 11334–42.

[331] Hames BR, Thomas SR, Sluiter AD, Roth CJ, Templeton DW. Rapid biomass analysis. New tools for compositional analysis of corn stover feedstocks and process intermediates from ethanol production. Appl Biochem Biotechnol 2003;105–108:5–16.

[332] Xu F, Yu J, Tesso T, Dowell F, Wang D. Qualitative and quantitative analysis of lignocellulosic biomass using infrared techniques: a mini-review. Appl Energy 2013;104:801–9.

[333] McCreery RL. Raman spectroscopy for chemical analysis. New York/Chichester/ Weinheim/Brisbane/Singapore/Toronto: Wiley Interscience; 2000. p. 448.

[334] Smith W, Dent G. Modern Raman spectroscopy. Chichester, UK: John Wiley & Sons; 2005.

[335] Shenk JS, Workman Jr. JJ, Westerhaus MO. Application of NIR spectroscopy to agricultural products. Pract Spectrosc 2008;35:347–86.

[336] DeThomas FA, Brimmer PJ. Monochromators for near-infrared spectroscopy. In: Chalmers JMaG PR, editor. Handbook of vibrational spectrscopy. Chichester, UK: John Wiley & Sons; 2002. p. 383–92.

[337] Stark EW. Near-infrared array spectrometers. In: Chalmers JMaG PR, editor. Handbook of vibrational spectroscopy. Chichester, UK: John Wiley & Sons; 2002. p. 393–422.

[338] Goldman DS. Near-infrared spectroscopy in process analysis. In: Peterson JW, editor. Encyclopedia of analytical chemistry-process instrumental methods. New York (NY): John Wiley and Sons; 2000. p. 8256–64.

[339] Gjersing E, Happs RM, Sykes RW, Doeppke C, Davis MF. Rapid determination of sugar content in biomass hydrolysates using nuclear magnetic resonance spectroscopy. Biotechnol Bioeng 2013;110:721–8.

[340] Skoog DA, Holler FJ, Nieman TA. Principles of instrumental analysis. 5th ed.. Philadelphia (PA): Harcourt, Brace, & Company; 1998.

[341] Jehlicka J, Vitek P, Edwards HGM, Heagraves M, Capoun T. Application of portable Raman instruments for fast and non-destructive detection of minerals on outcrops. Spectrochim Acta, Part A Mol Biomol Spectrosc 2009;73A:410–9.

[342] Vitek P, Ali EMA, Edwards HGM, Jehlicka J, Cox R, Page K. Evaluation of portable Raman spectrometer with 1064 nm excitation for geological and forensic applications. Spectrochim Acta, Part A Mol Biomol Spectrosc 2012;86:320–7.

[343] Dao NQ. Dispersive Raman spectroscopy, current instrumental designs. In: Meyers RA, editor. Encyclopedia of analytical chemistry. Hoboken (NJ): John Wiley & Sons; 2006. p. 13024–58.

[344] Agarwal UP, Reiner RS. Near-IR surface-enhanced Raman spectrum of lignin. J Raman Spectrosc 2009;40:1527–34.

[345] Agarwal UP, Kawai N. Self-absorption phenomenon in near-infrared Fourier transform Raman spectroscopy of cellulosic and lignocellulosic materials. Appl Spectrosc 2005;59:385–8.

[346] Lu F, Ralph J. Detection and determination of p-coumaroylated units in lignins. J Agric Food Chem 1999;47:1988–92.

[347] Faix O. Classification of lignins from different botanical origins by FT-IR spectroscopy. Holzforschung 1991;45:21–7.

[348] Faix O. Fourier transform infrared spectroscopy [of lignin in solid state]. In: Lin SY, Dence CW, editors. Methods in lignin chemistry. Berlin, Germany: Springer-Verlag; 1992. p. 83–109.

[349] Hergert HL. Infrared spectra [of lignin]. In: Sarkanen KV, Ludwig CH, editors. Lignins: occurrence and formation, structure, chemical and macromolecular properties, and utilization. New York (NY): John Wiley & Sons; 1971. p. 267–97.

[350] Sills DL, Gossett JM. Using FTIR to predict saccharification from enzymatic hydrolysis of alkali-pretreated biomasses. Biotechnol Bioeng 2012;109:353–62.

[351] Michell AJ, Schimleck LR. NIR spectroscopy of woods from Eucalyptus globulus. App J 1996;49:23–6.

[352] Workman Jr. J, Weyer L, editors. Practical guide to interpretive near-infrared spectroscopy. Boca Raton (FL): CRC Press; 2007.

[353] Alves A, Santos A, Rozenberg P, Paques LE, Charpentier J-P, Schwanninger M, et al. A common near infrared-based partial least squares regression model for the prediction of wood density of Pinus pinaster and Larix × eurolepis. Wood Sci Technol 2012;46:157–75.

[354] Sonoda T, Ona T, Yokoi H, Ishida Y, Ohtani H, Tsuge S. Quantitative analysis of detailed lignin monomer composition by pyrolysis-gas chromatography combined with preliminary acetylation of the samples. Anal Chem 2001;73:5429–35.

[355] Chen L, Auh C, Chen F, Cheng X, Aljoe H, Dixon RA, et al. Lignin deposition and associated changes in anatomy, enzyme activity, gene expression, and ruminal degradability in stems of tall fescue at different developmental stages. J Agric Food Chem 2002;50:5558–65.